

# Effects of the stochasticity of galaxy angular momentum growth on star formation

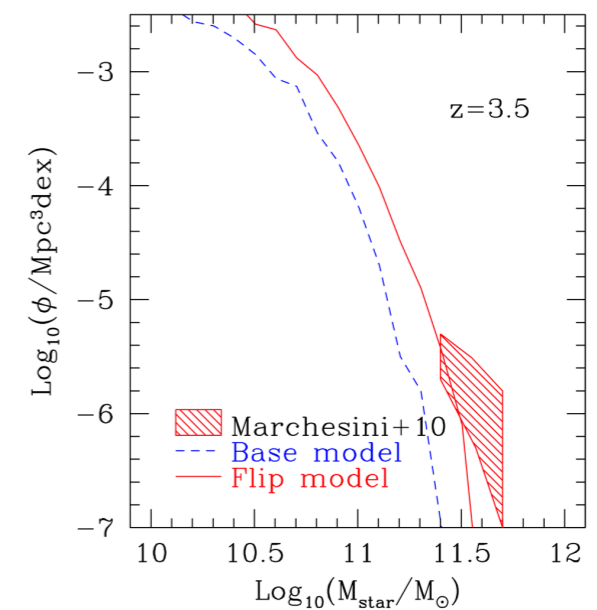
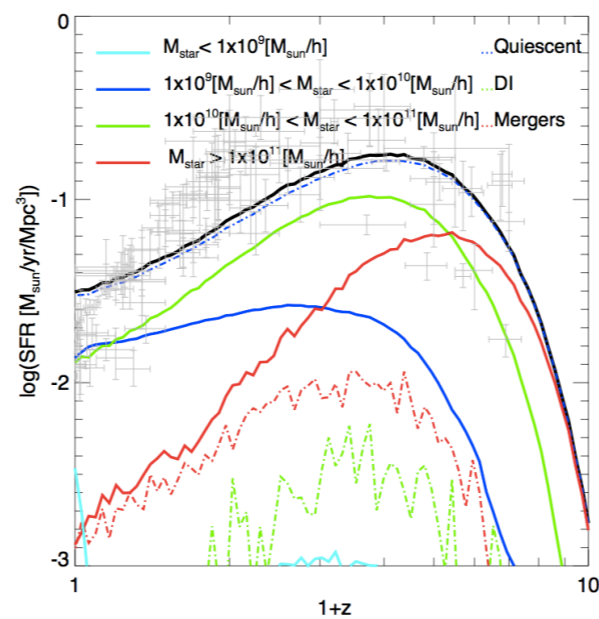
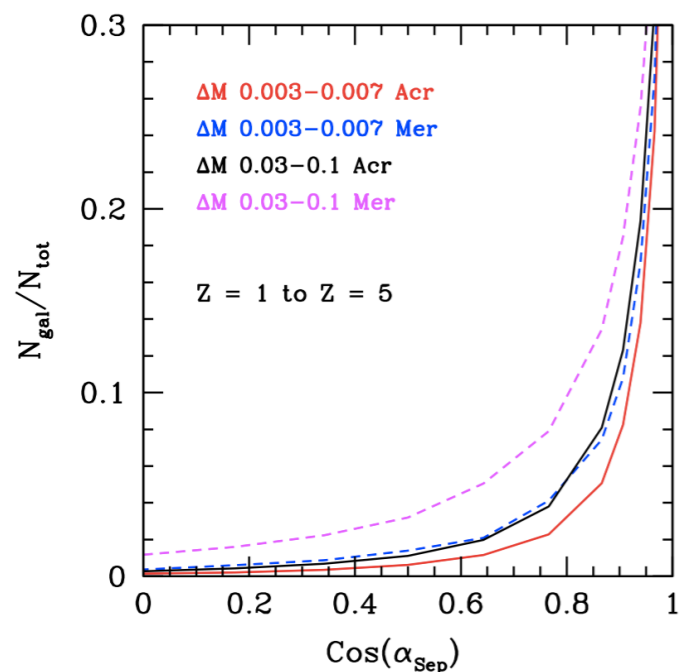
NELSON PADILLA  
PUC CHILE

Sergio Contreras (PUC), Salvador Salazar (MPE), Álvaro Orsi (PUC),  
Andrés Ruiz (UNC), Sofía Cora (La Plata)



# OUTLINE

- 1 Models of galaxy formation
- 2 Angular mom. of infalling material and its effect in a SAM
- 3 Results



# 1) MODELS OF GALAXY FORMATION

Hydrodynamical simulations:

- Detailed processes of gas cooling, turbulence, preheating, star-formation, feedback (SN and AGN).

- Difficulties: over cooling, no grand-design spirals, difficulty to obtain statistical samples, lack of universality in codes.

Sales+12, Scannapieco+12, Marinacci+13,  
Crain+09, Powell+11, Brook+11,  
Nagamine10, Hopkins+11, Tasker+11,  
Kannan+13

Semi-analytic models

- Baryons via a set of equations per sub-halo of a merger tree extracted from cosmological DM-only simulations.

- Difficulties: simplified assumptions do not contain full complexity of galaxy evolution; e.g., by fitting  $z=0$  LF, they make little SF at high- $z$ .

Springel+01, Lagos, Cora & Padilla 08, Lagos,  
Padilla & Cora 09, Tecce+10, Lagos+11,  
Padilla+13

# 1) MODELS OF GALAXY FORMATION

Hydrodynamical simulations:

- Detailed processes of gas cooling, turbulence, preheating, star-formation, feedback (SN and AGN).

- Difficulties: over cooling, no grand-design spirals, difficulty to obtain statistical samples, lack of universality in codes.

Sales+12, Scannapieco+12, Marinacci+13,  
Crain+09, Powell+11, Brook+11,  
Nagamine10, Hopkins+11, Tasker+11,  
Kannan+13

Semi-analytic models

- Baryons via a set of equations per sub-halo of a merger tree extracted from cosmological DM-only simulations.

- Difficulties: simplified assumptions do not contain full complexity of galaxy evolution; e.g., by fitting  $z=0$  LF, they make little SF at high- $z$ .

Springel+01, Lagos, Cora & Padilla 08, Lagos,  
Padilla & Cora 09, Tecce+10, Lagos+11,  
Padilla+13

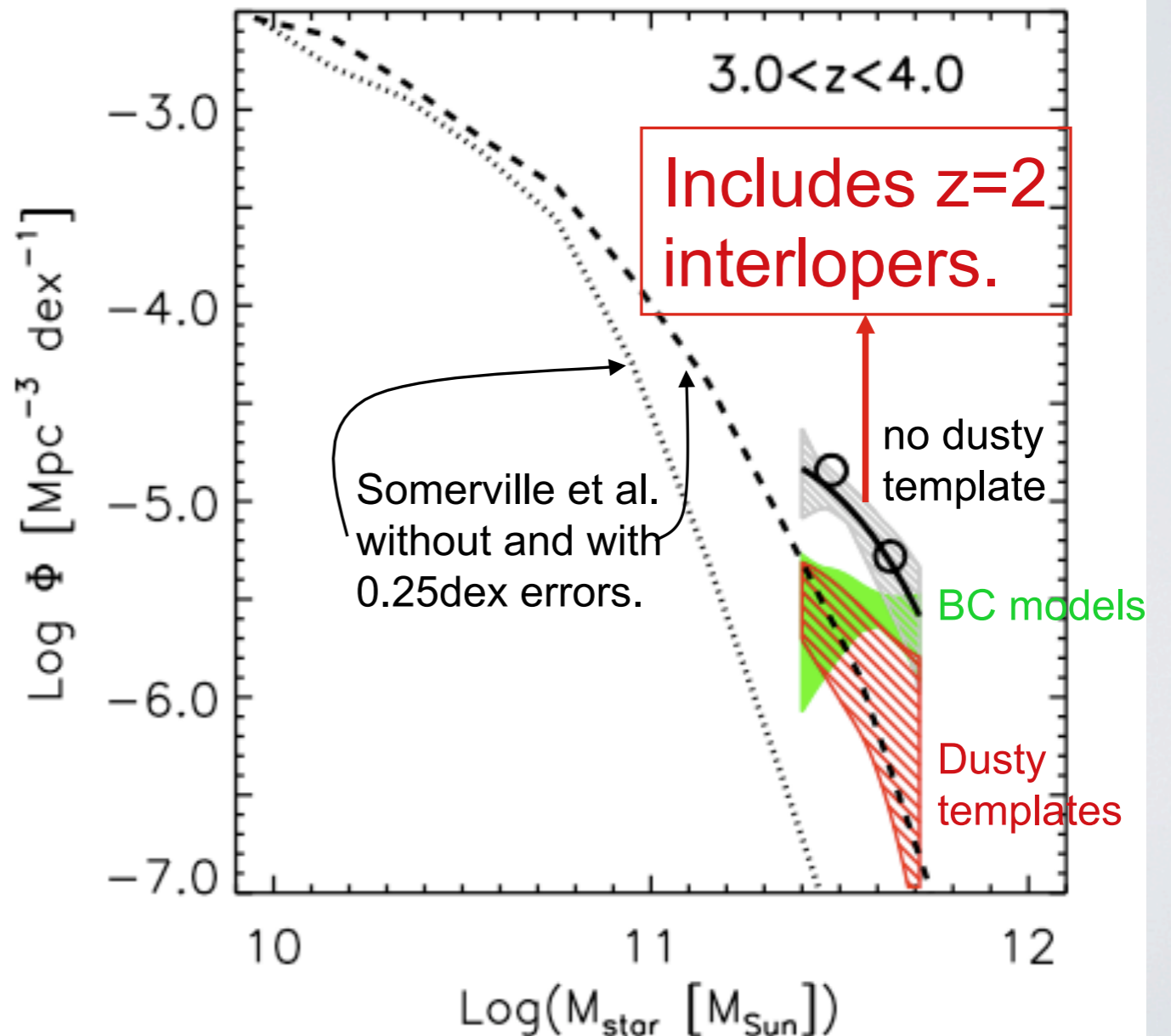
# I) SAM PERFORMANCE AT HIGH-Z

General deficit of high-z massive galaxies

Example:

NEWFIRM Medium Band Survey  
Marchesini et al. (2010)

By fitting the  $z=0$  LF, and  
having large initial  
angular momenta in discs, SAMs  
slow down the high-z SF



## 2) ANGULAR MOMENTUM

*Simplified assumption in SAM:* dimensionless spin parameter is constant due to limited resolution in large cosmological volume simulations.

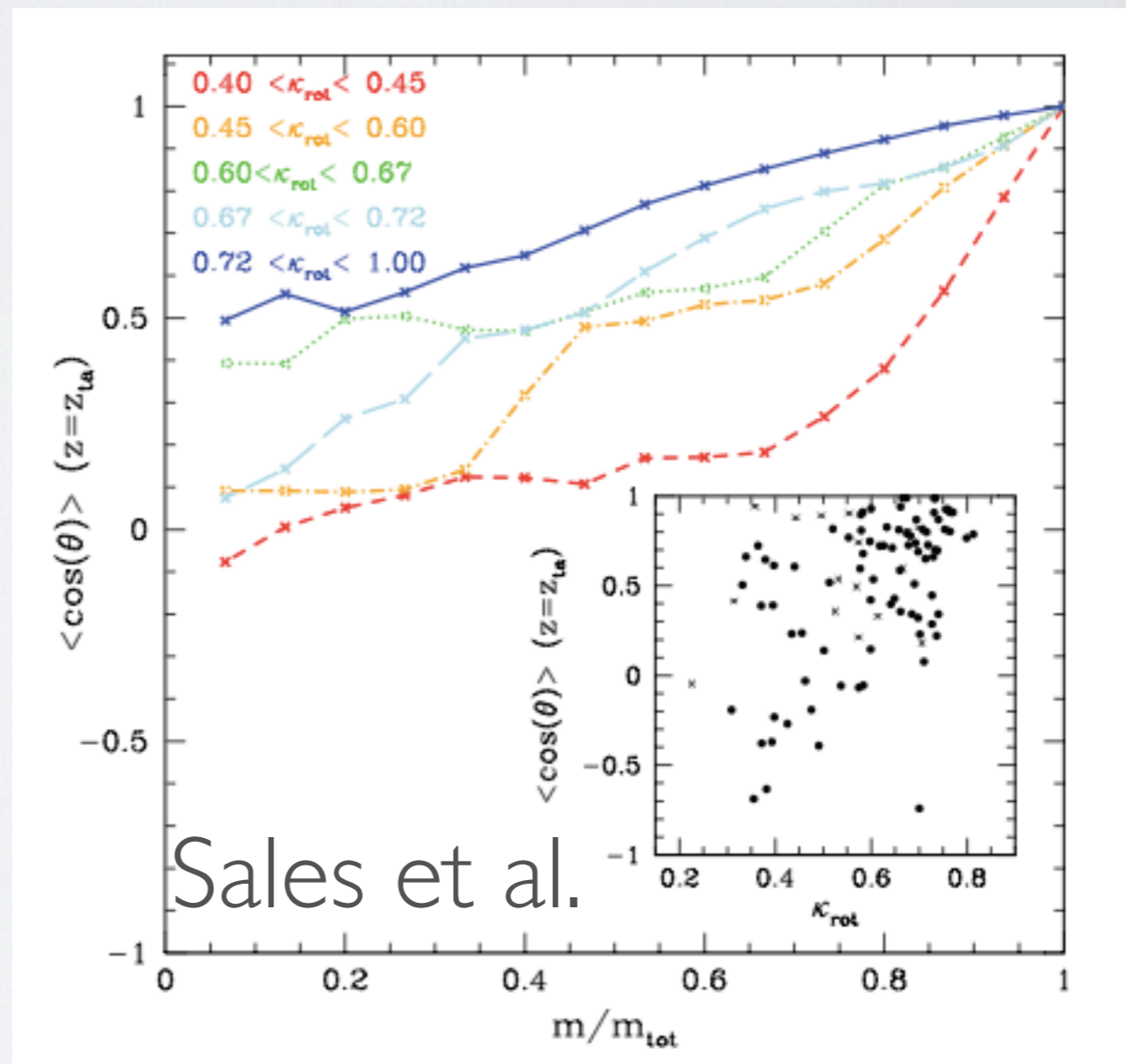
## 2) ANGULAR MOMENTUM

**Simplified assumption in SAM:** dimensionless spin parameter is constant due to limited resolution in large cosmological volume simulations.

Using Hydro, Sales et al. (2012) show that surviving discs ( $\kappa_{\text{rot}}$  high) in GIMIC show good alignment of angular momentum of mass enclosed in given radius ( $m/m_{\text{tot}}$ ) with total angular momentum at time of turn-around.

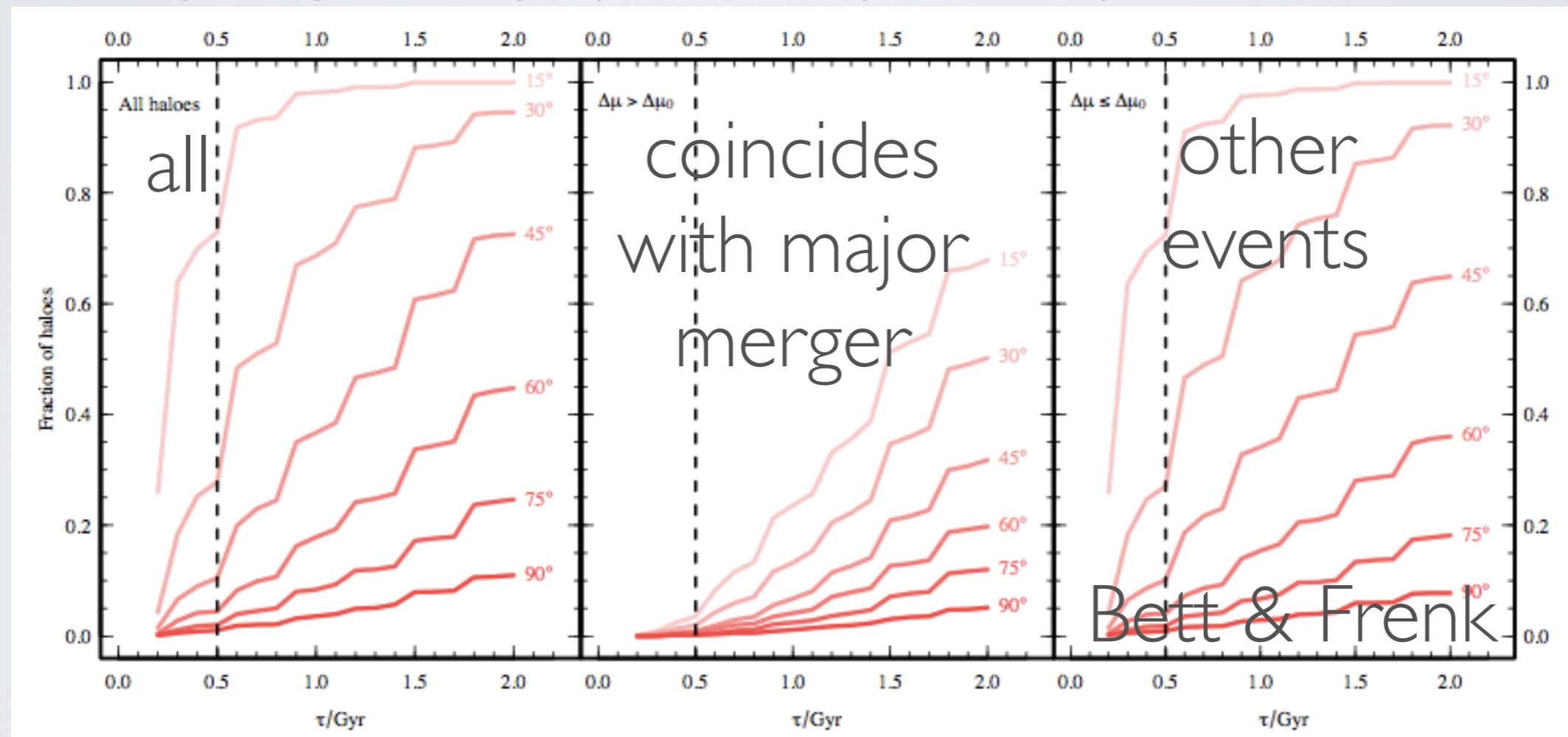
Missalignments by accretion of material destroy the disc, and a new disc starts to form.

**Discs are episodic and their spins not constant.**



## 2) ANGULAR MOMENTUM

SAMs do not follow gas: Bett & Frenk (2011) study the occurrence of spin flips in DM halos in a high resolution simulation (using enough particles per halo):

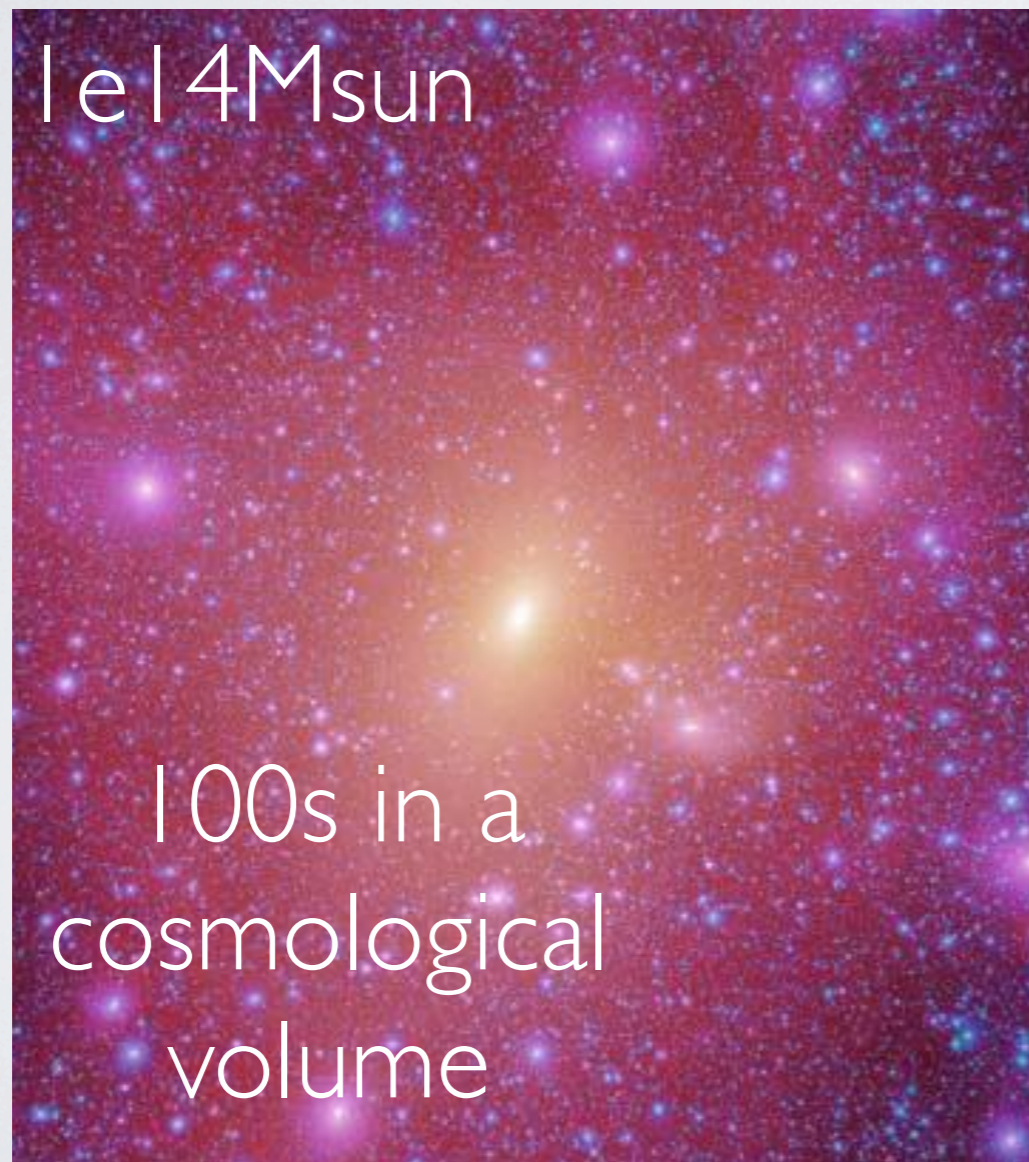


flips produced by infalling material with angular momentum misaligned with that of DM halo.



## 2) ANGULAR MOMENTUM IN SAMs

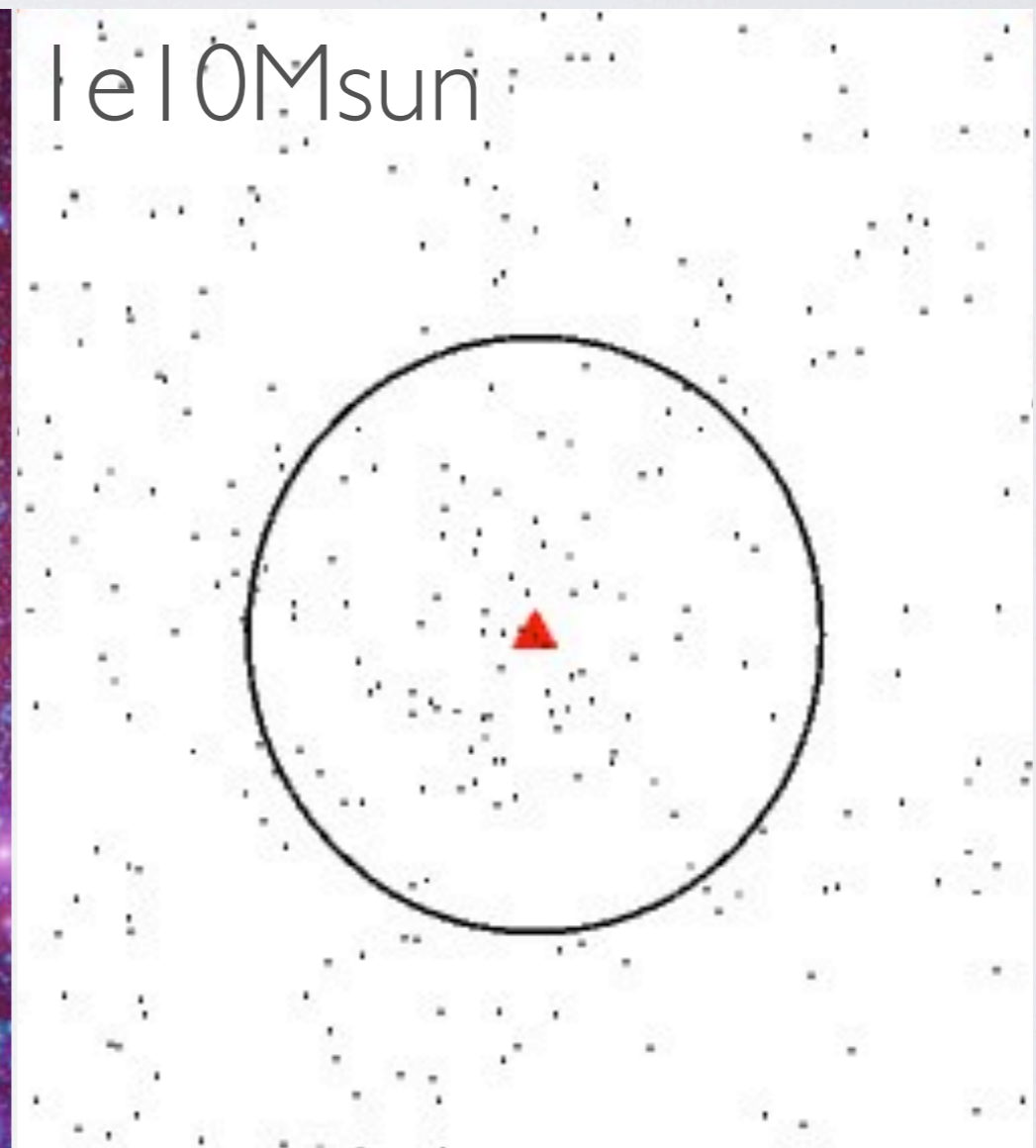
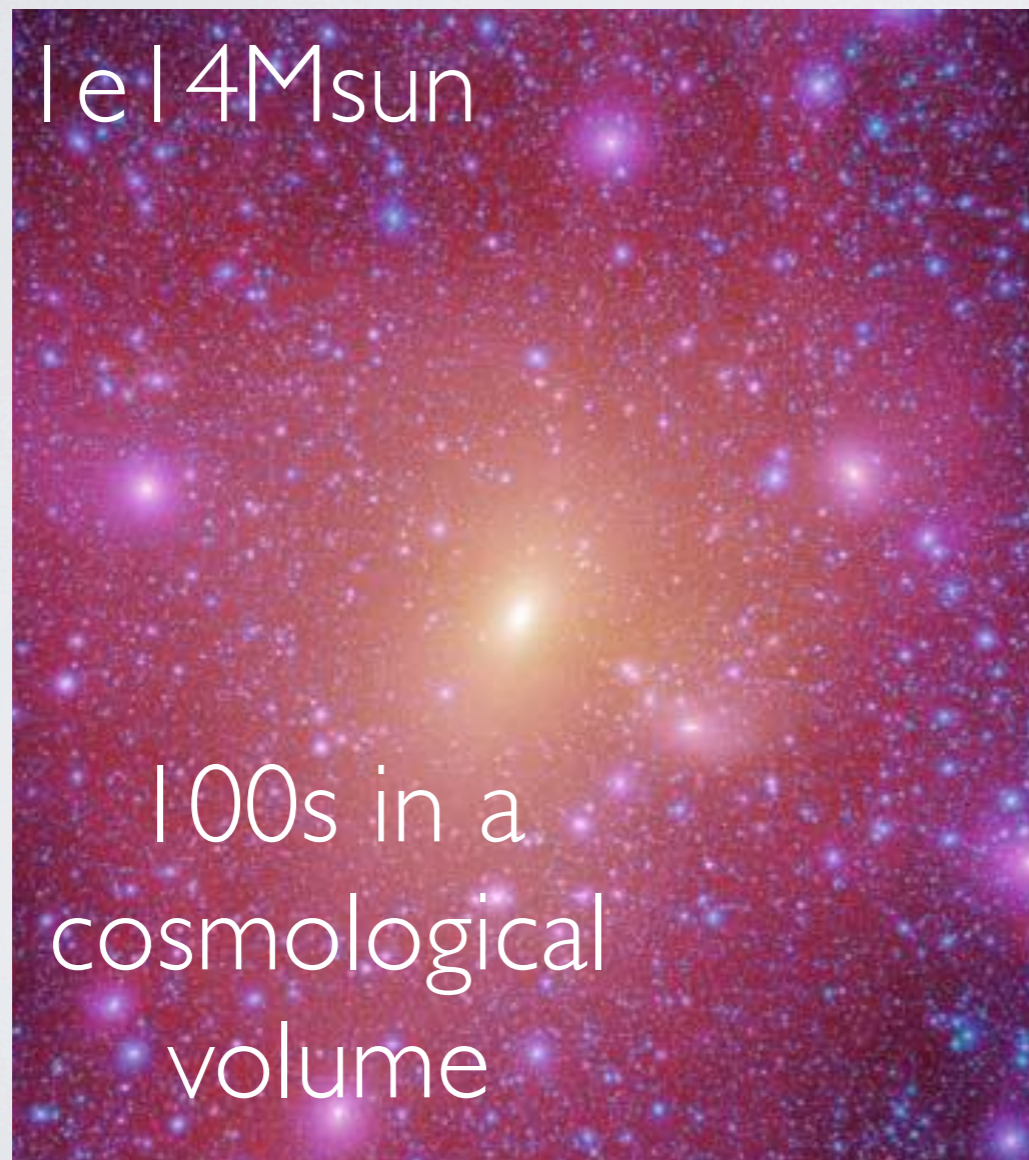
In a SAM there are no particles tracing a disk, they trace DM halos. The angular momentum is easy to measure for well resolved ones.



But halos in SAMs are sometimes resolved with 10 particles

## 2) ANGULAR MOMENTUM IN SAMs

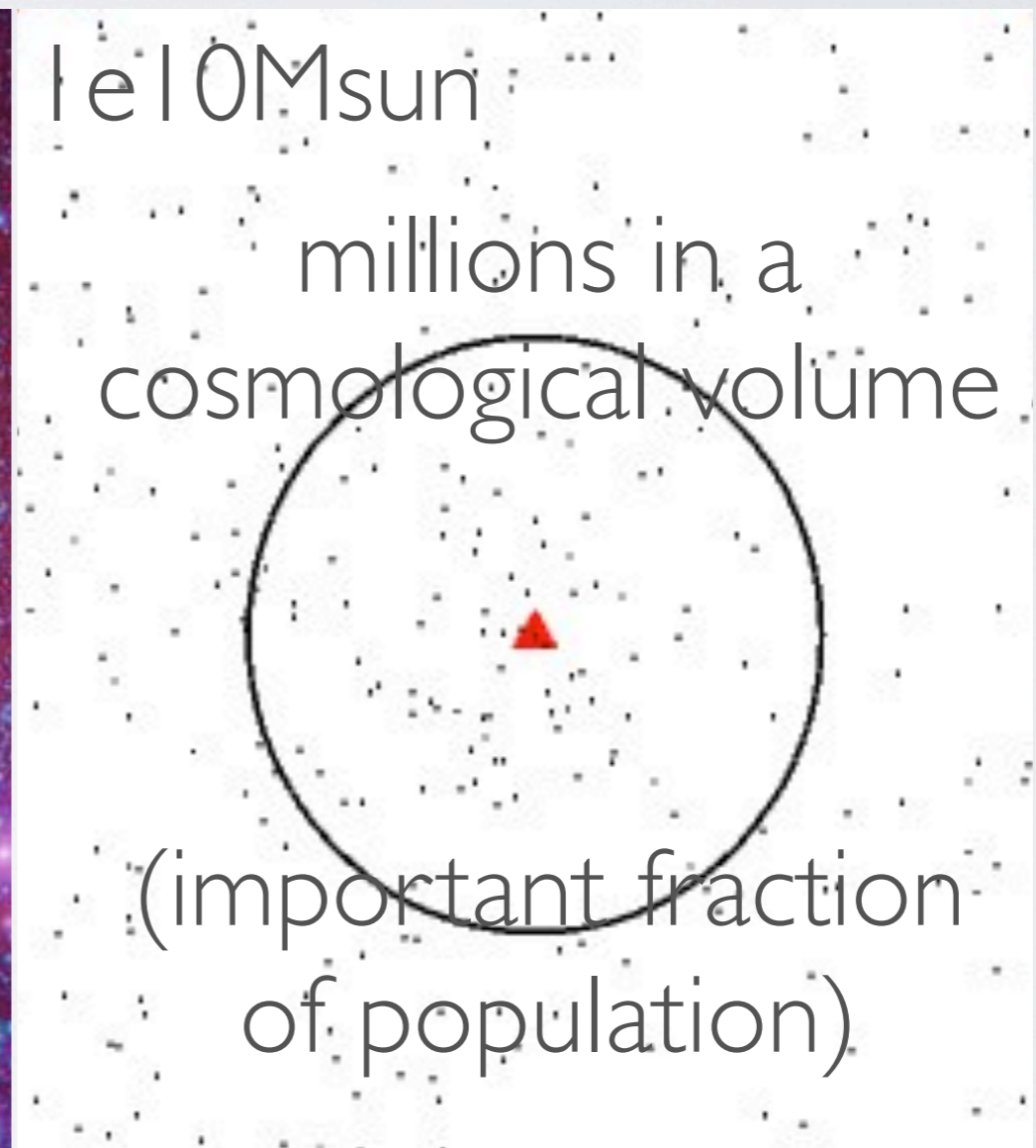
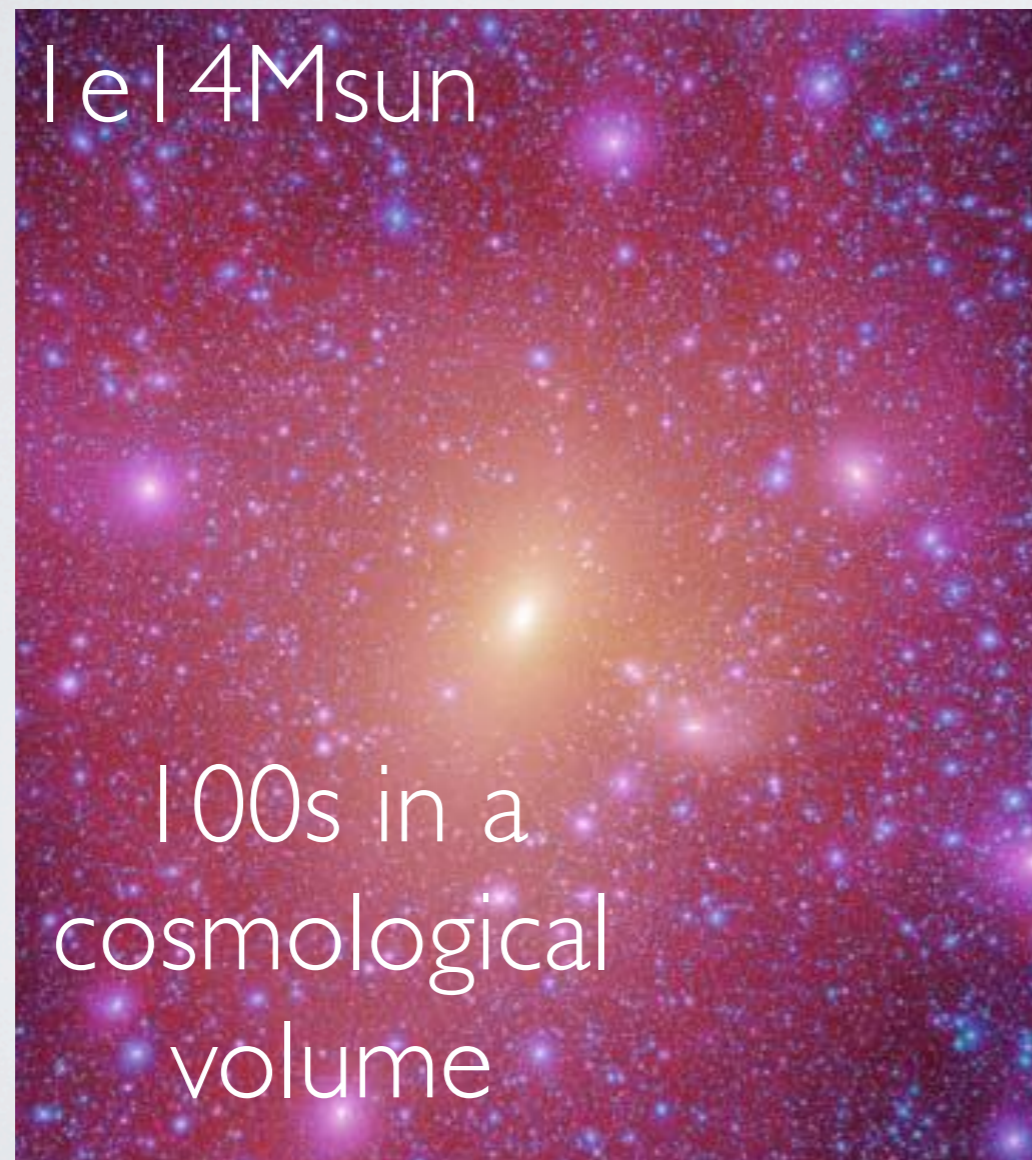
In a SAM there are no particles tracing a disk, they trace DM halos. The angular momentum is easy to measure for well resolved ones.



But halos in SAMs are sometimes resolved with 10 particles

## 2) ANGULAR MOMENTUM IN SAMs

In a SAM there are no particles tracing a disk, they trace DM halos. The angular momentum is easy to measure for well resolved ones.



But halos in SAMs are sometimes resolved with 10 particles

## 2) ANGULAR MOMENTUM IN SAMs

Use high resolution Millennium II simulation:

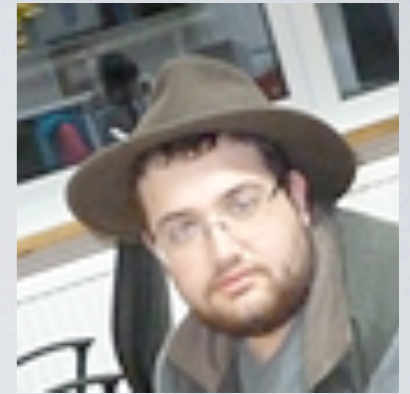
Angular momentum followed numerically

A halo needs to have at least 1000 particles for a reliable measurement of the three components of its angular momentum vector.

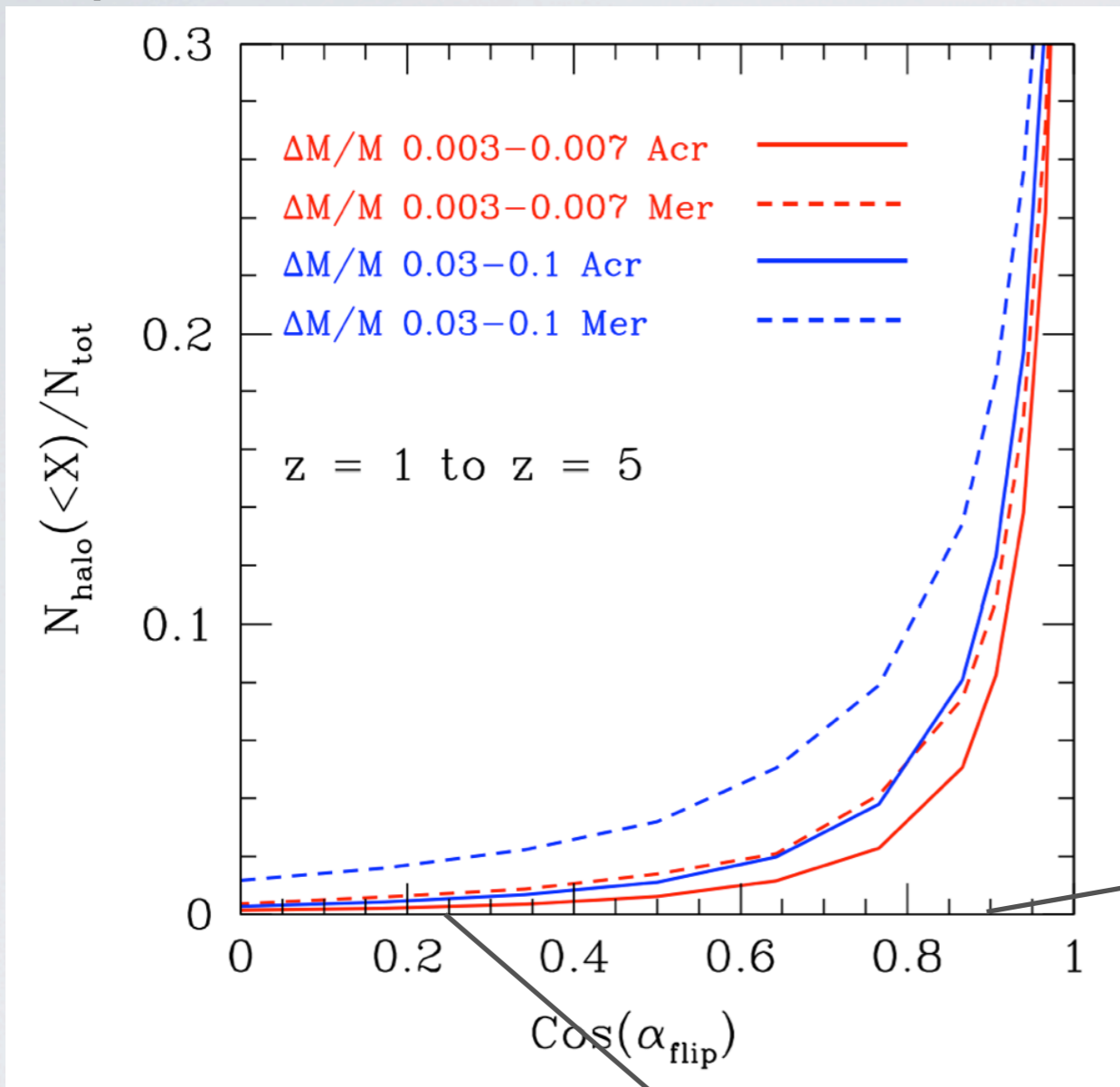
Low resolution (SAMs):

Directions of spins assigned using MC simulations

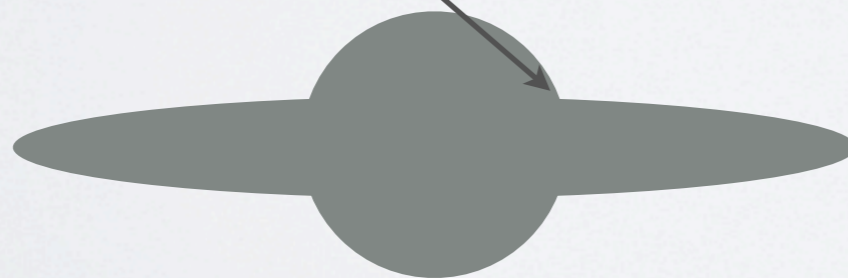
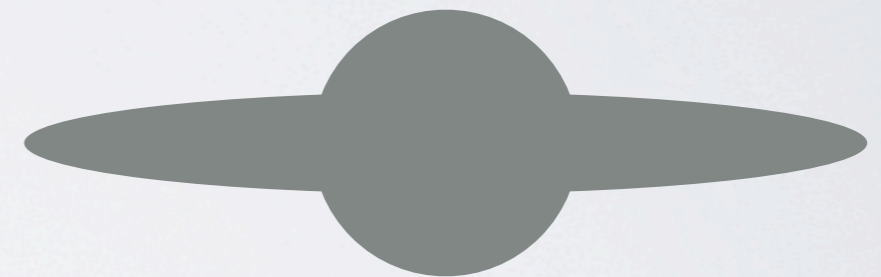
# 2) ANGULAR MOMENTUM IN SAMs



S. Contreras

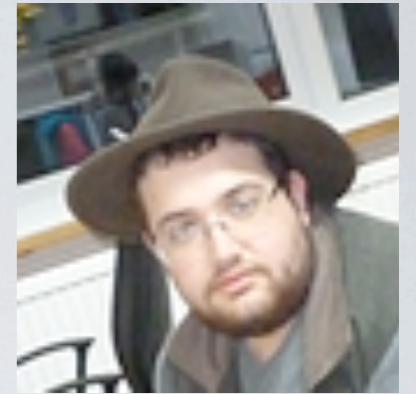


Interpretation for a semi-analytic galaxy:



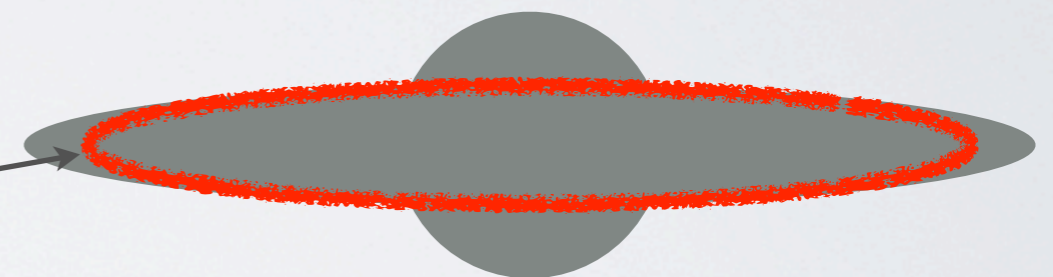
Convert into probability of  $\alpha_{\text{sep}}$  for a given accretion event.

# 2) ANGULAR MOMENTUM IN SAMs



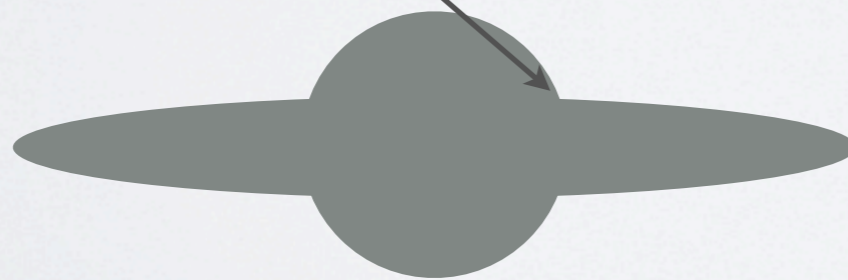
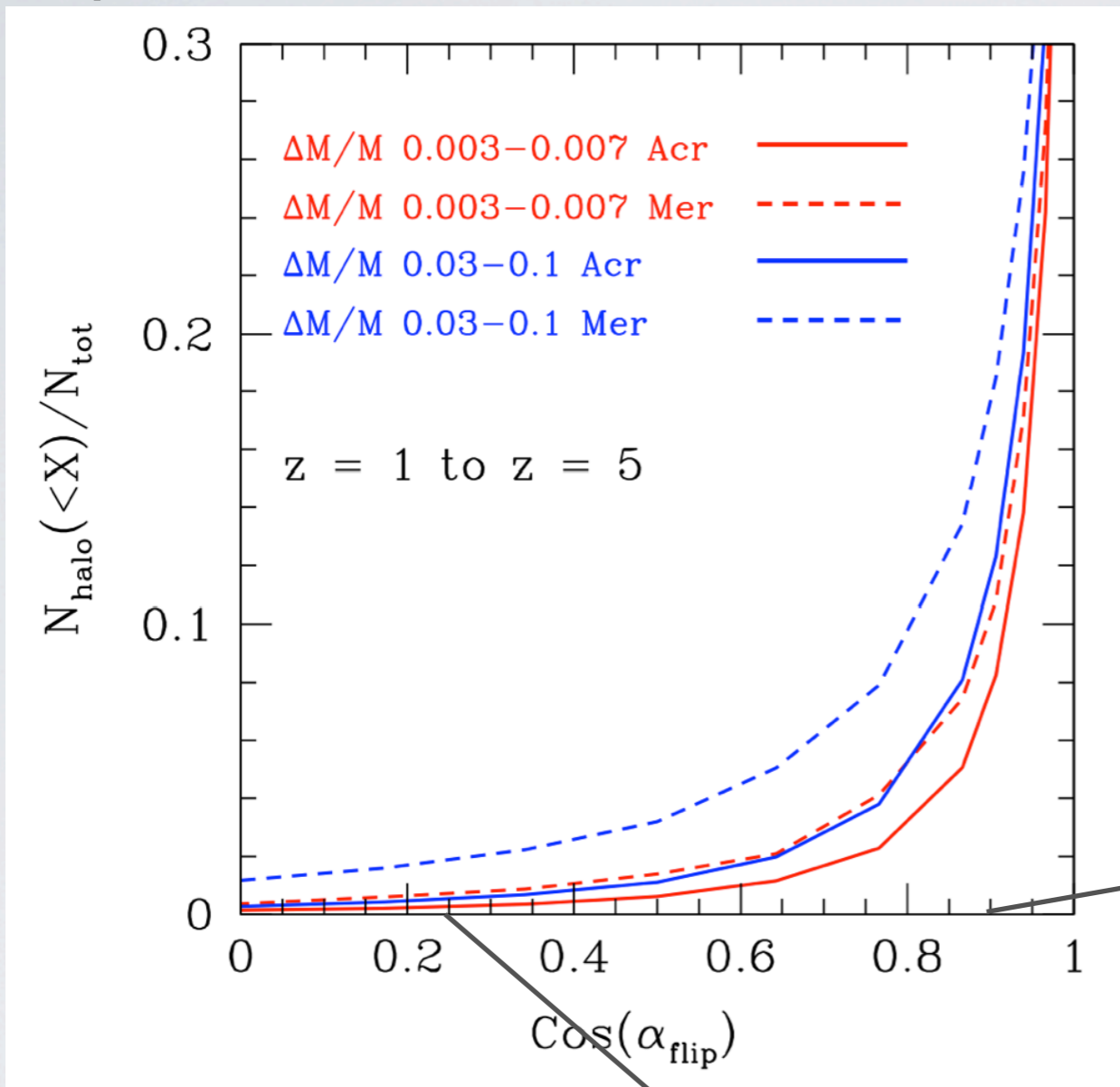
S. Contreras

Interpretation for a semi-analytic galaxy:

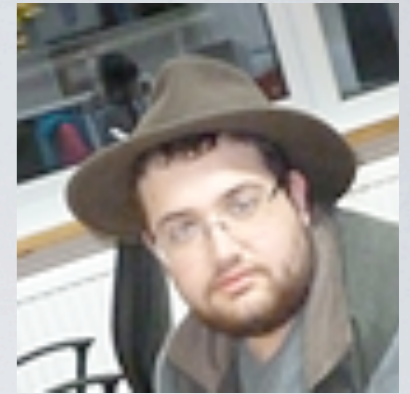


Angular momentum and size increase

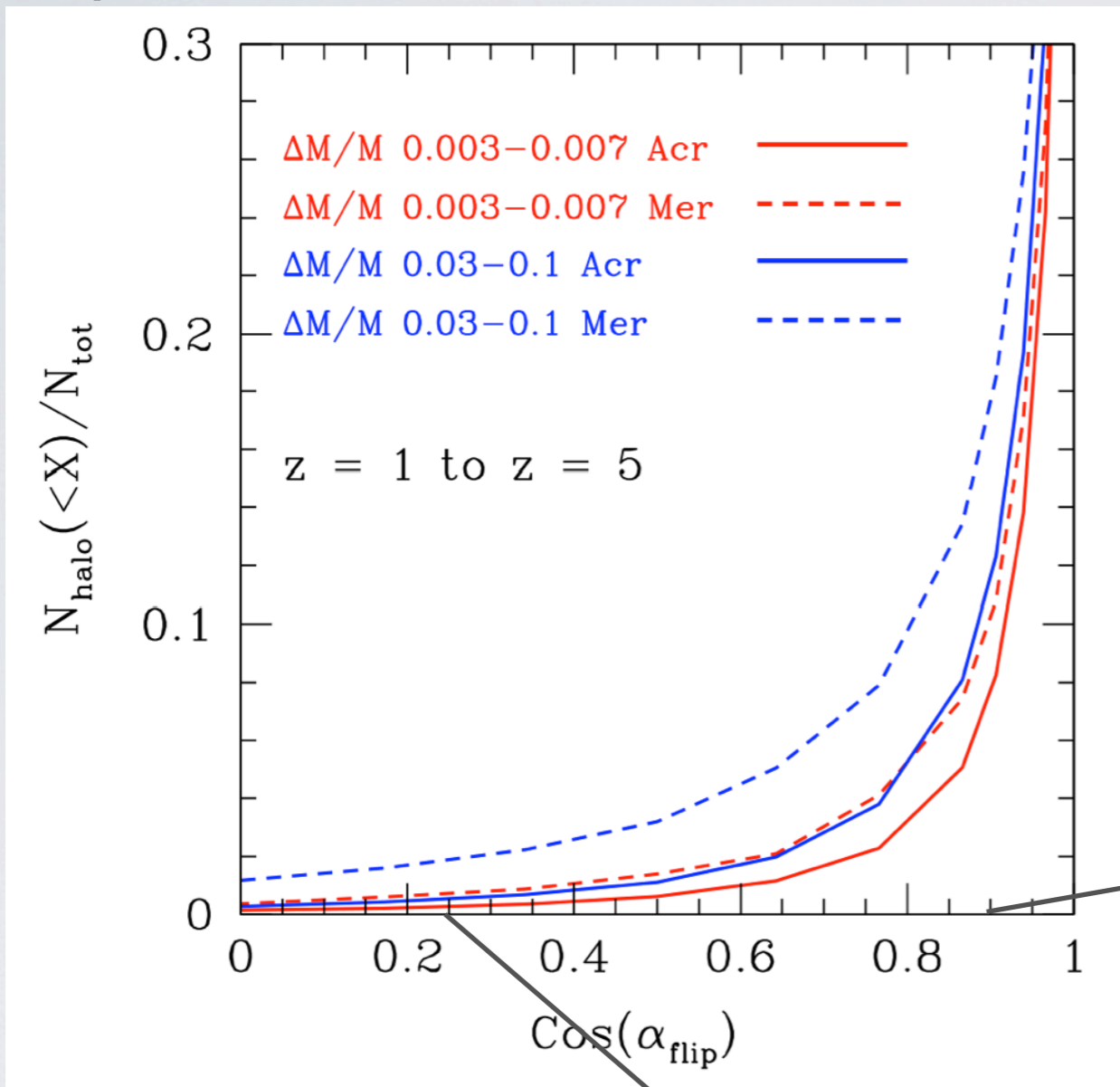
Convert into probability of  $\alpha_{sep}$  for a given accretion event.



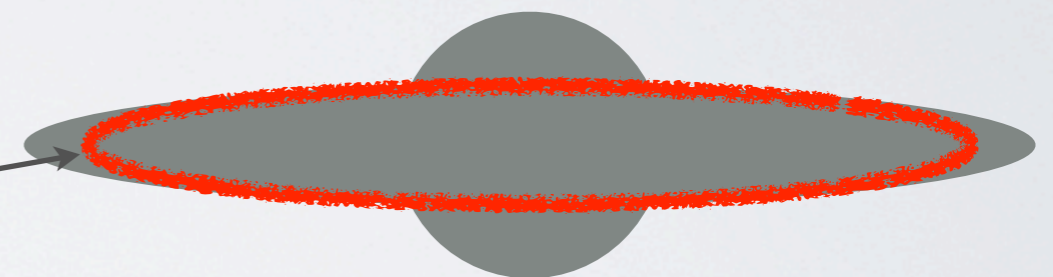
# 2) ANGULAR MOMENTUM IN SAMs



S. Contreras



Interpretation for a semi-analytic galaxy:



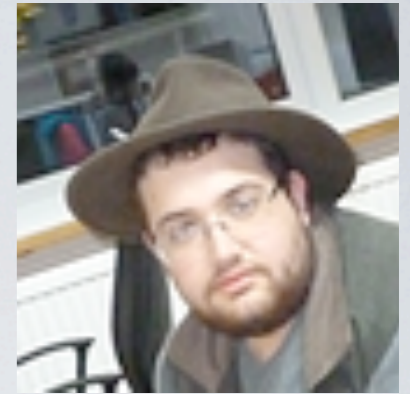
Angular momentum and size increase

Convert into probability of  $\alpha_{\text{sep}}$  for a given accretion event.



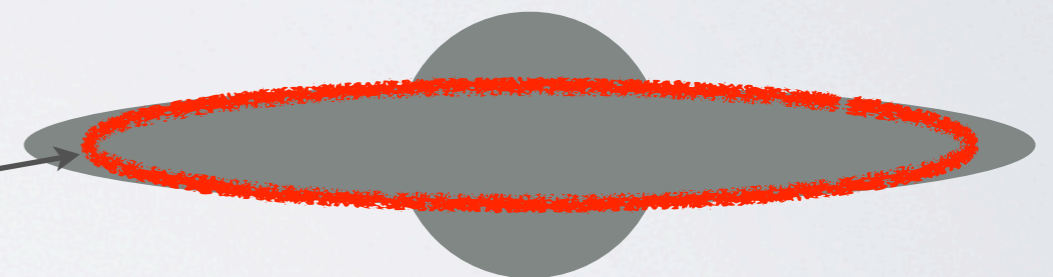
Angular momentum does not increase

# 2) ANGULAR MOMENTUM IN SAMs



S. Contreras

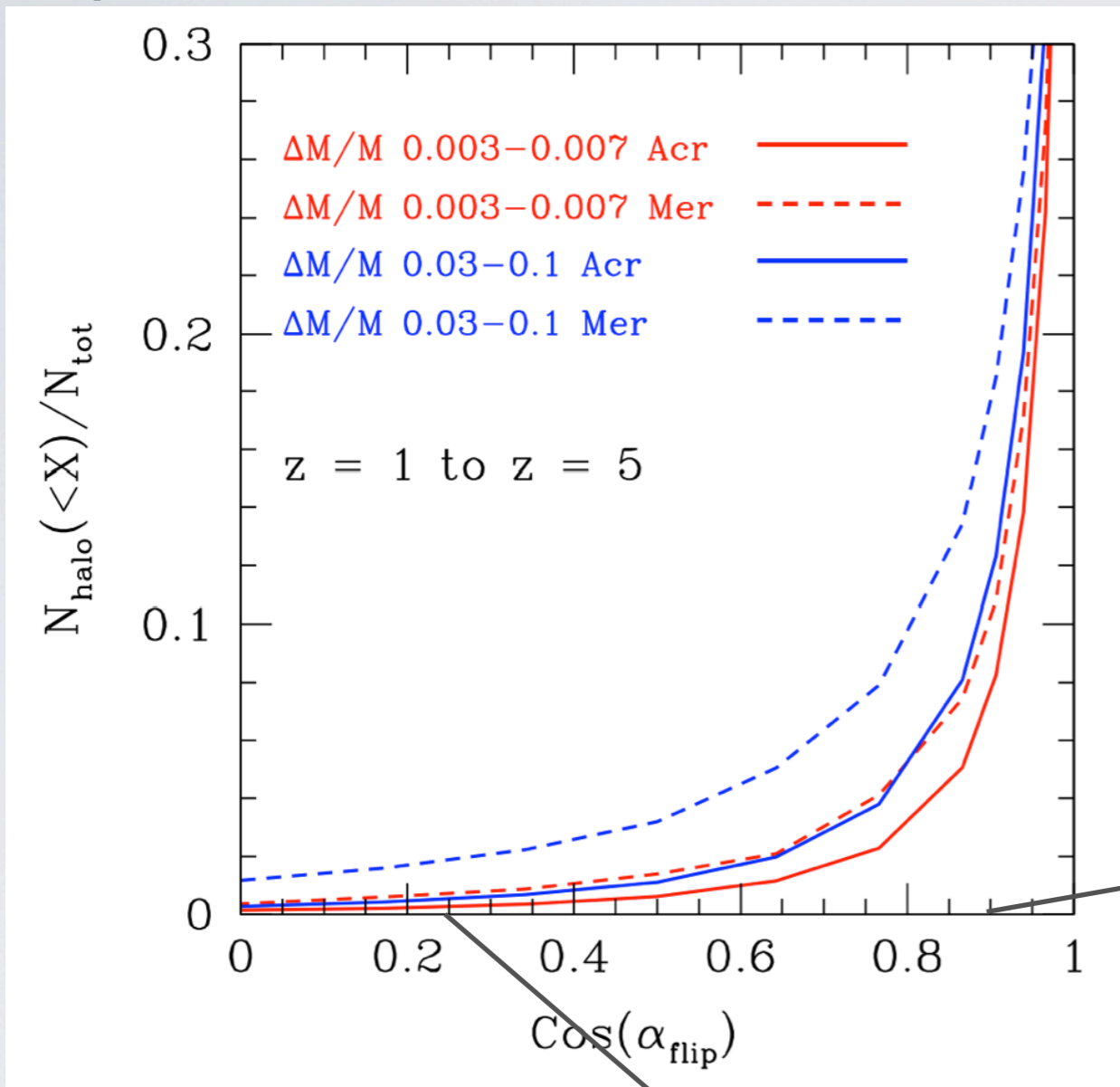
Interpretation for a semi-analytic galaxy:



Angular momentum and size increase

Convert into probability of  $\alpha_{sep}$  for a given accretion event.

$$Rd_{new} = Rd_{init} * \cos(\alpha_{flip})$$

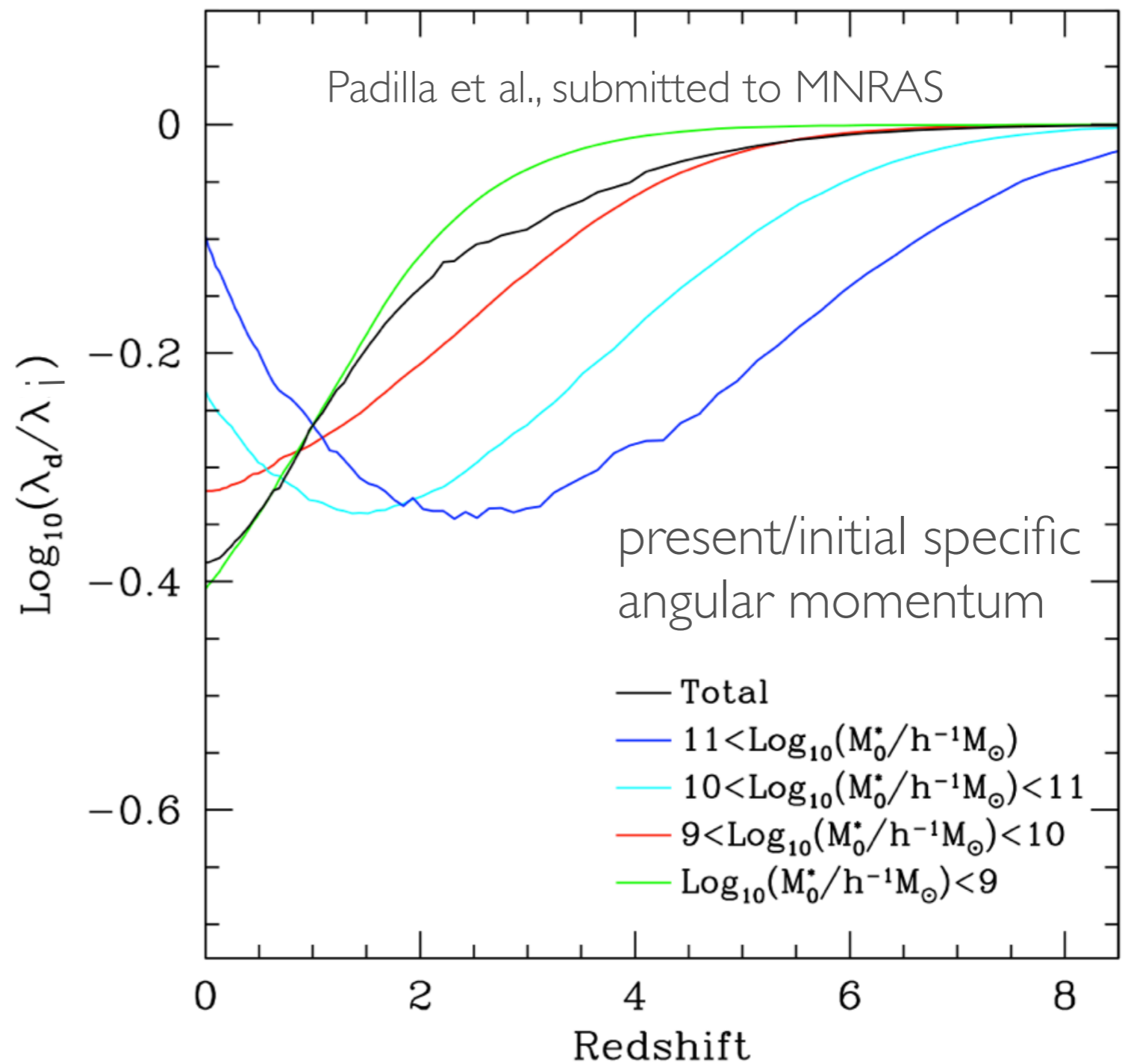


Angular momentum does not increase



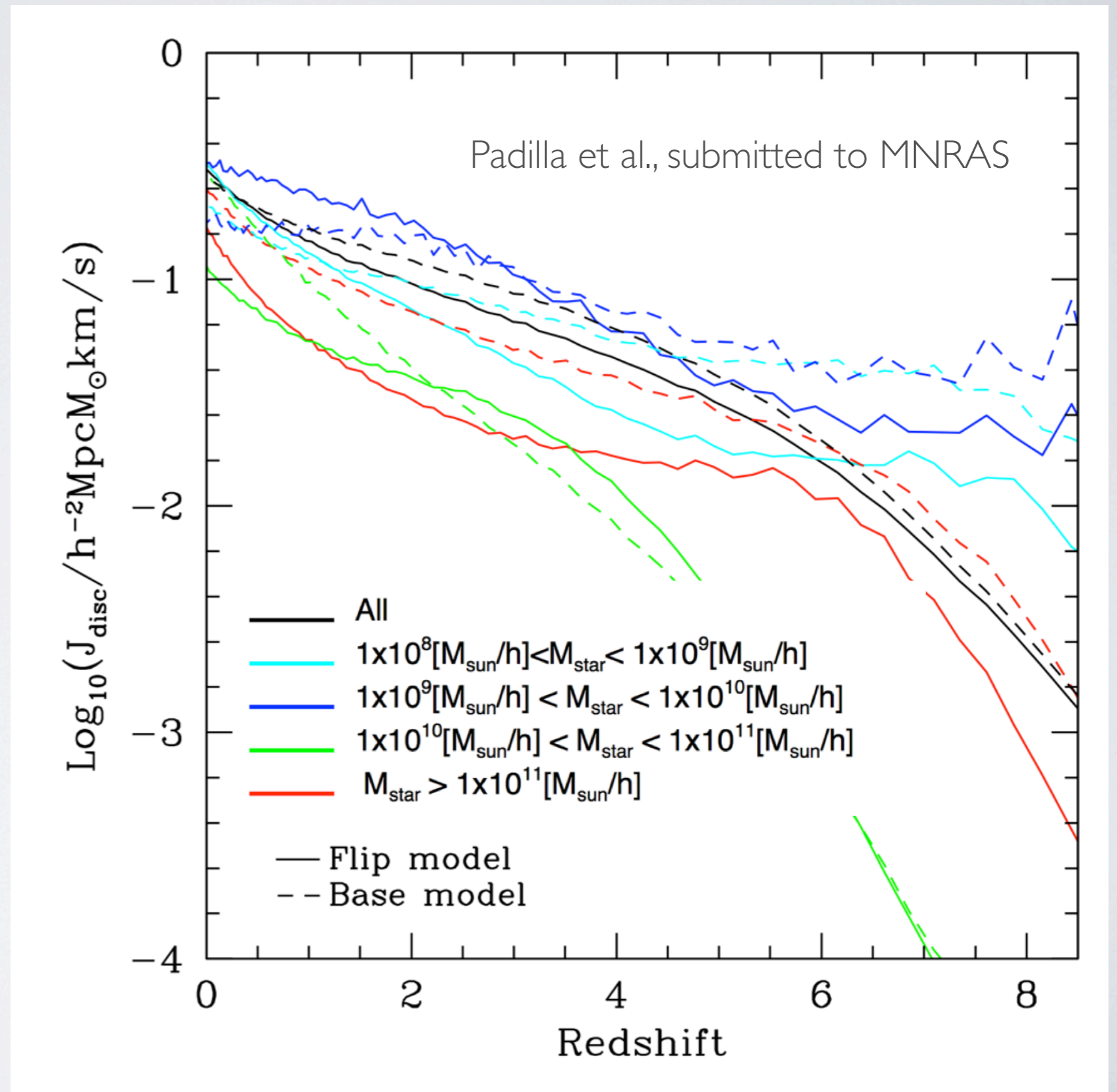
## 2) ANGULAR MOMENTUM IN SAMs

Resulting ratios between present-day and initial specific angular momentum of disc



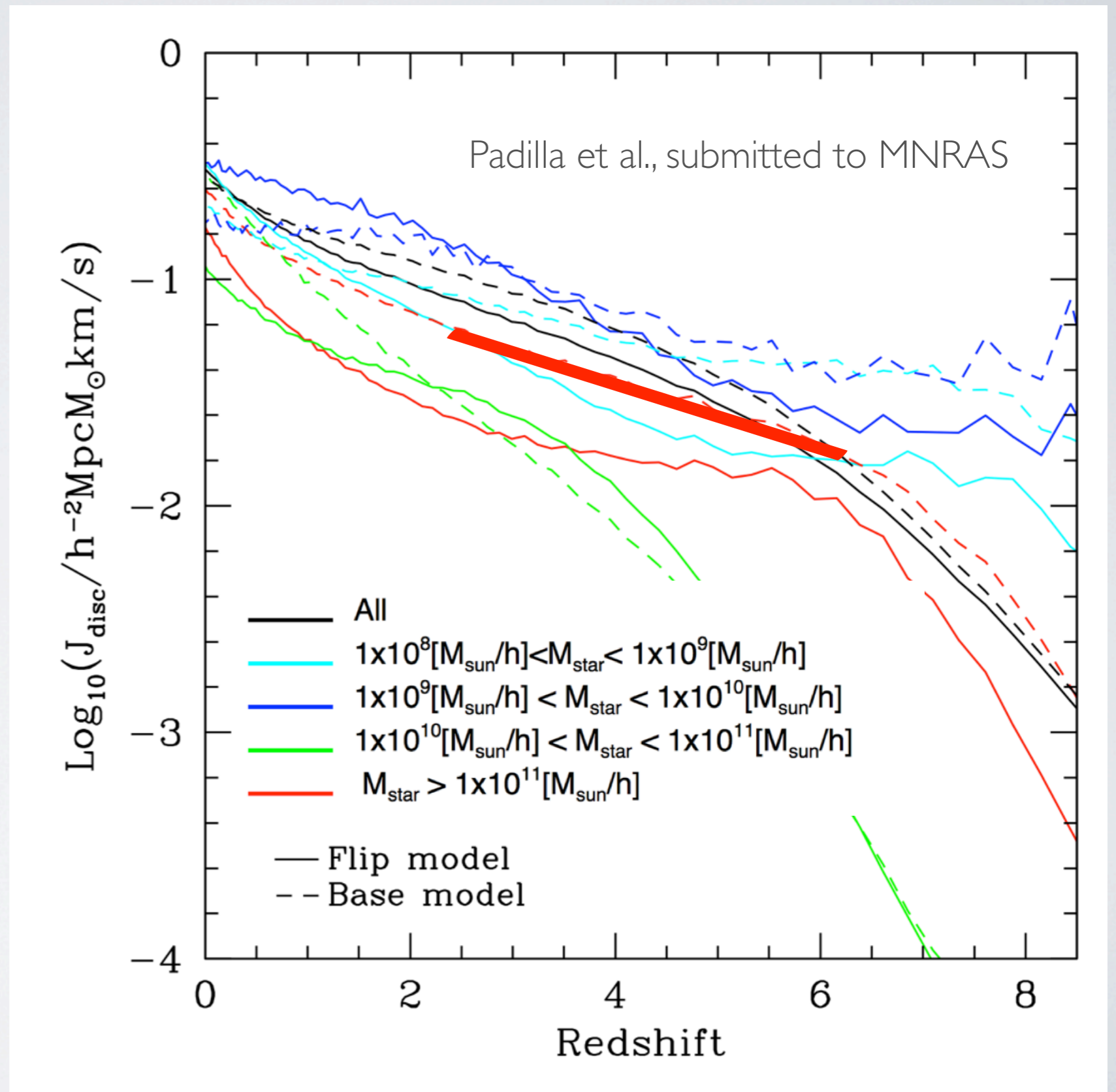
## 2) ANGULAR MOMENTUM IN SAMs

Resulting  
slower increase  
of disc  
angular  
momentum



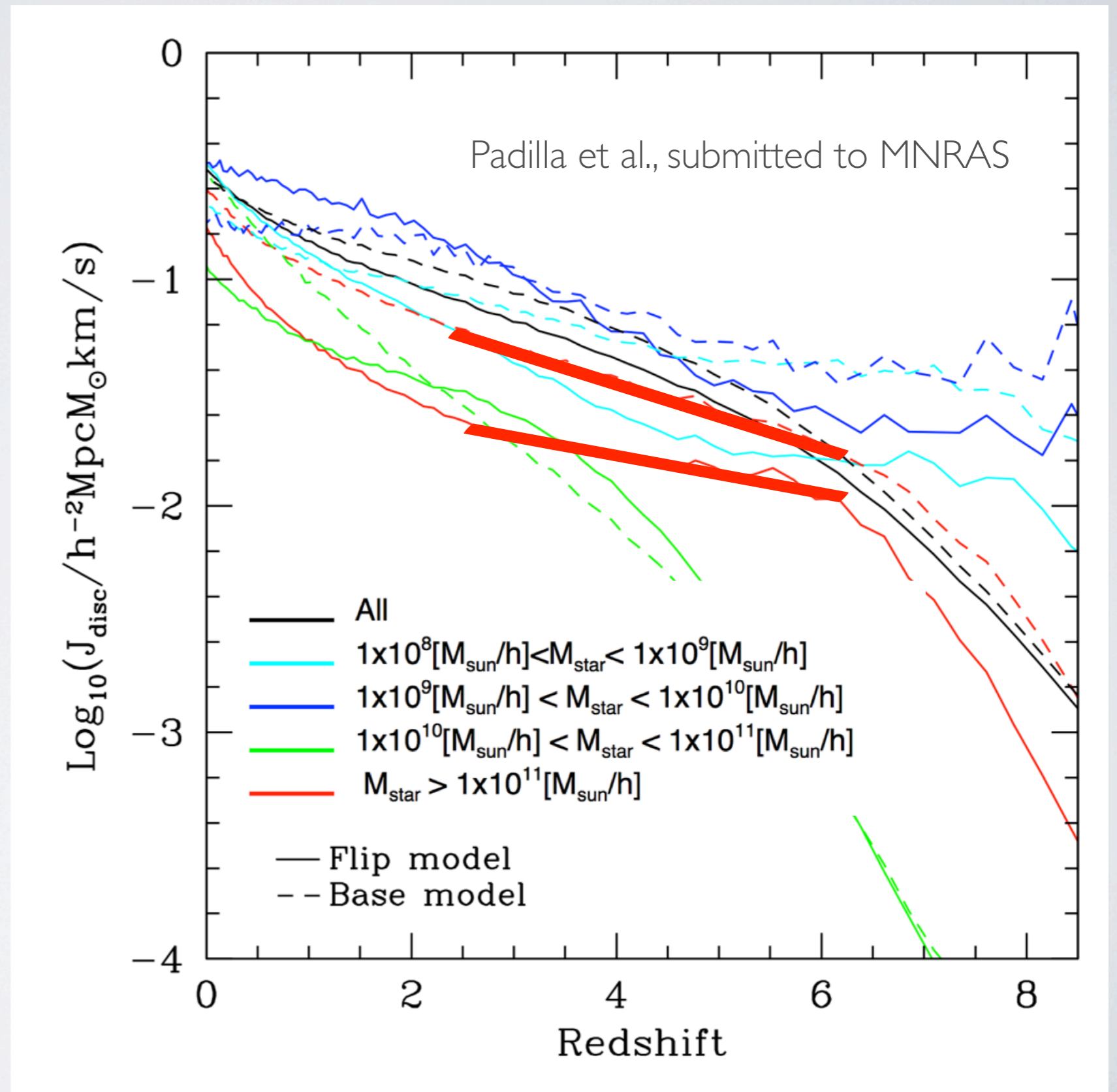
## 2) ANGULAR MOMENTUM IN SAMs

Resulting  
slower increase  
of disc  
angular  
momentum



## 2) ANGULAR MOMENTUM IN SAMs

Resulting  
slower increase  
of disc  
angular  
momentum



## 2) EFFECT ON SF

Using the SF law from Croton et al. (2006) which considers a threshold surface density of gas to form stars.

$$R_d = \frac{1}{\sqrt{2}} \left( \frac{j_d}{m_d} \right) \lambda r_{\text{vir}} f_c^{-1/2} f_R(\lambda, c, m_d, j_d).$$

MMW

$$f_c \simeq \frac{2}{3} + \left( \frac{c}{21.5} \right)^{0.7}, \quad f_R(\lambda, c, m_d, j_d) = 2 \left[ \int_0^\infty e^{-u} u^2 \frac{V_c(R_d u)}{V_{\text{vir}}} du \right]^{-1}$$

Star formation on dense enough discs (Croton+06):

$$m_{\text{crit}} = 3.8 \times 10^9 \left( \frac{V_{\text{vir}}}{200 \text{ km s}^{-1}} \right) \left( \frac{r_{\text{disc}}}{10 \text{ kpc}} \right) M_\odot$$

$$\dot{m}_* = \alpha_{\text{SF}} (m_{\text{cold}} - m_{\text{crit}}) / t_{\text{dyn, disc}}$$

$$t_{\text{dyn}} = r_{\text{disc}} / V_{\text{vir}}$$

## 2) EFFECT ON SF

Using the SF law from Croton et al. (2006) which considers a threshold surface density of gas to form stars.

$$R_d = \frac{1}{\sqrt{2}} \left( \frac{j_d}{m_d} \right) \lambda r_{\text{vir}} f_c^{-1/2} f_R(\lambda, c, m_d, j_d).$$

MMW

$$f_c \simeq \frac{2}{3} + \left( \frac{c}{21.5} \right)^{0.7}, \quad f_R(\lambda, c, m_d, j_d) = 2 \left[ \int_0^\infty e^{-u} u^2 \frac{V_c(R_d u)}{V_{\text{vir}}} du \right]^{-1}$$

Star formation on dense enough discs (Croton+06):

$$m_{\text{crit}} = 3.8 \times 10^9 \left( \frac{V_{\text{vir}}}{200 \text{ km s}^{-1}} \right) \left( \frac{r_{\text{disc}}}{10 \text{ kpc}} \right) M_\odot$$

$$\dot{m}_* = \alpha_{\text{SF}} (m_{\text{cold}} - m_{\text{crit}}) / t_{\text{dyn, disc}}$$

$$t_{\text{dyn}} = r_{\text{disc}} / V_{\text{vir}}$$

Smaller disc size  $\Rightarrow$  higher star formation rates

## 2) EFFECT ON SF

Disk instabilities:

$$\epsilon = \frac{V_{\max}}{(GM_{\text{disc}}/r_{\text{disc}})^{1/2}},$$

if lower than critical value  
disc is unstable

Smaller radius makes  
more frequent instabilities

After a disk instability driven starburst, disc forms again with initial halo angular momentum.

## 2) EFFECT ON SF

Disk instabilities:

$$\epsilon = \frac{V_{\max}}{(GM_{\text{disc}}/r_{\text{disc}})^{1/2}},$$

if lower than critical value  
disc is unstable

Flip from merger lowers  
 $r_{\text{disc}}$  and triggers instabilities

After a merger driven starburst, disc forms again with initial halo angular momentum.



## 2) EFFECT ON SF

Disk instabilities:

Disc instability  
as the only driver  
of bursts in the  
model.

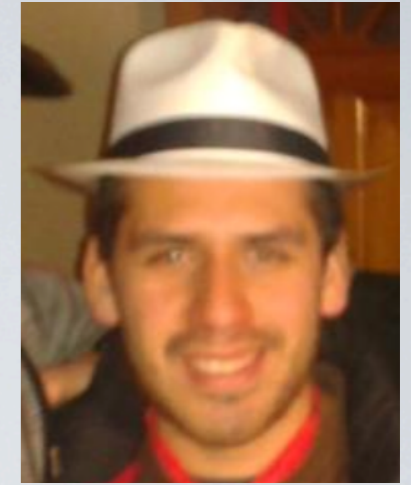
$$\epsilon = \frac{V_{\max}}{(GM_{\text{disc}}/r_{\text{disc}})^{1/2}},$$

if lower than critical value  
disc is unstable

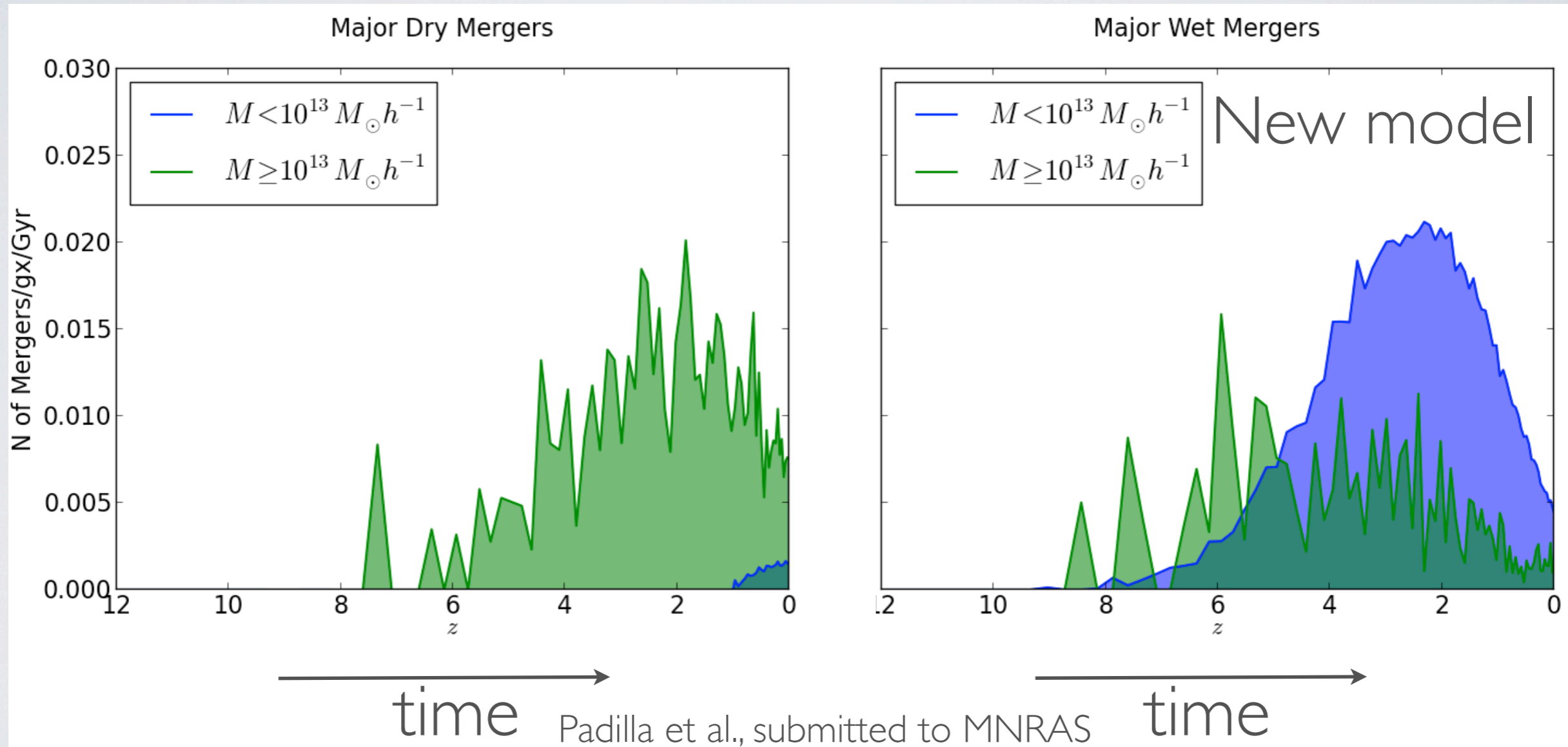
**Flip from merger** lowers  
 $r_{\text{disc}}$  and triggers instabilities

After a merger driven starburst, disc forms again with initial halo angular momentum.

# 2) EFFECT ON MERGERS



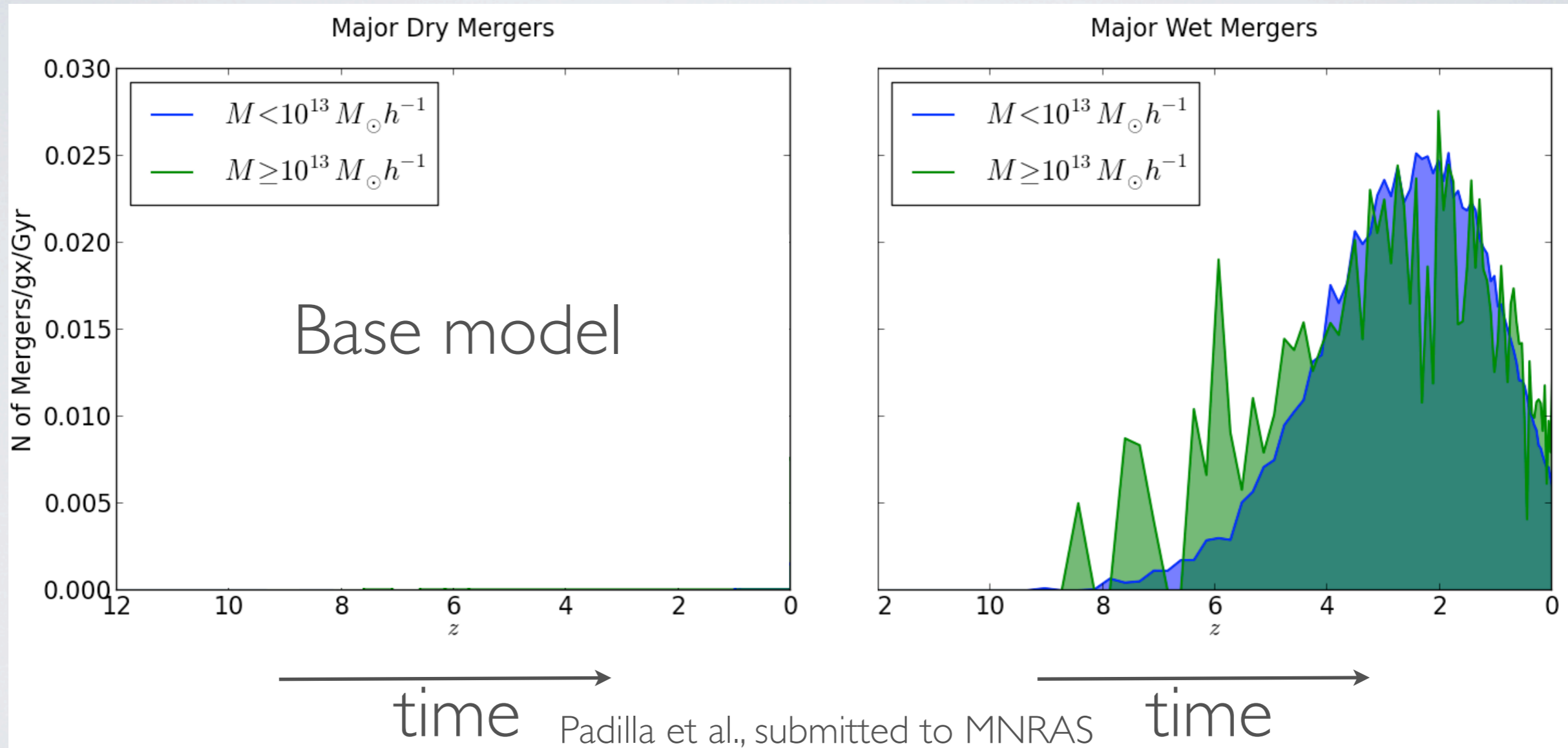
S. Salazar



# 2) EFFECT ON MERGERS

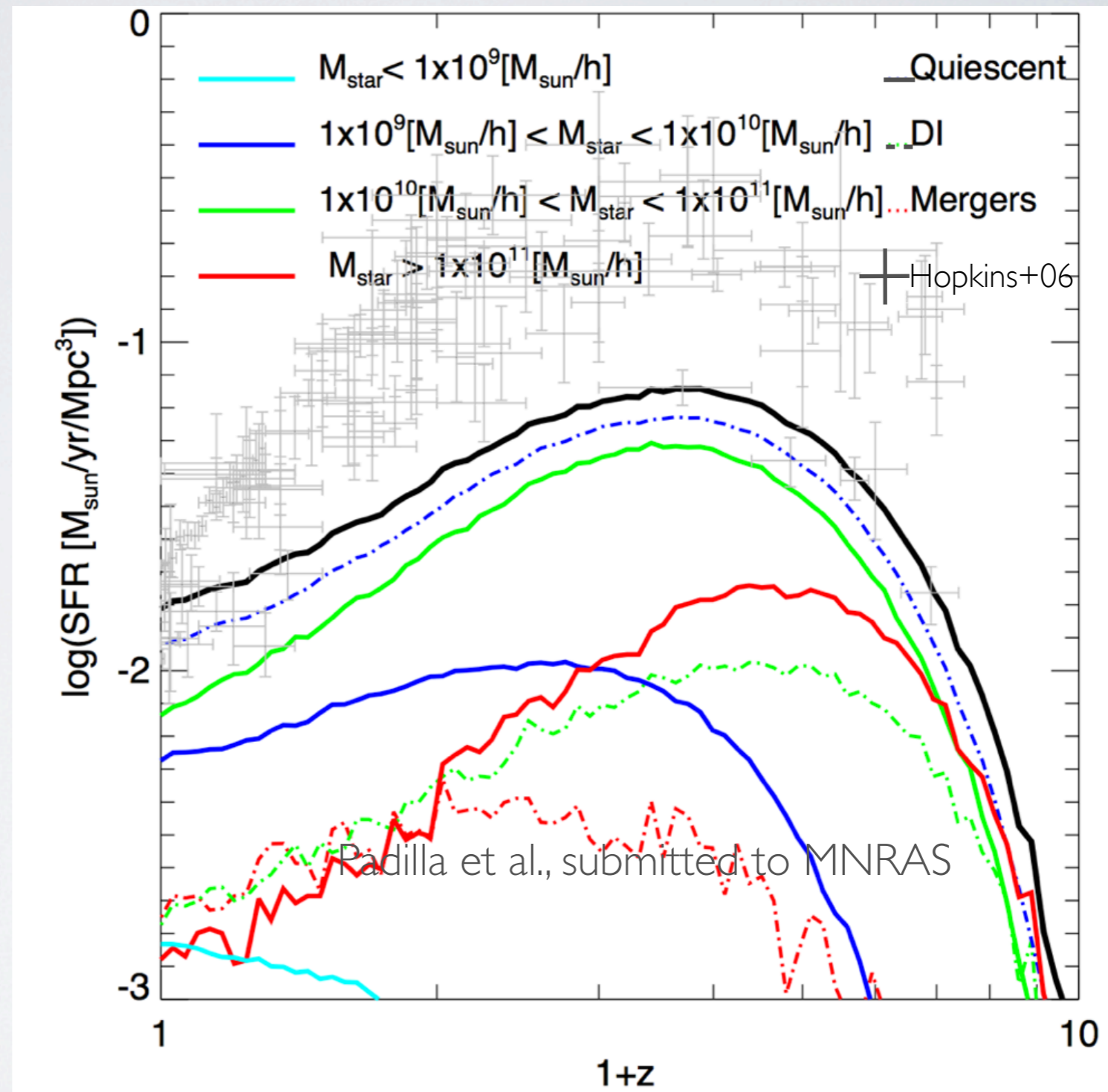


S. Salazar



## 2) EFFECT ON SF

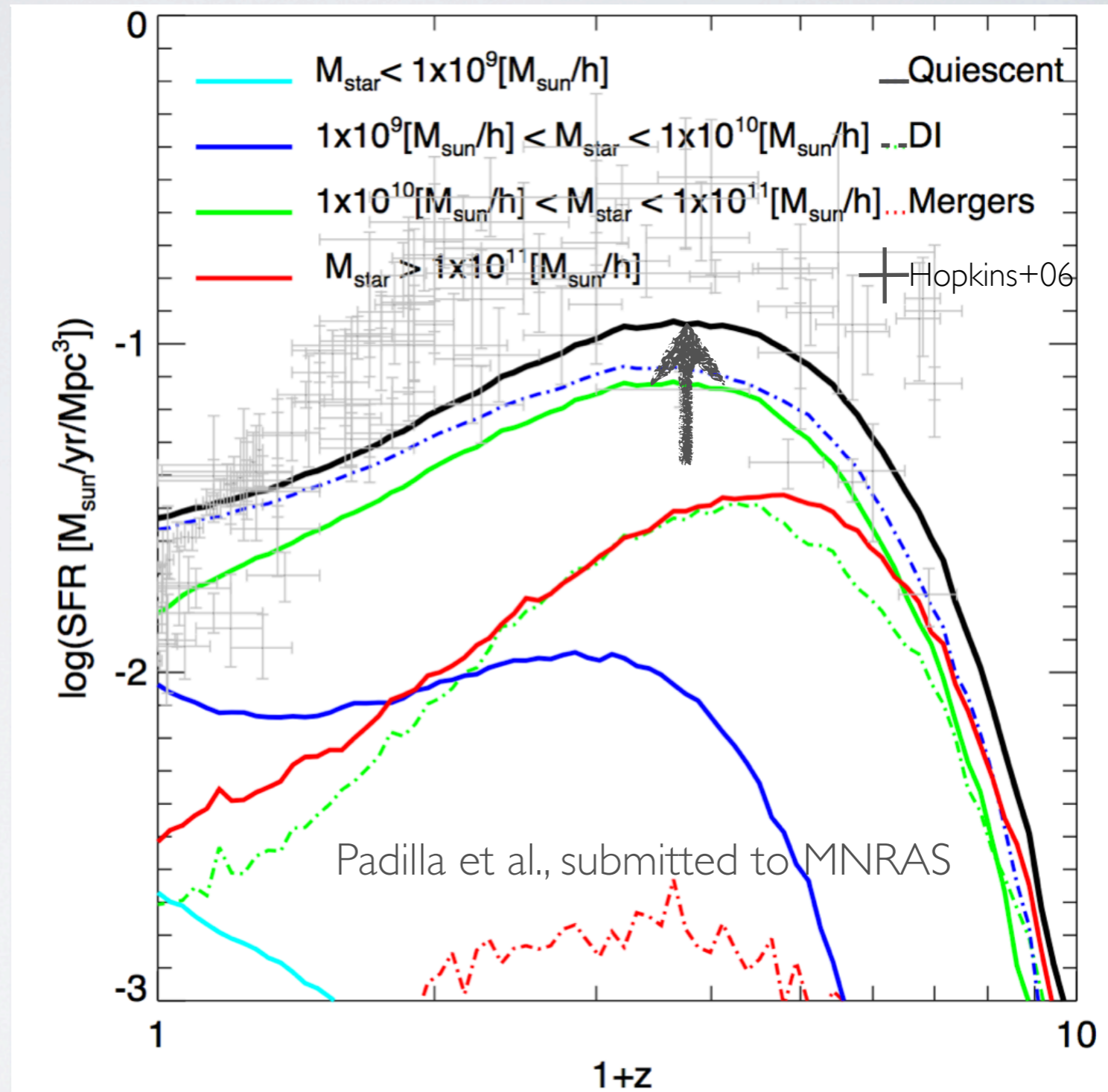
Smooth  
growth  
in disc size



## 2) EFFECT ON SF

With episodic  
discs

$R_{\text{disk}}$  is smaller,  
 $T_{\text{dyn}}$  is smaller,  
SFR is higher,  
comparatively

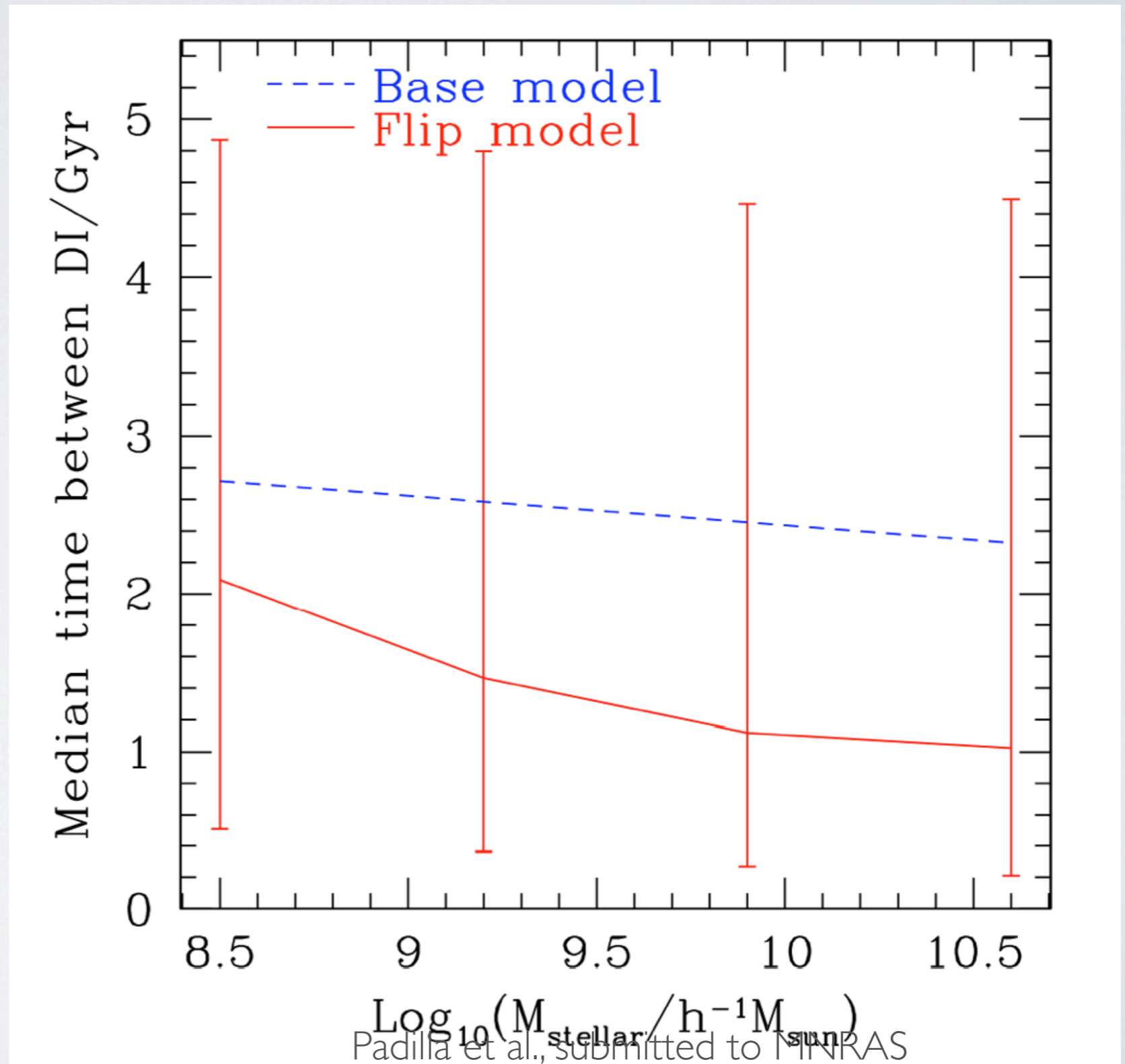


## 2) EFFECT ON SF

Disc life-times

Base Model

With episodic  
discs

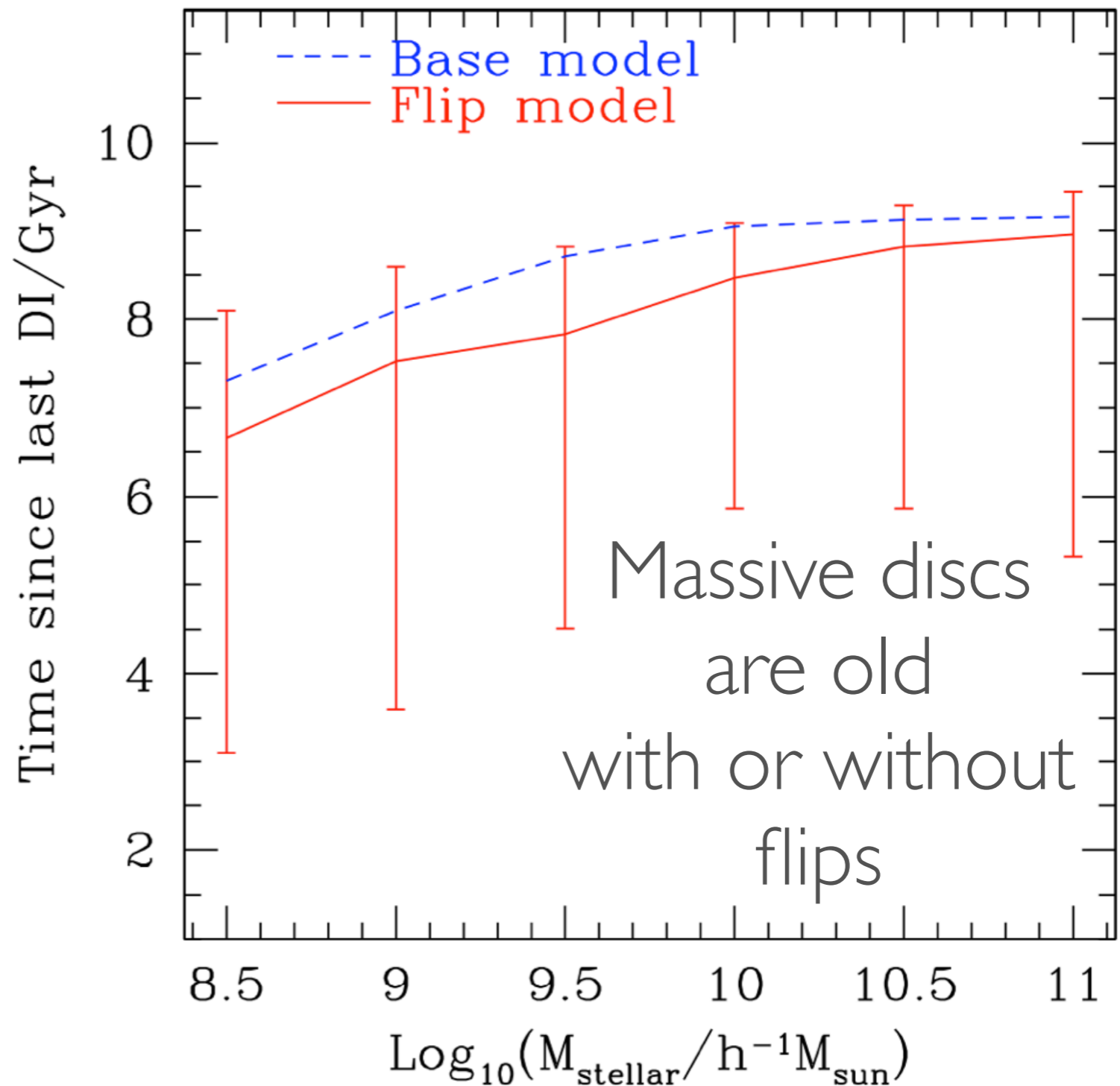


## 2) EFFECT ON SF

Disc life-times

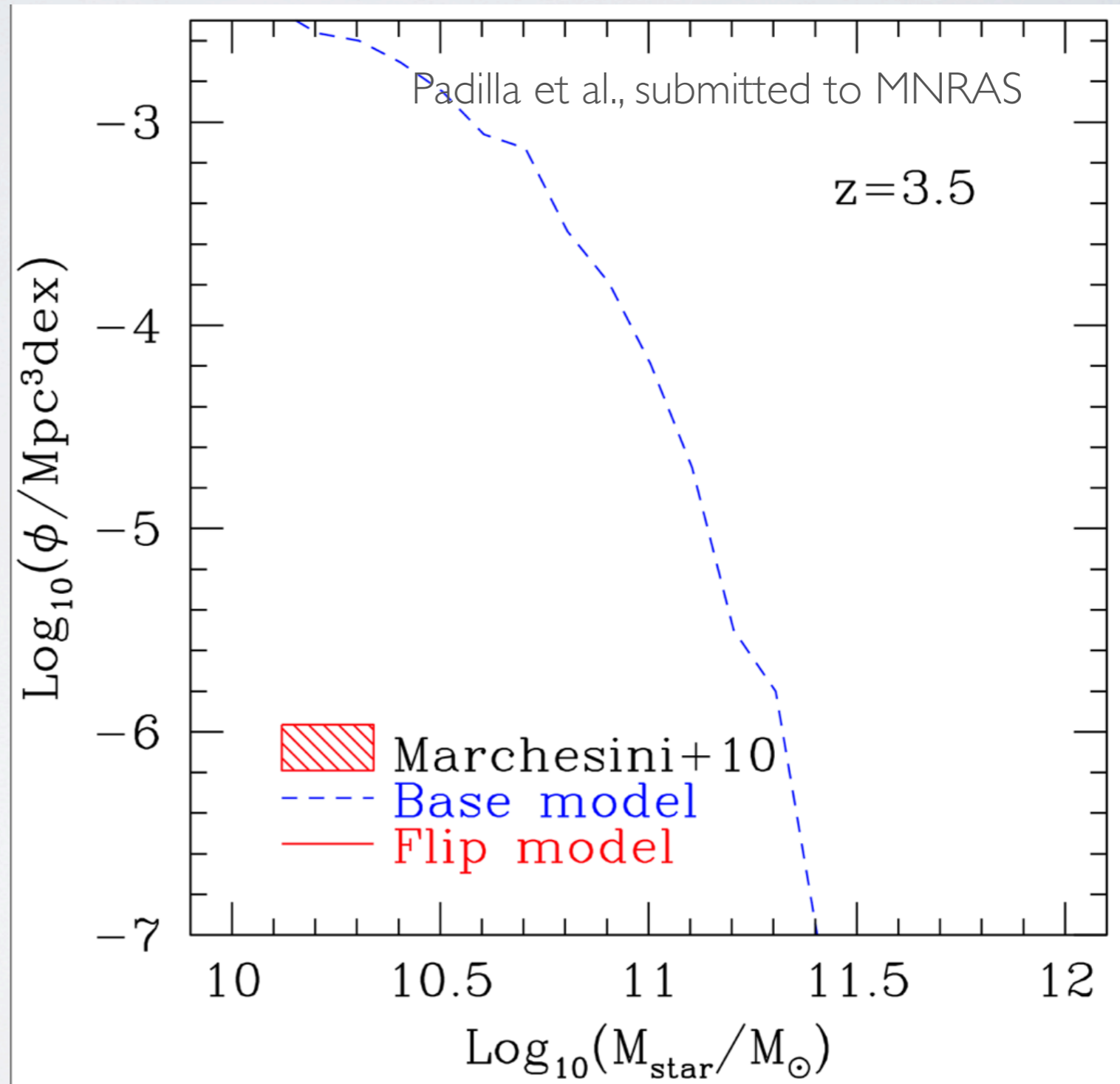
Base Model

With episodic  
discs



# 3) RESULTS: HIGH-Z MASSES

The stellar mass function at  $z=3.5$

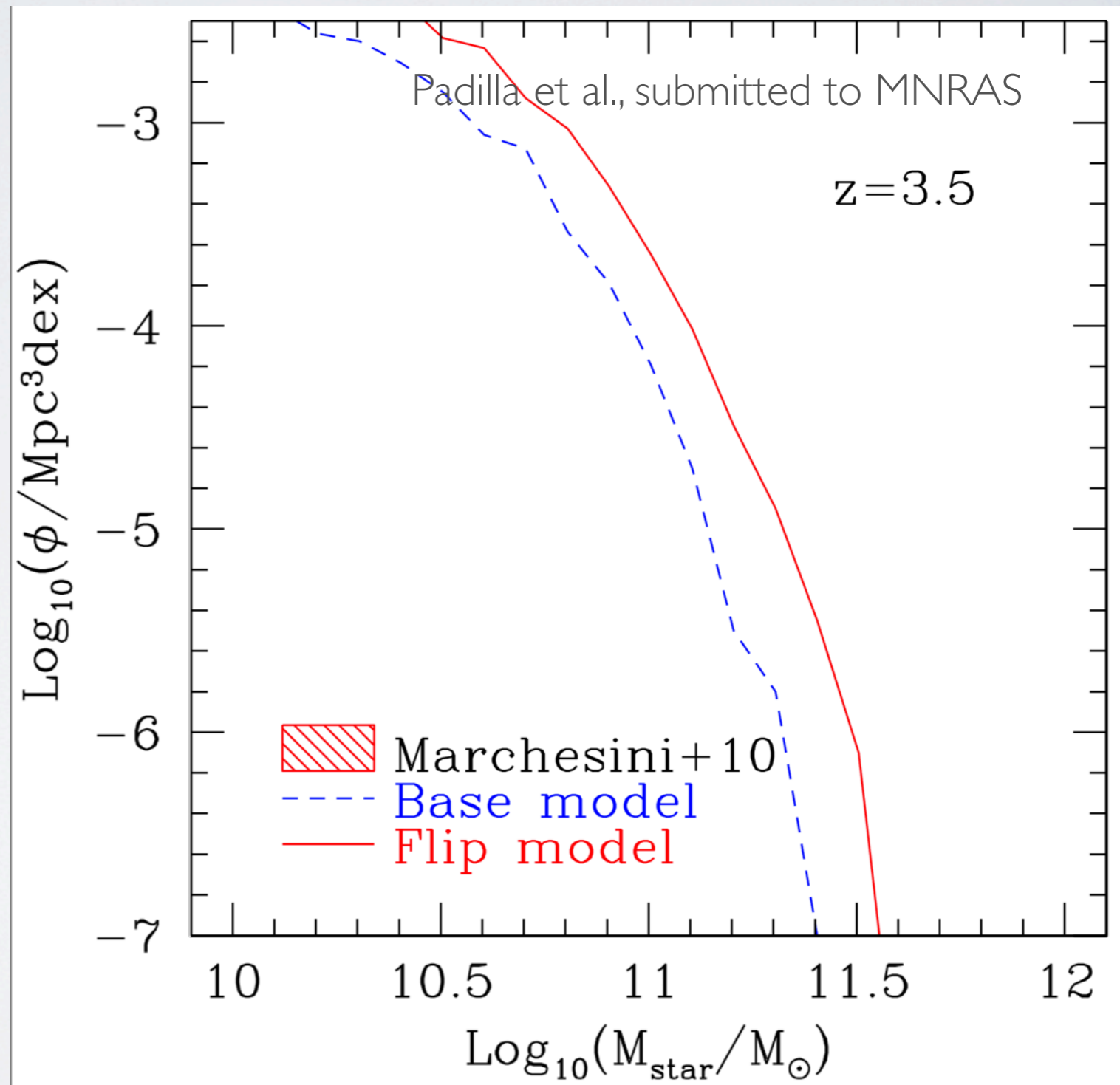




# 3) RESULTS: HIGH-Z MASSES

The stellar mass function at  $z=3.5$

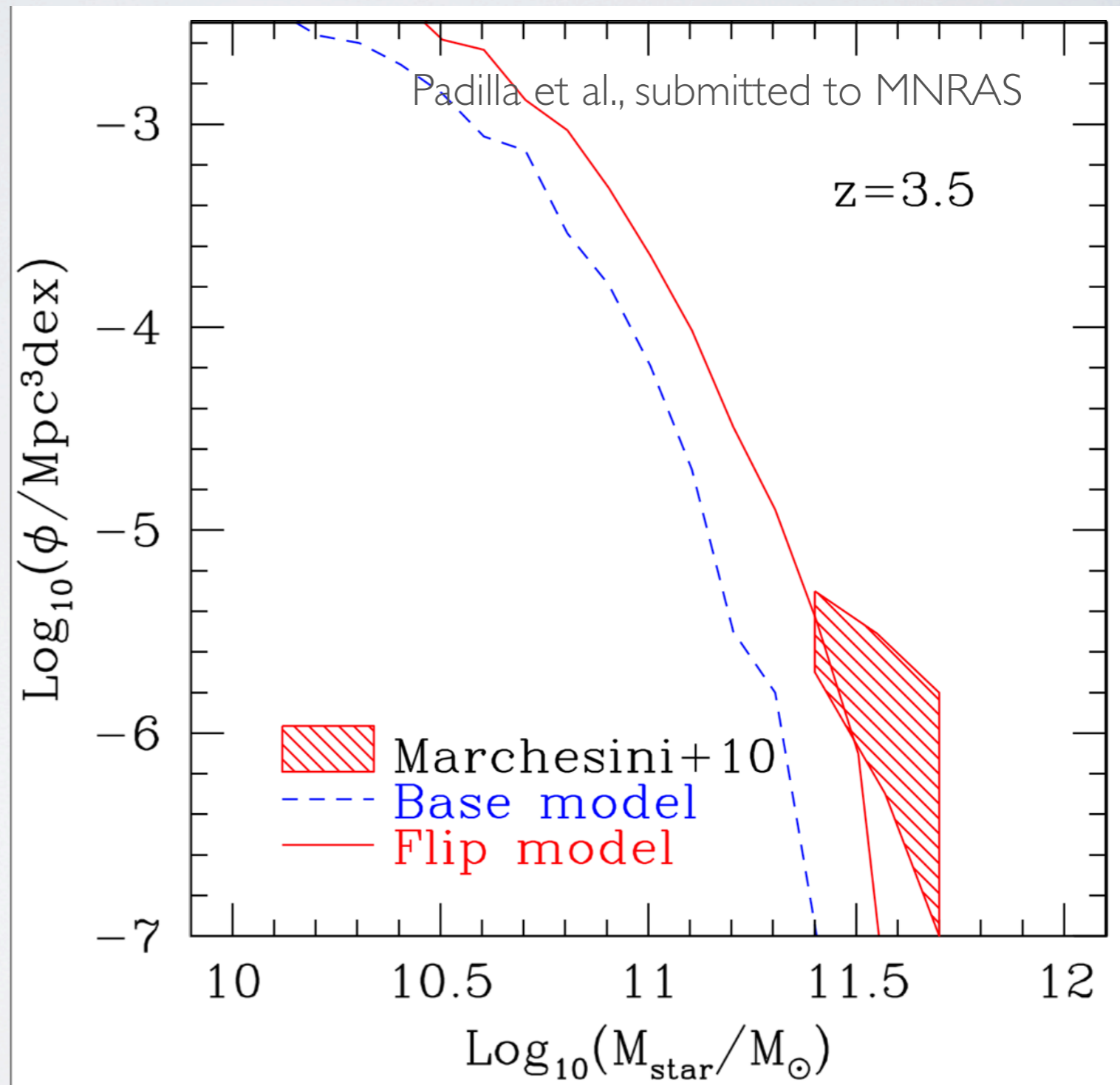
Stellar mass growth is faster at high  $z$  due to the more frequent instabilities of discs.



# 3) RESULTS: HIGH-Z MASSES

The stellar mass function at  $z=3.5$

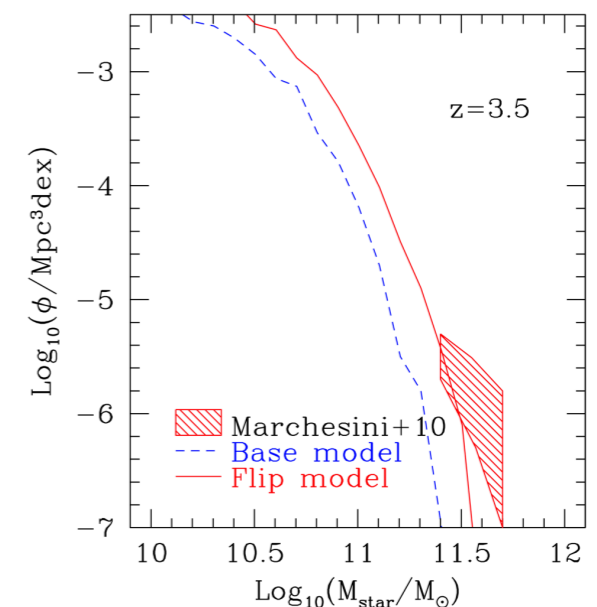
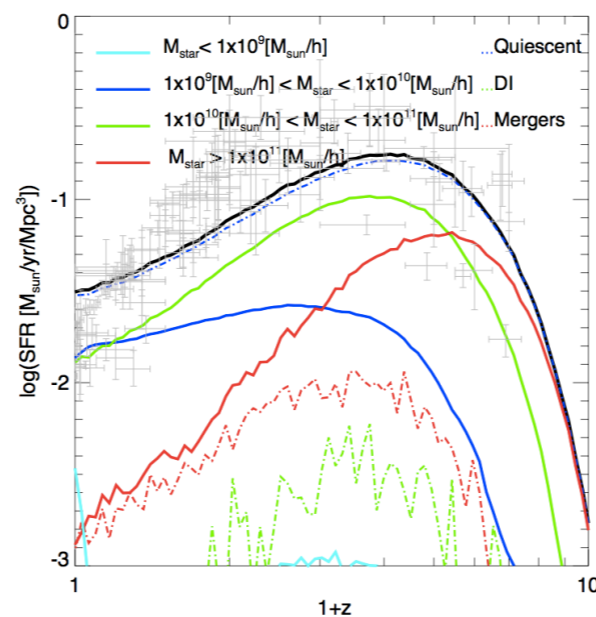
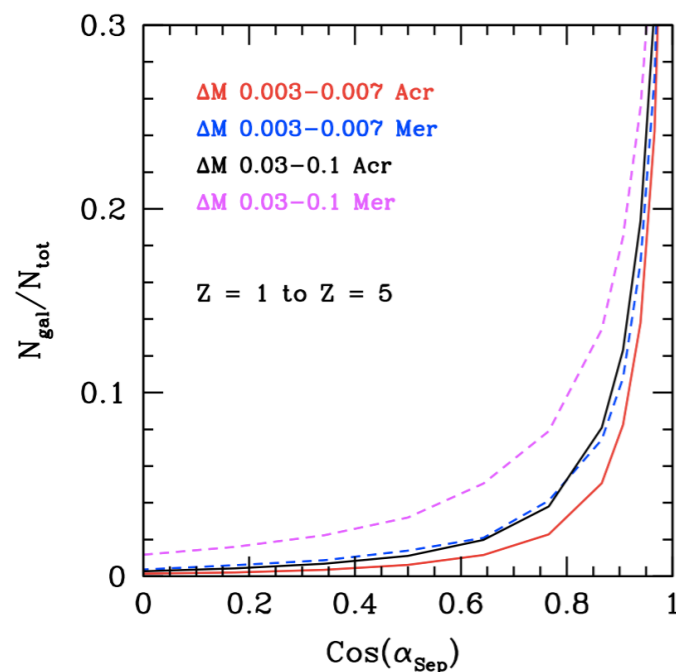
Stellar mass growth is faster at high  $z$  due to the more frequent instabilities of discs.



# CONCLUSIONS

Padilla et al., tonight in arXiv!

- High redshift abundances in models and observations have been difficult to reconcile. Observational and modeling techniques are still evolving...
- The infalling material carries only a small contribution to the increase of the angular momentum, with a strong stochastic component => discs become short-lived. Merger driven starbursts are obtained naturally.
- Galaxy sizes are more compatible with observations at low and high redshift and stellar mass grows more rapidly at high redshifts..



# Alejandra Muñoz



# Jorge Diaz



## Properties of Submillimeter Galaxies in a Semi-analytic Model using the "Count Matching" Approach: Application to the ECDFS

Alejandra M. Muñoz Arancibia<sup>1</sup>, Felipe P. Navarrete<sup>2,3</sup>, Nelson D. Padilla<sup>1,4</sup>, Sofia A. Cora<sup>5,6</sup>, Eric Gawiser<sup>7</sup>, Peter Kurczynski<sup>7</sup> and Andrés N. Ruiz<sup>8</sup>

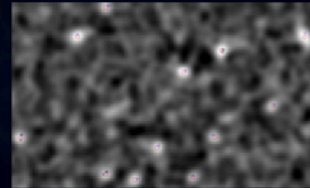
<sup>1</sup>Instituto de Astrofísica, Pontificia Universidad Católica de Chile, Santiago, Chile  
<sup>2</sup>Argelander-Institut für Astronomie, Bonn, Germany  
<sup>3</sup>Max-Planck-Institut für Radioastronomie, Bonn, Germany  
<sup>4</sup>Centro de Astro-Ingeniería, Pontificia Universidad Católica de Chile, Santiago, Chile  
<sup>5</sup>Consejo Nacional de Investigaciones Científicas y Técnicas, Buenos Aires, Argentina  
<sup>6</sup>Facultad de Ciencias Astronómicas y Geofísicas, Universidad Nacional de La Plata, and Instituto de Astrofísica de La Plata, La Plata, Argentina  
<sup>7</sup>Department of Physics and Astronomy, Rutgers University, Piscataway NJ, USA  
<sup>8</sup>Observatorio Astronómico de Córdoba, Universidad Nacional de Córdoba, Córdoba, Argentina



### MOTIVATION

Fitting submillimeter galaxies (SMGs) into the current theory of galaxy formation has been a challenge since their discovery. They are the most luminous star-forming sources at the epoch where galaxy formation peaks, being detected by their redshifted FIR emission from warm dust in the submm wavebands. Recent ALMA observations of the Extended Chandra Deep Field South (ECDFS) show that the brightest sources detected by LABOCA (LESS, Weiss et al. 2009) are comprised by emission from multiple fainter sources (ALESS, Karim et al. 2013).

With the aim of exploring the properties of SMGs in this field, and in analogy to the now-standard abundance matching approach, we perform a "Count Matching" approach through lightcones drawn from a semi-analytic model. We choose various physical galaxy properties given by the model as proxies for their submillimeter luminosities, assuming a monotonic relationship so that the combined LABOCA plus bright-end ALMA observed number counts are reproduced.



Example: section of the simulated map (lightcone #1, MDS proxy).  
 Red big circles: extracted sources.  
 Blue small circles: matched input sources.  
 Black crosses: components of the blended source.  
 The map resolution is 6"pix.

### METHODOLOGY

After turning the catalogs of galaxy positions and fluxes given by the different proxies into submillimeter maps (LABOCA beamwidth), we perform a source extraction. With this we study the effects of the observational process in the recovered counts, as well as the galaxy properties derived from the detected sources for each proxy.

We perform a cross-match between the extracted sources and input ones (brighter than 0.4 mJy), assigning the properties of the brightest source within the search radius to the extracted one. In addition, when finding multiple sources for a given extraction, we compute the separation in redshift between the components of the blended source.

Exploring the distribution of properties as redshift, SFR, stellar mass and host halo mass can help us to find the best proxy. Moreover, sources with the highest submm fluxes will have different clustering depending on the assumed proxy, since the sources with the highest value of a given property will be clustered in a particular way.

### APPLYING THE TECHNIQUE: STEPS

a) Select a galaxy sample. We construct 10 lightcones from the semi-analytic model SAG (Cora 2006, Lagos et al. 2006). Each lightcone covers 30x30', having an orientation in the sky such that the repetition of structure is minimum. All sources belonging to one lightcone comprise a unique galaxy sample.  
 b) Choose a physical galaxy property (given by SAG) as a proxy for the 870 μm luminosity, and sort the galaxy values of that proxy in increasing order.

$$c) \text{Assign a submm flux to each galaxy according to } N\left(\frac{\text{Proxy}}{f_k D_L^2}\right) > y = N(\text{Flux} > x)$$

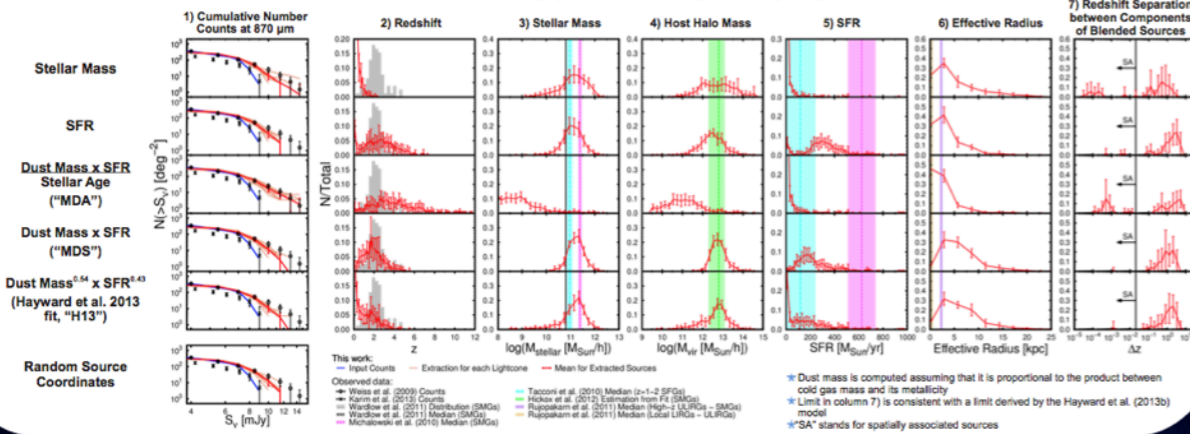
with  $D_L$  luminosity distance and  $f_k$  a factor giving the corresponding k-correction, assuming an Arp220 spectrum. Submillimeter fluxes are drawn from a Monte Carlo simulation following the observed cumulative number counts, where we have combined the LABOCA counts at low fluxes and ALMA counts at fluxes brighter than 8 mJy (we want to test whether we are able to recover LESS counts after simulating the observational process, while avoiding biases in the counts arising from targeting only LESS sources and not other regions in the ECDFS having S/N slightly lower than the LESS threshold).

### CONCLUSIONS

- For all proxies, there are lines of sight giving counts consistent with those derived from LABOCA observations. This is found even for input sources with randomized positions in the simulated map.
- MDS proxy gives redshift, stellar mass and host halo mass distributions consistent with observed ones. Our model still is not able to reproduce the observed SFRs assuming a Salpeter IMF.
- The majority of components of blended sources are spatially unassociated. However, for the stellar mass and MDA proxies the amount of sources being spatially associated is not negligible.

### RECOVERED DISTRIBUTIONS

## PROXIES



### References

- A.M.M.A. acknowledges the support from CONICYT Doctoral Fellowship program. Simulations were run using the Geryon cluster of the Centro de Astro-Ingeniería UC (AIUC). Correspondence and requests for materials should be addressed to A.M.M.A. (amunoz@astro.puc.cl).
- Cora, S. A., Mon. Not. R. Astron. Soc. 368 (2006), 1540.  
 Lagos, C. et al., Mon. Not. R. Astron. Soc. 388 (2008), 587.  
 Hayward, C. C. et al., Mon. Not. R. Astron. Soc. 428 (2013), 2529.  
 Hayward, C. C. et al., Mon. Not. R. Astron. Soc. 434 (2013b), 2572.  
 Hickox, R. C., Mon. Not. R. Astron. Soc. 421 (2012), 284.  
 Karim, A. et al., Mon. Not. R. Astron. Soc. 432 (2013), 2.  
 Michalowski, M. et al., Astron. & Astrophys. 514 (2010), A67.  
 Rujopakarn, W. et al., Astrophys. J. 726 (2011), 93.  
 Tacconi, L. J. et al., Nature 463 (2010), 781.  
 Wardlow, J. L., Mon. Not. R. Astron. Soc. 415 (2011), 1479.  
 Weiss, A. et al., Astrophys. J. 707 (2009), 1201.

## Star Formation Activity in Balmer Break Galaxies at $z < 1.5$ .

J. Díaz Tello<sup>1,4</sup>, C. Donzelli<sup>1</sup>, N. Padilla<sup>2</sup>, N. Fujishiro<sup>3</sup>, M. Akiyama<sup>4</sup>.

<sup>1</sup> Instituto de Astronomía Teórica y Experimental (IATE-Conicet), Argentina  
<sup>2</sup> DAA, Pontificia Universidad Católica de Chile (PUC), Chile  
<sup>3</sup> Koyama Astronomical Observatory, Kyoto Sangyo University, Japan  
<sup>4</sup> Astronomical Institute, Tohoku University, Japan  
 \* jdiaz@iate.uncor.edu

We derived star formation rates (SFR) and investigated the evolution of the SFR–stellar mass, specific SFR (SSFR)–stellar mass and SSFR–color relations as function of the redshift. The studied sample composed of star-forming and post-starburst galaxies, span a redshift range from 0.094 to 1.47, and they have stellar masses from  $10^8$ – $10^{12}$  Msun. We observe that for a given mass or color, high-redshift galaxies have higher SFR and SSFR values than local galaxies. A break in the star-forming sequence appears when post-starburst galaxies are included, revealing an increasing trend with redshift for the SFR/SSFR values. These results let us hypothesize about a characteristic mass and color at which the red sequence could mostly be formed at a given redshift.

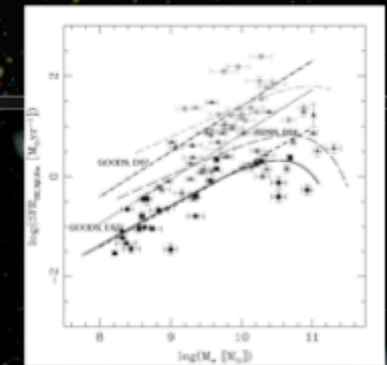
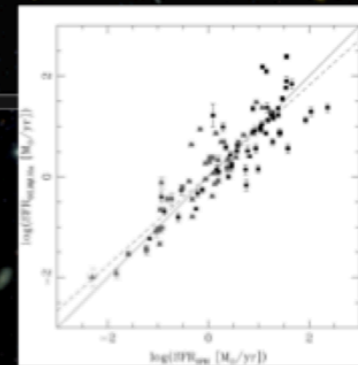


Fig. 1: - LEFT: Comparison between  $SFR_{\text{OHL/ELH}}$  versus  $SFR_{\text{LABOCA}}$  obtained using exponentially declining SFHs. Black squares show the SFR values obtained for the spectroscopic sample presented in this work, while gray triangles show the SFR values obtained from the Díaz Tello et al. (2013) sample. The solid line represent a 1:1 relation, while the dashed line shows the linear fit applied to the sample. It can be seen that the SFR derived from both methods correlate fairly well but with a slightly trend of SFH models to give higher SFR values at larger SFRs.  
 - RIGHT: SFR as function of total stellar mass. Black squares represent our low-redshift galaxies ( $0 < z < 0.5$ ), gray triangles are our intermediate-redshift galaxies ( $0.5 < z < 1.0$ ), while light gray diamonds are our high-redshift galaxies ( $1.0 < z < 1.5$ ). The solid, long-dashed and short-long-dashed lines show the fitting function (power-law and break component) applied to each group. The short-dashed line shows the trend observed in SDSS at redshift  $z < 0.2$  (Brinchmann et al. 2004), the dotted line shows the trend observed in GOODS by Elbaz et al. (2007) at redshift  $0.8 < z < 1.2$ , while the dot-dashed line shows the trend found by Daddi et al. (2007) in GOODS at  $1.4 < z < 2.5$ . It can be seen how the mass break in the power-law shape appear to be necessary for following the trends showed by star-forming and post-starburst galaxies.

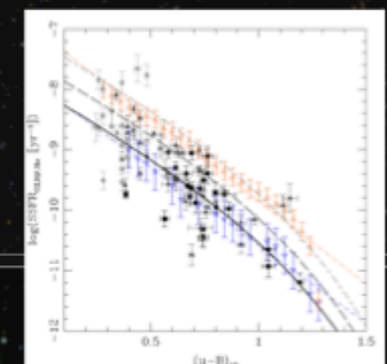
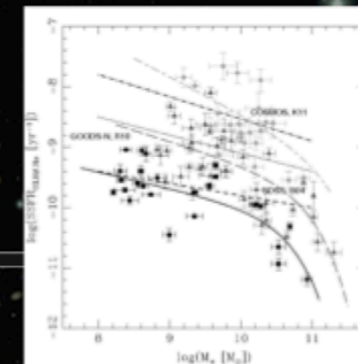


Fig. 2: - LEFT: SSFR as function of total stellar mass. As was shown in Figure 9, black squares are our low-redshift galaxies, gray triangles our intermediate-redshift galaxies and light gray diamonds our high-redshift galaxies. The solid, long-dashed and short-long-dashed lines show the fitting function applied to each group. As comparison, the short-dashed line shows the trend observed in SDSS at redshift  $z < 0.2$  (Brinchmann et al. 2004), the dotted line shows the trend observed in GOODS by Elbaz et al. (2007) at redshift  $0.8 < z < 1.2$ , while the dot-dashed line shows the trend found by Daddi et al. (2007) in GOODS at  $1.4 < z < 2.5$ . It can be seen how the mass break in the power-law shape appear to be necessary for following the trends showed by star-forming and post-starburst galaxies.

# I A) MODELS OF GALAXY FORMATION

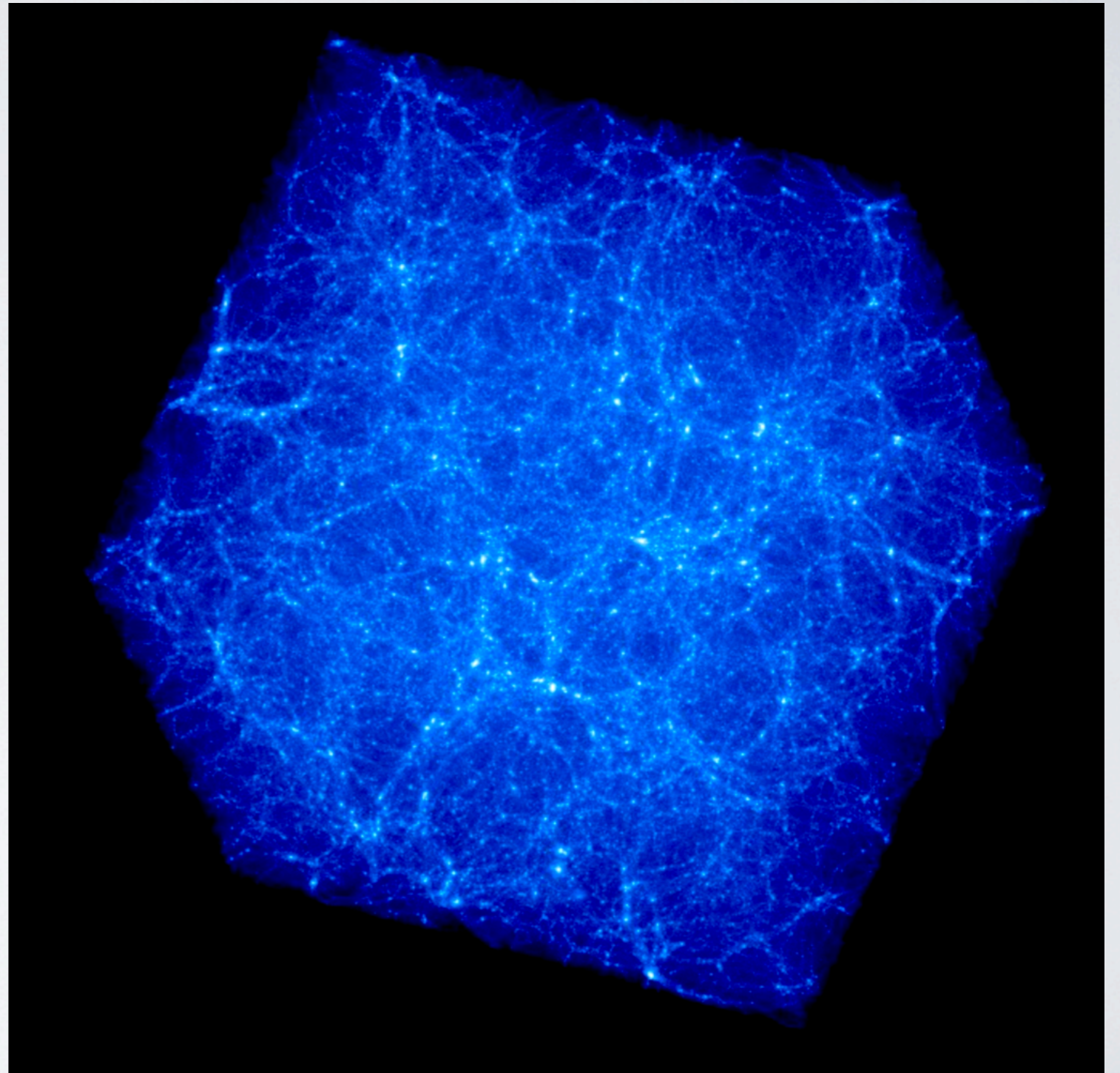
Cosmological  
periodic  
comoving  
boxes.

DM-only:  
halos of  $1e10M_{\text{sun}}$  and up.

Our sim:  $640^3$  particles

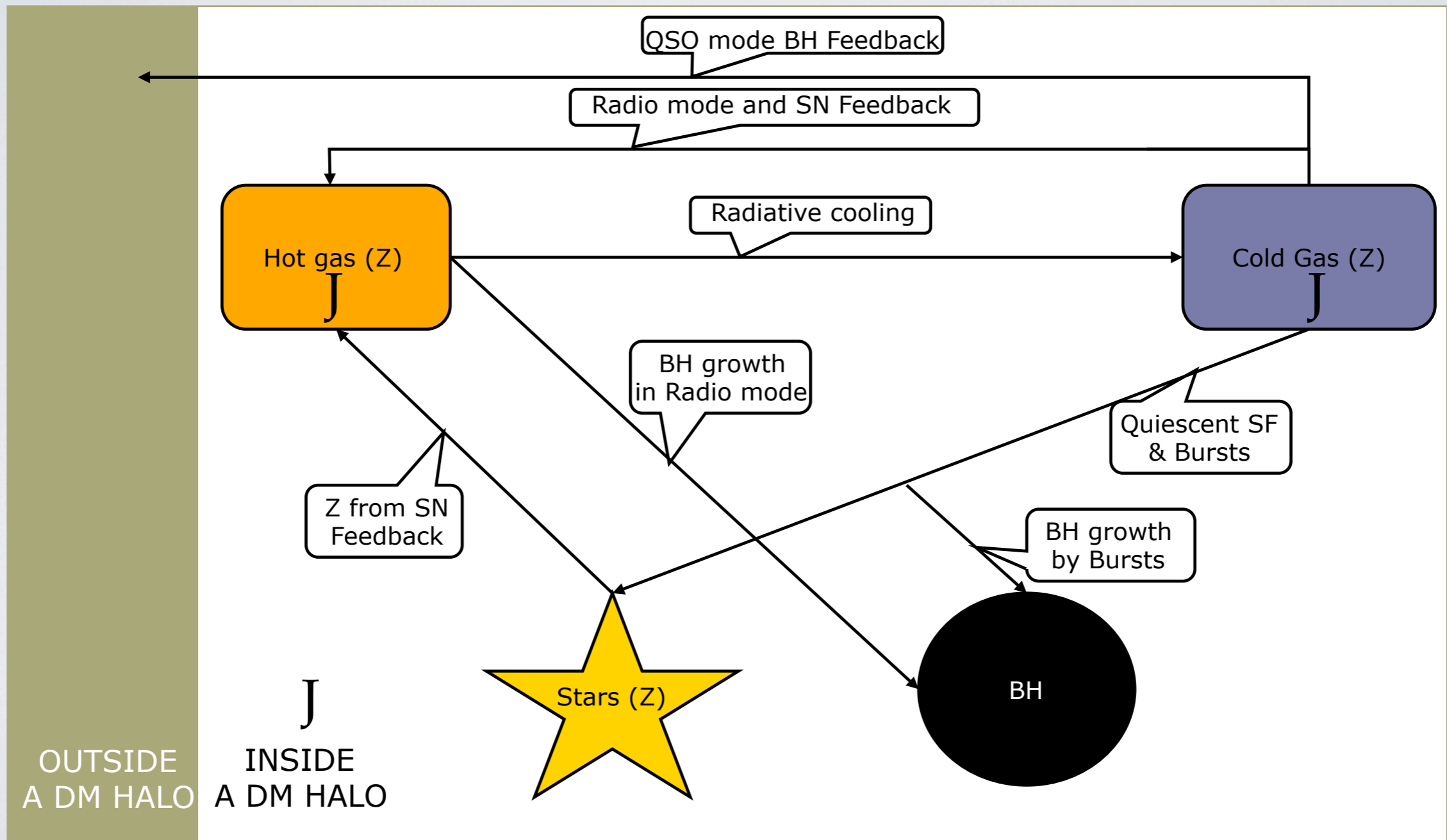
Millennium II:  
 $2000^3$  particles

MII 100xparticles per halo of  
equal mass



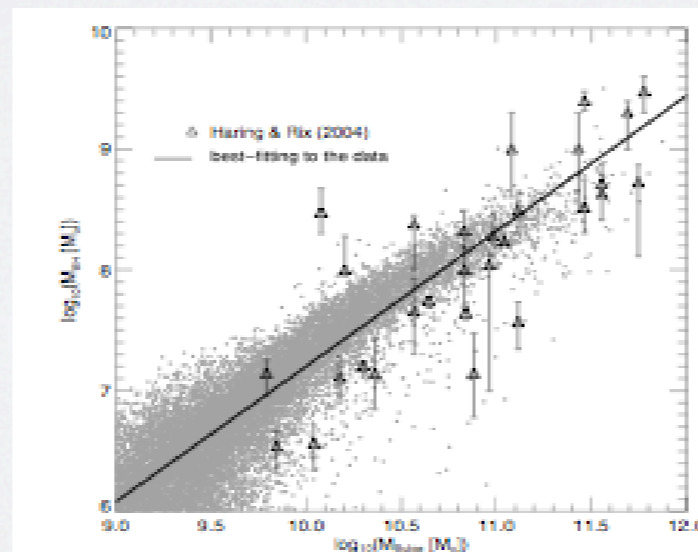
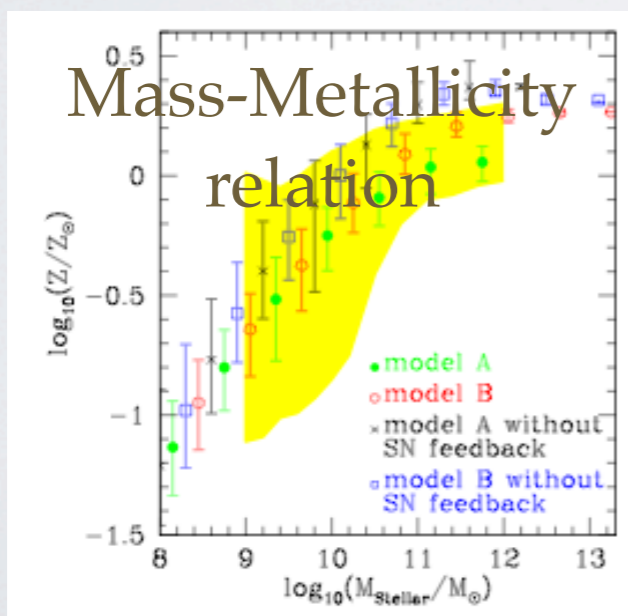
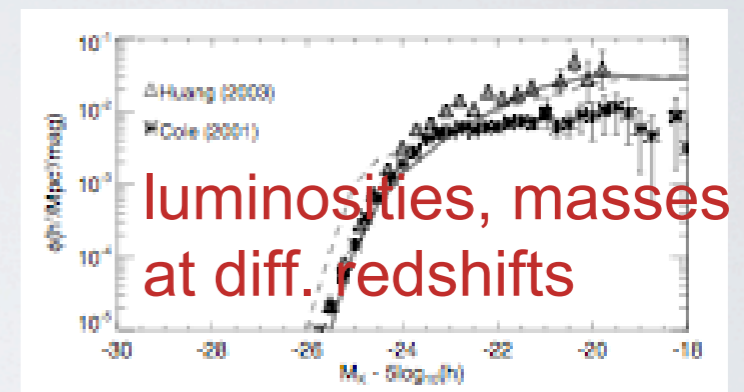
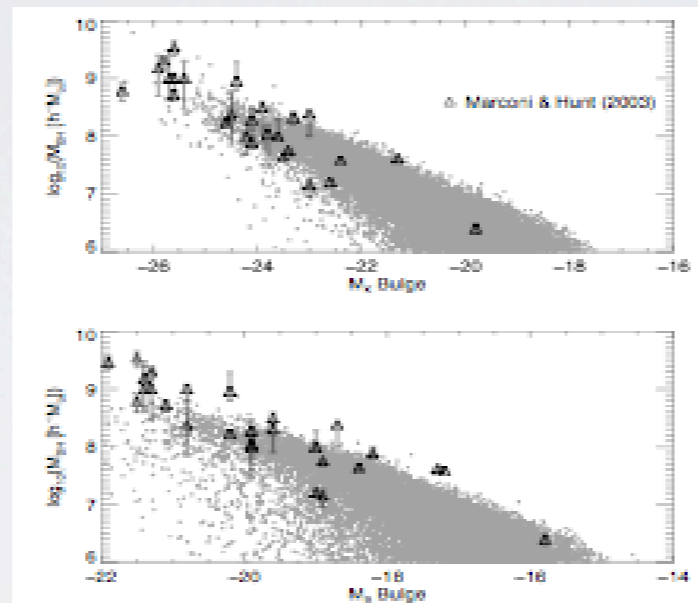
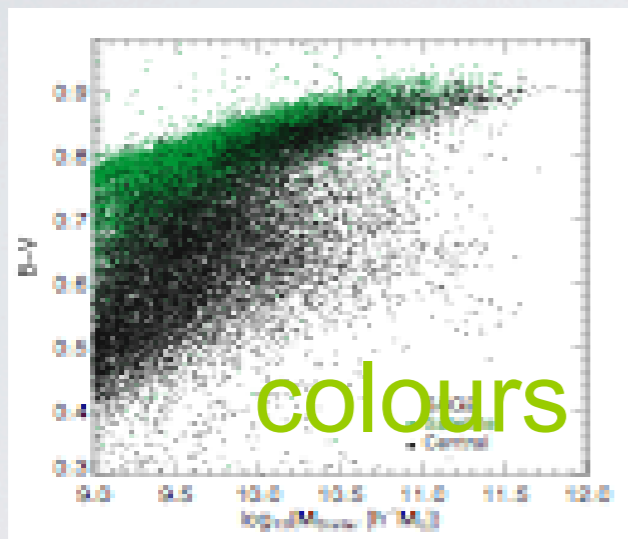
# I B) SEMI-ANALYTIC MODELS

Summary of processes:



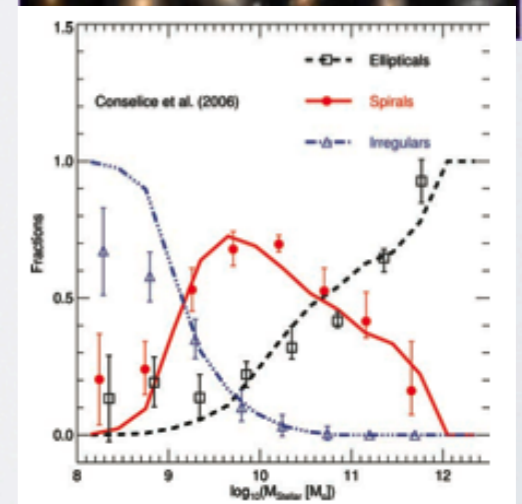
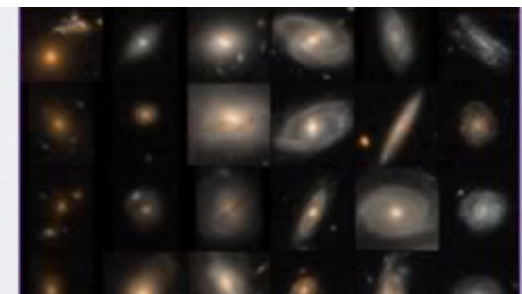
# I B) SEMI-ANALYTIC MODEL

Fix free parameters using a set of  $z=0$  statistics:



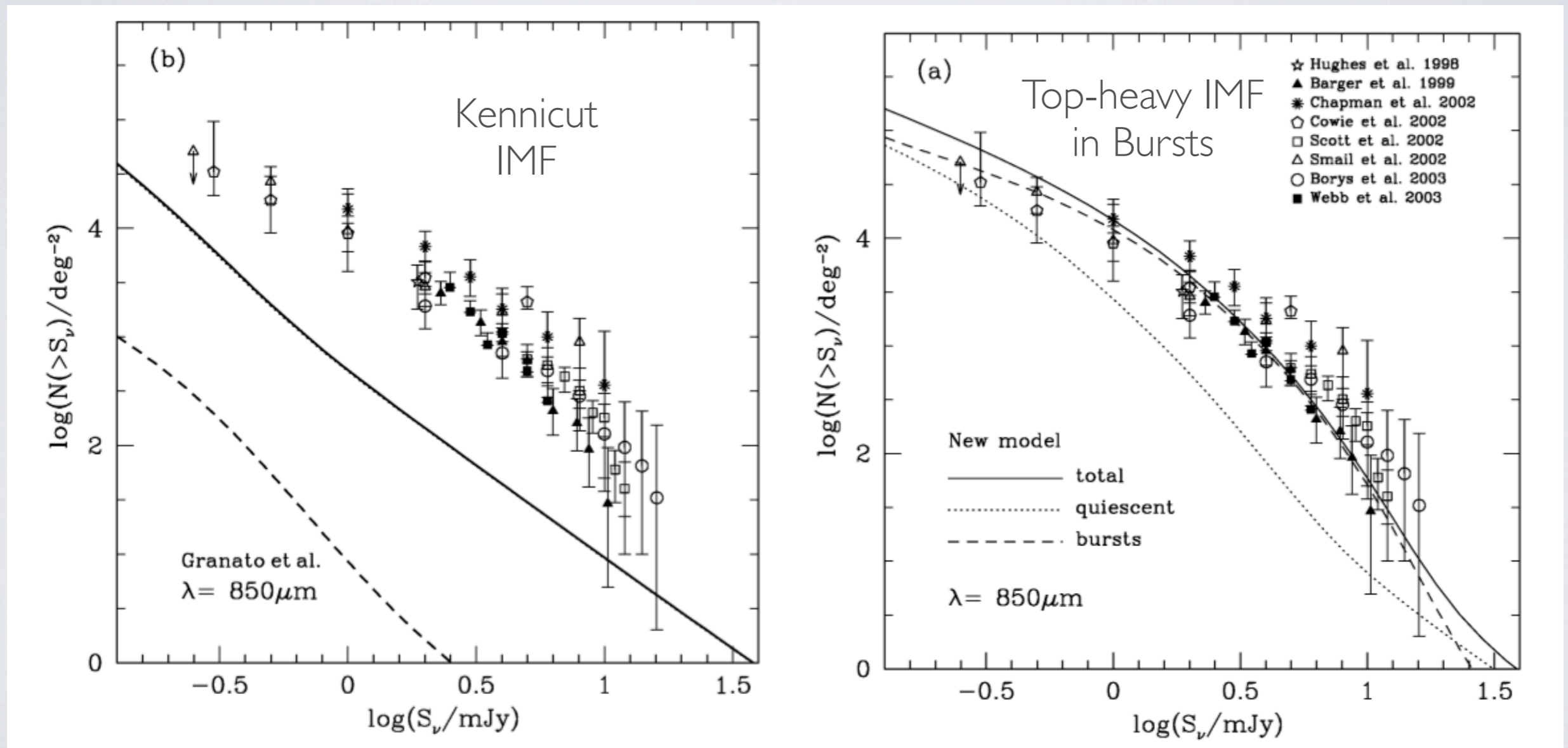
Black hole-host relations

morphologies



# I C) MODELS PERFORMANCE AT HIGH-Z

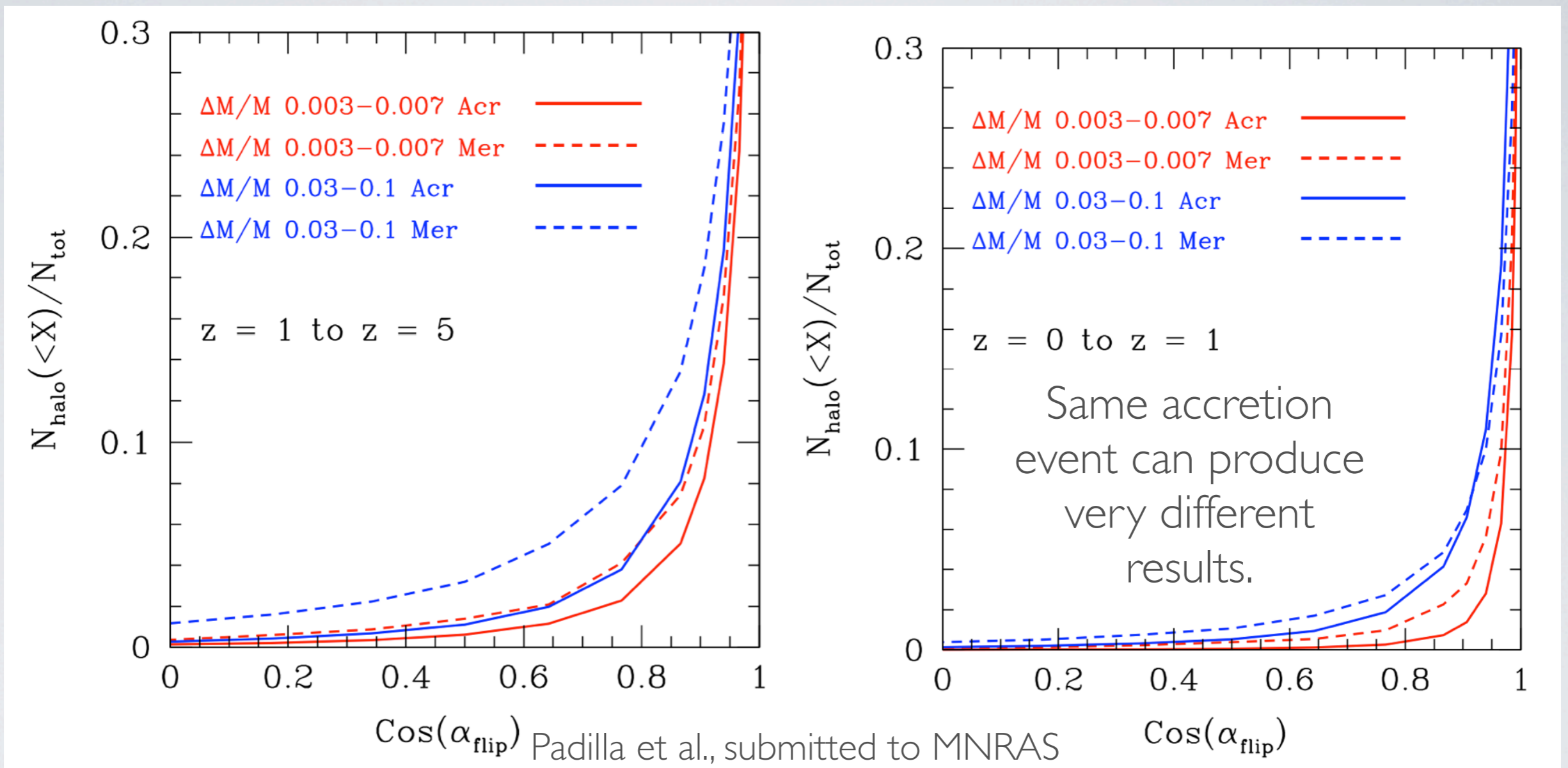
Submm counts:



Baugh et al. 2005



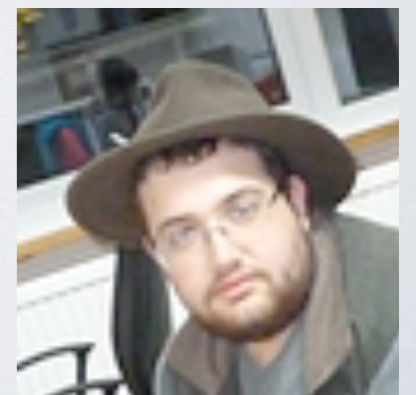
# 2) MILLENNIUM II ANALYSIS



Notice that change in direction is larger for mergers.



$\text{Cos}(\alpha_{\text{sep}})$  as a function of fraction of accreted mass.



S. Contreras

## 2) ANGULAR MOMENTUM IN SAMS

Assumption:

The angular momentum of the dark matter is carried by the baryons.

Flips in DM => Flip in baryons

Cooling baryons will find a disc with a different L.

Missaligned accretion prevents the angular momentum of the disc from growing.

(i.e., no need to follow the amplitude of the angular momentum of DM haloes).

## 2) EFFECT ON MERGERS

Disc instability  
as the only driver of bursts in  
the model naturally produces  
short-lived discs when loss of  
angular momentum due to  
accretion is considered.

## 2) EFFECT ON MERGERS

Disc instability  
as the only driver  
of bursts in the  
model.

$$\epsilon = \frac{V_{\max}}{(GM_{\text{disc}}/r_{\text{disc}})^{1/2}},$$

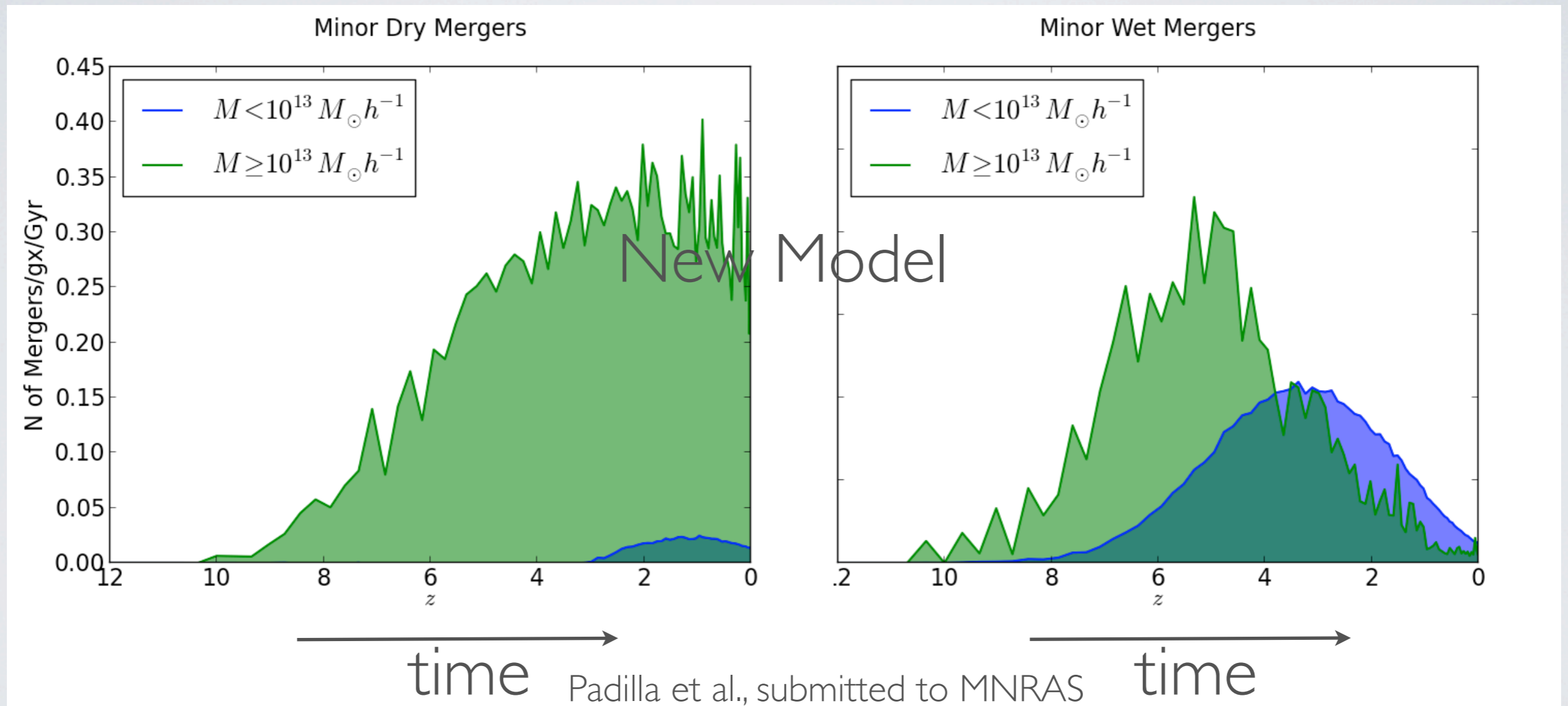
if lower than critical value  
disc is unstable

Mergers also  
which make epsilon very low

# 2) EFFECT ON MERGERS



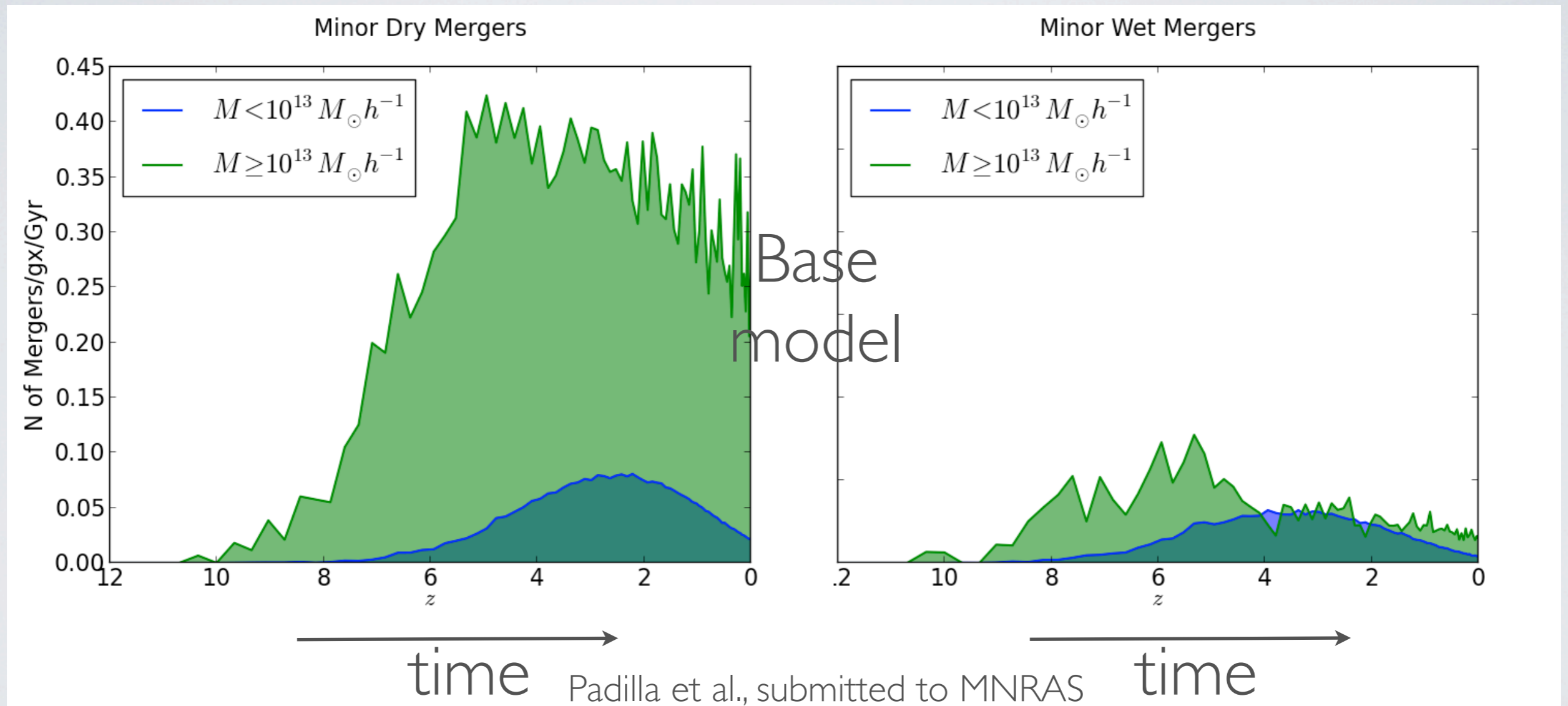
S. Salazar



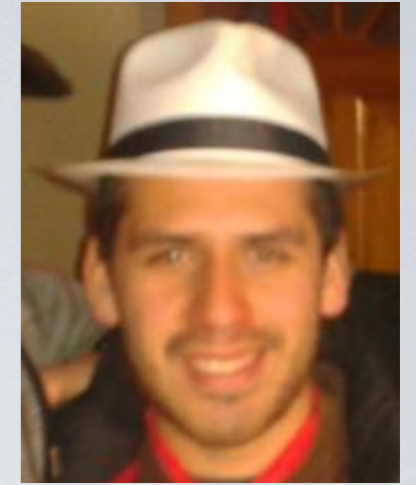
# 2) EFFECT ON MERGERS



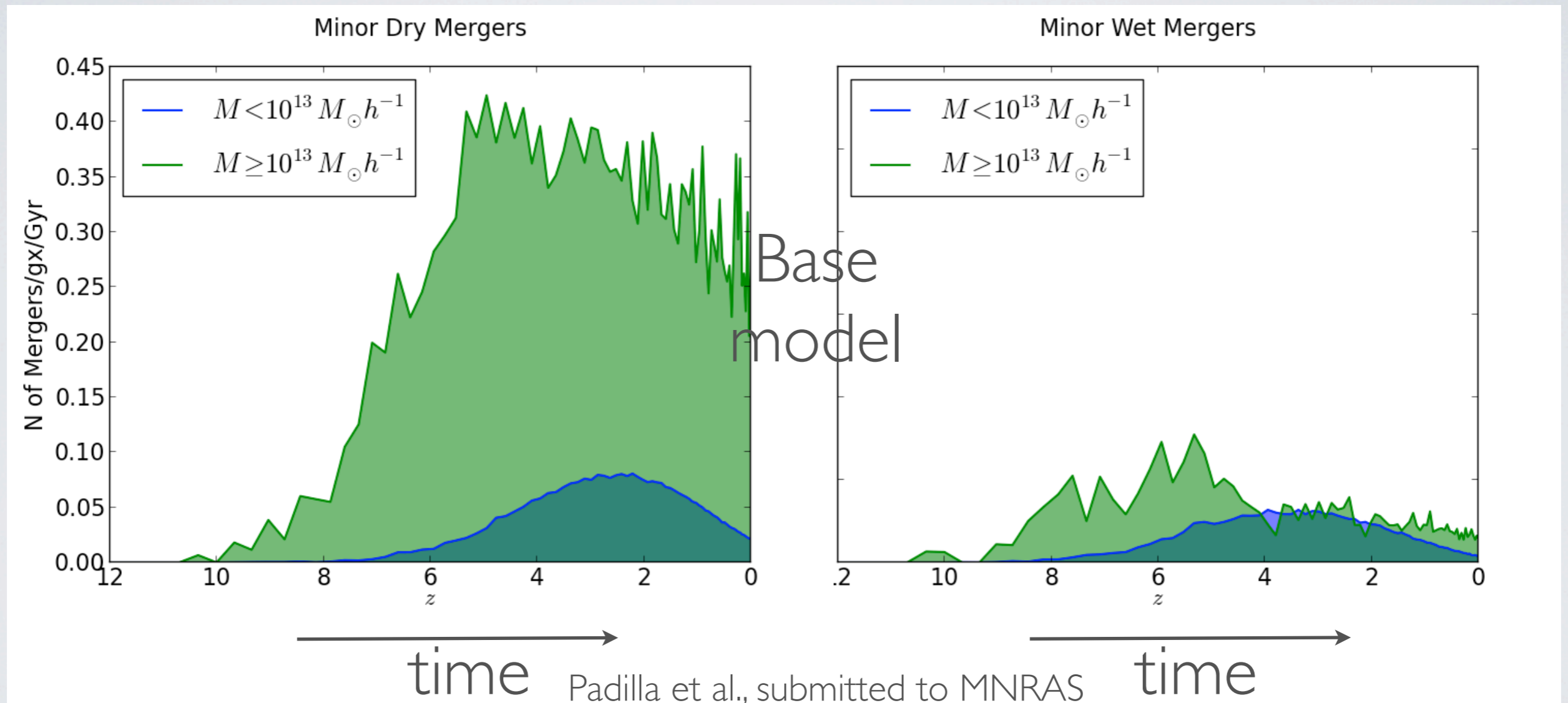
S. Salazar



# 2) EFFECT ON MERGERS



S. Salazar



Mergers+DI produce similar frequency of bursts  
(except for minor mergers)

$f_{\text{major}}$ ,  $f_{\text{gas}}$ ,  $f_{\text{disc}}$  no longer needed as parameters.

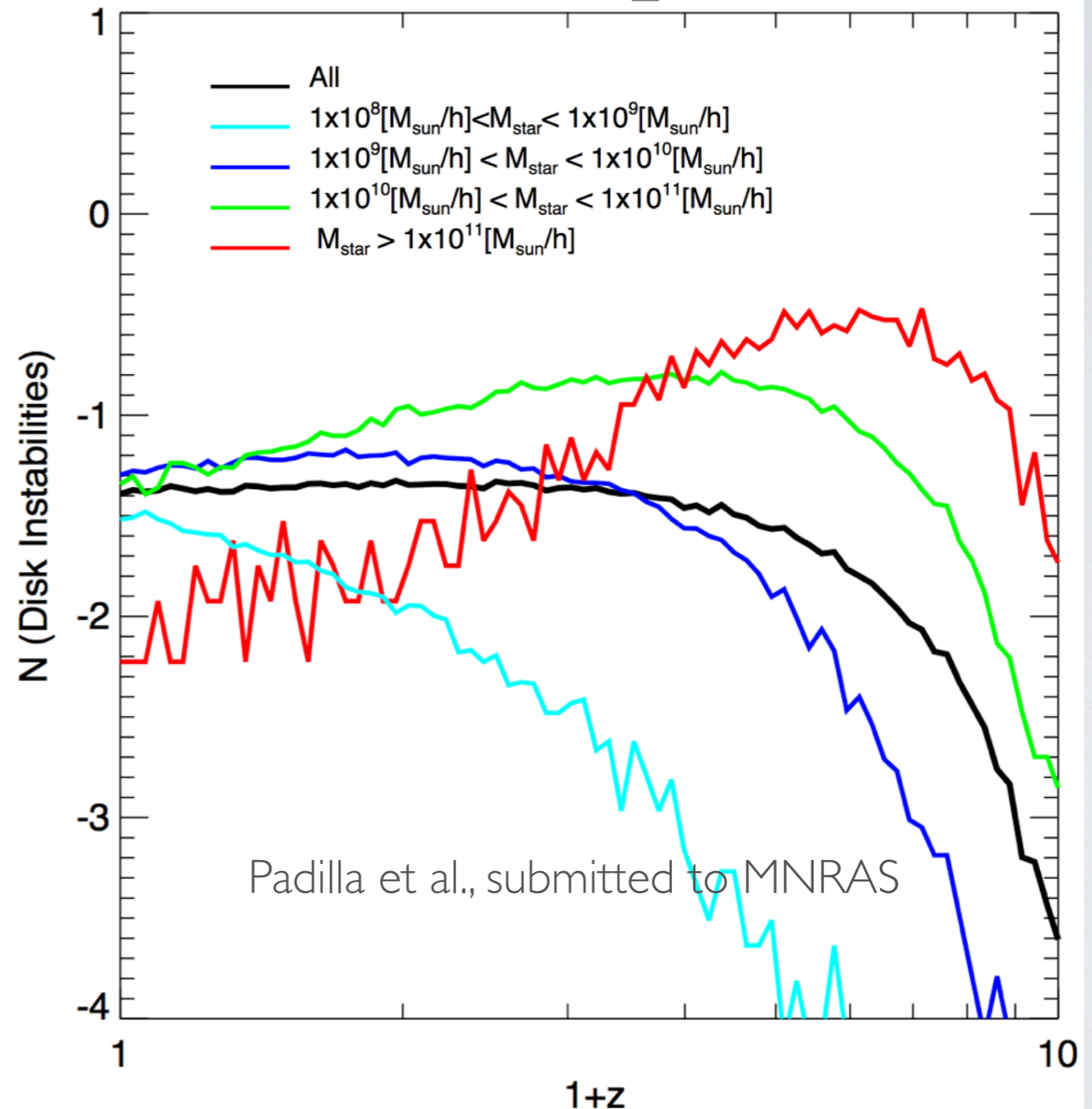
## 2) EFFECT ON SF

Number of disc instabilities

$$\epsilon = \frac{V_{\max}}{(GM_{\text{disc}}/r_{\text{disc}})^{1/2}},$$

if lower than critical value  
disc is unstable

$r_{\text{disc}}$  is now subject to  
changes due to accretion  
which make epsilon very low





## 2) EFFECT ON SF

Number of disc instabilities

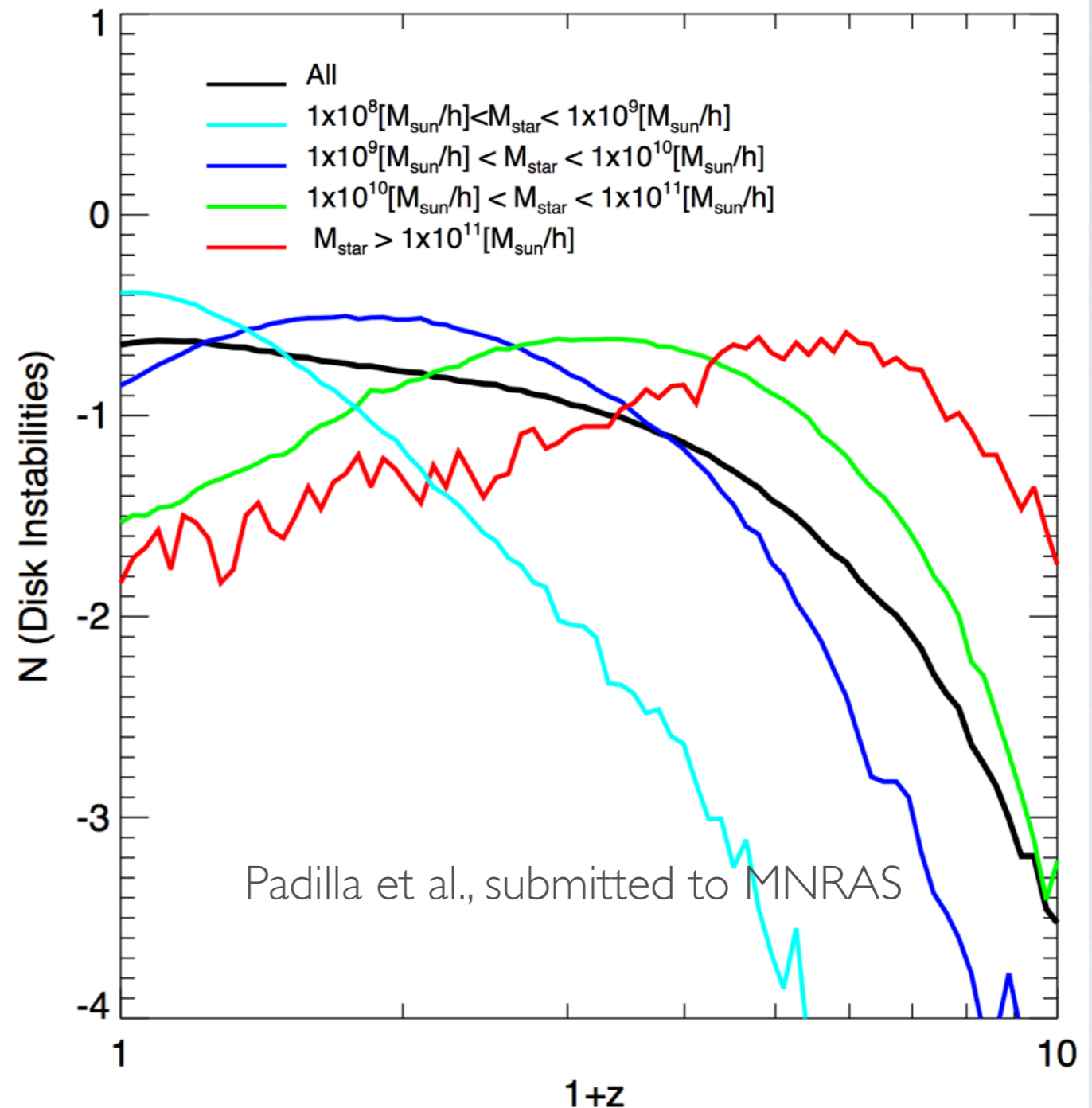
$$\epsilon = \frac{V_{\max}}{(GM_{\text{disc}}/r_{\text{disc}})^{1/2}},$$

if lower than critical value  
disc is unstable

$r_{\text{disc}}$  is now subject to  
changes due to accretion  
which make epsilon very low

With episodic discs:

- \* 50% global increase in instabilities at high masses
- \* 8% of galaxies with DI



## 2) EFFECT ON SF

Number of disc instabilities

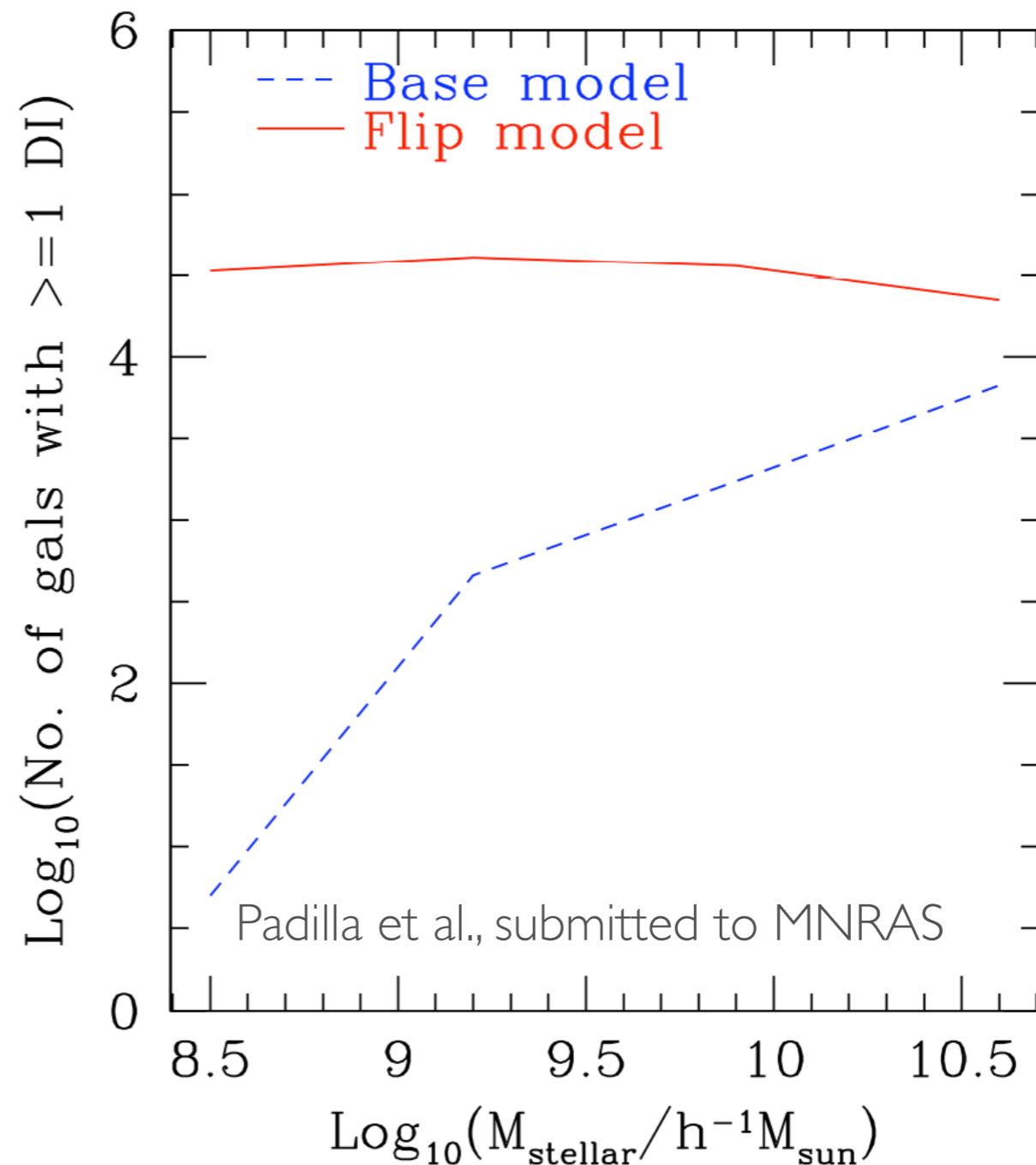
$$\epsilon = \frac{V_{\max}}{(GM_{\text{disc}}/r_{\text{disc}})^{1/2}},$$

if lower than critical value  
disc is unstable

$r_{\text{disc}}$  is now subject to  
changes due to accretion  
which make epsilon very low

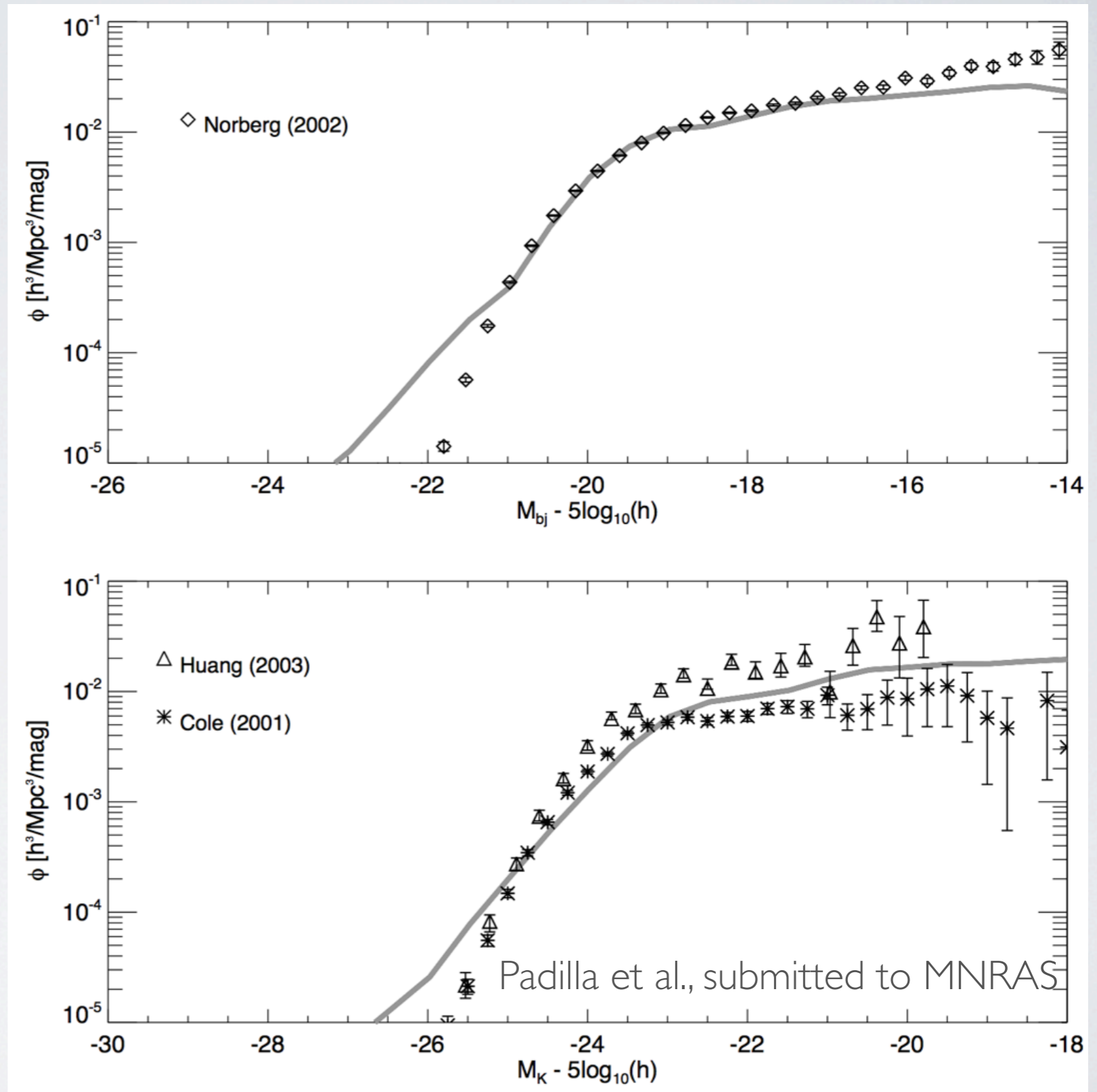
With episodic discs:

- \* 50% global increase in instabilities at high masses
- \* 8% of galaxies with DI



# SAM PARAMETERS FIXED WITH LF

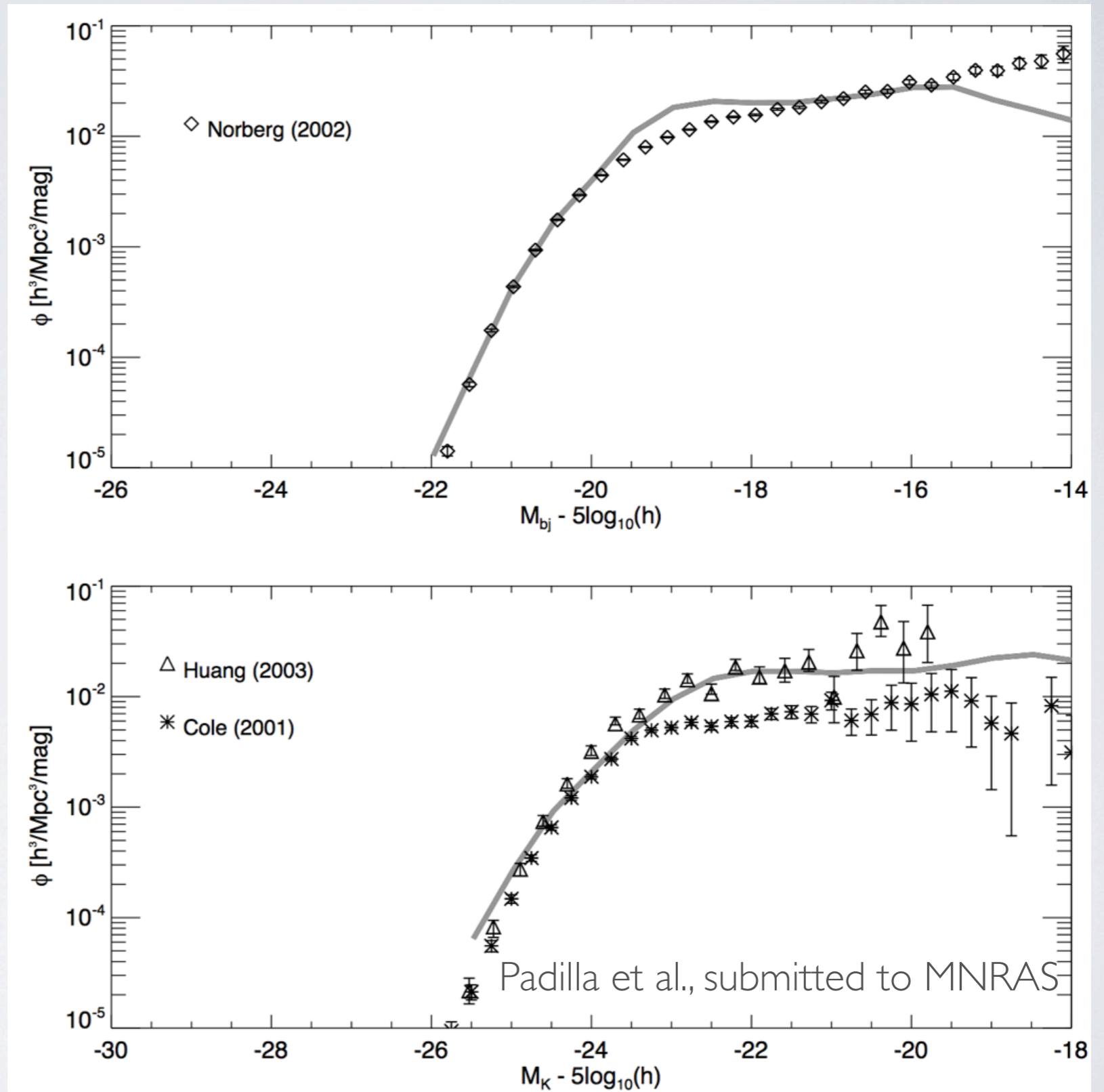
Smooth  
growth  
in disc size



# SAM PARAMETERS FIXED WITH LF

With episodic discs

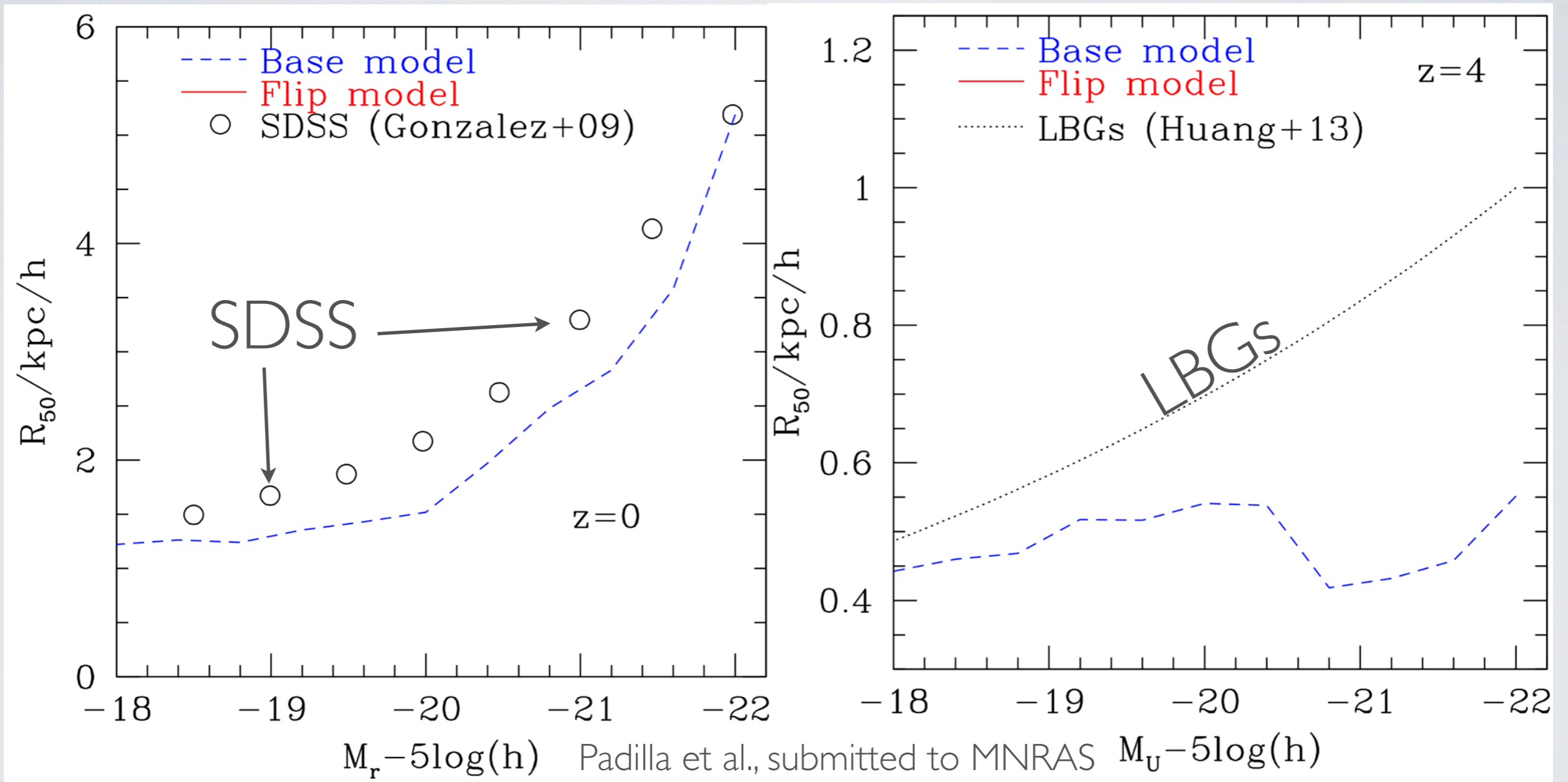
SF efficiency lowered to reproduce LF at  $z=0$



# 3) RESULTS: GALAXY SIZES

Low z:

High z:

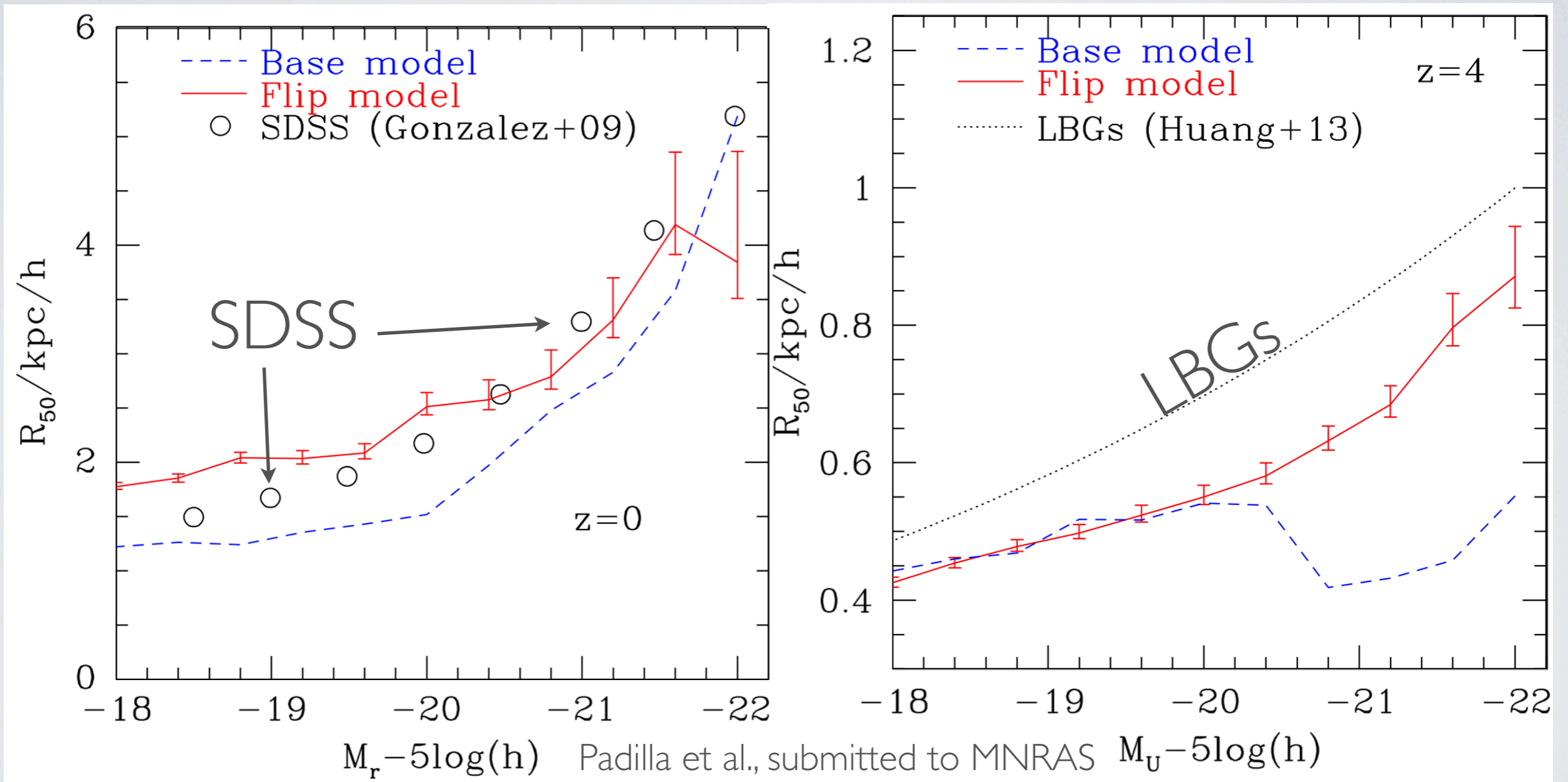


Even though discs would become smaller along with their spins, this makes only large discs survive perturbations: larger discs in the population.

# 3) RESULTS: GALAXY SIZES

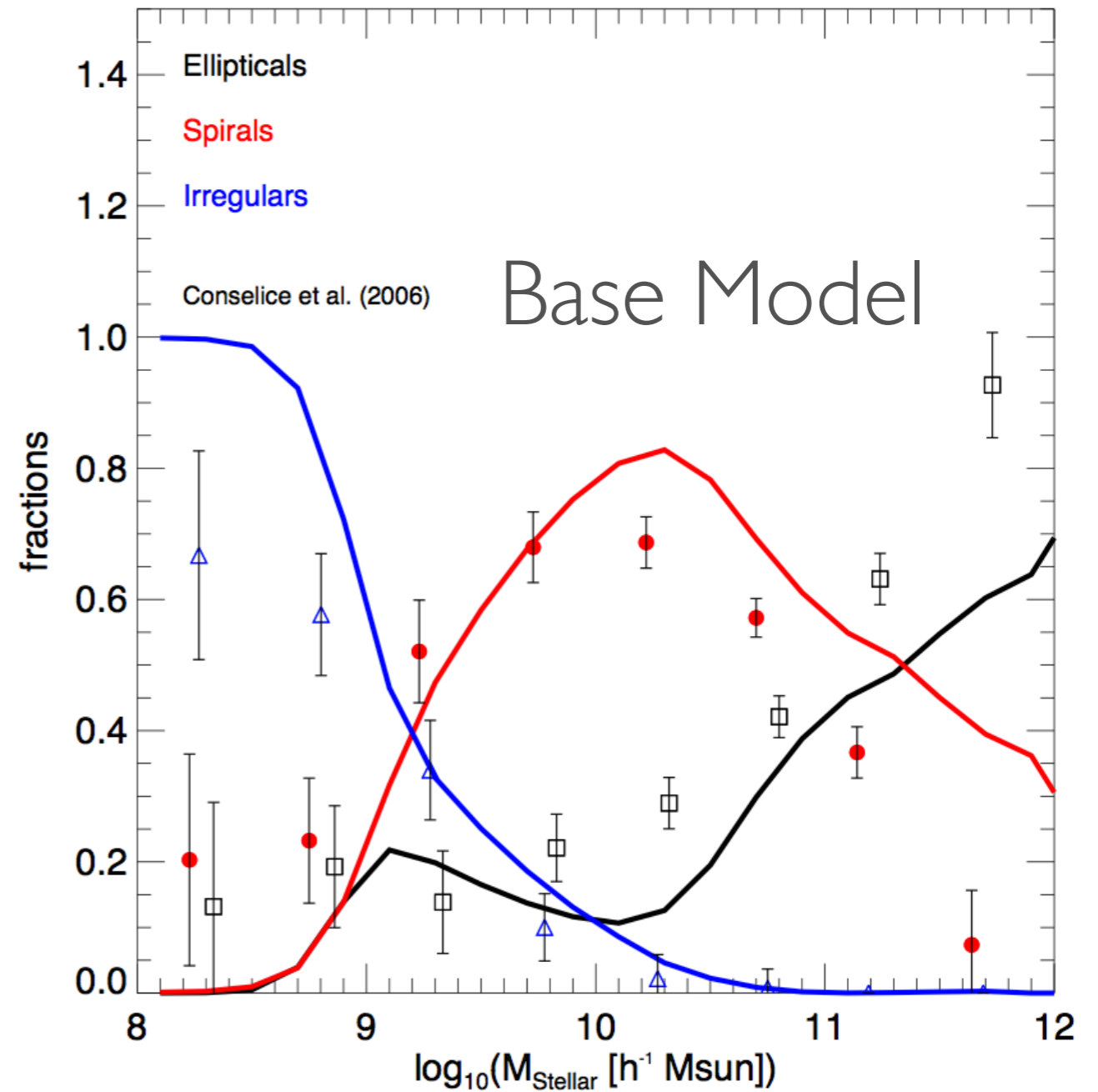
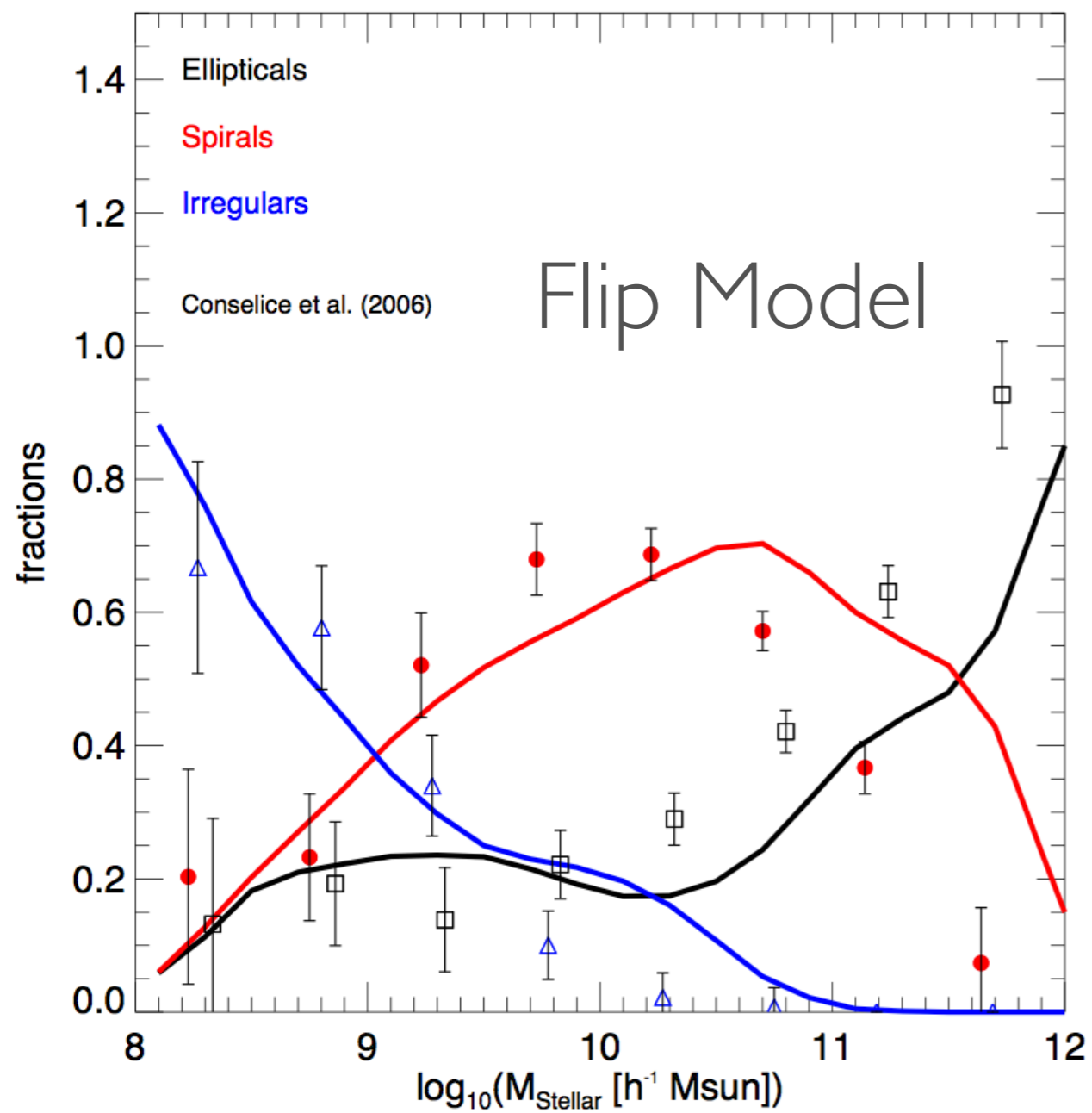
Low z:

High z:



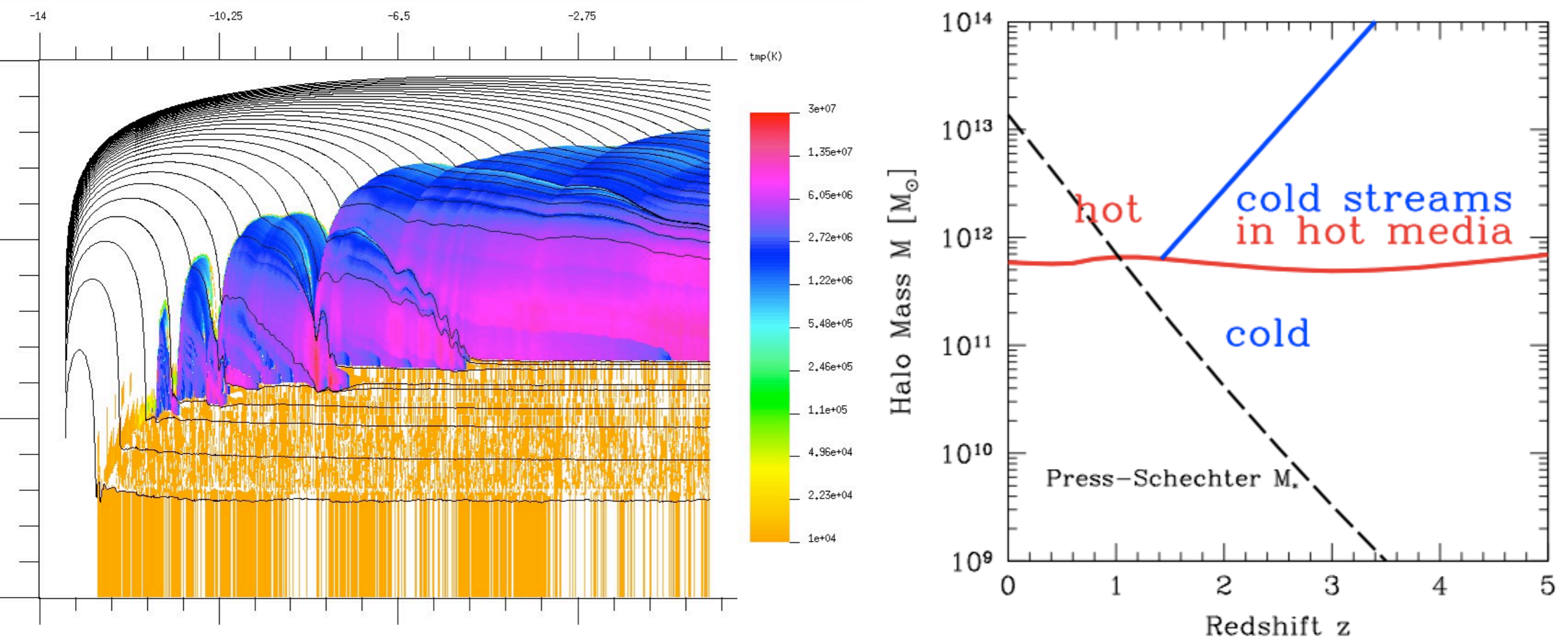
Even though discs would become smaller along with their spins, this makes only large discs survive perturbations: larger discs in the population.

# 3) RESULTS: MORPHOLOGIES



# 4) COLD GAS INFLOWS

High- $z$  low mass halos: most of the gas reaching the center of a galaxy is able to arrive cold without going through a heating phase.



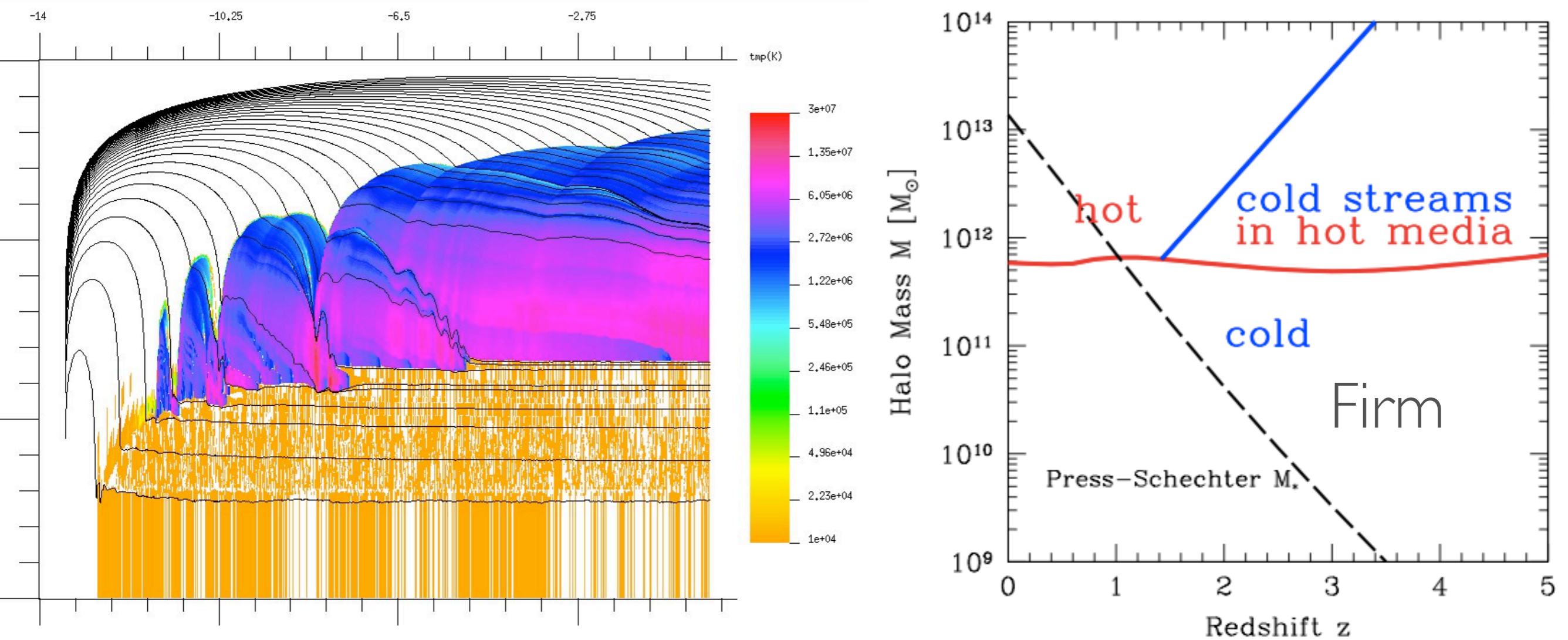
Dekel, Birnboim, et al., 2009

see also Keres et al., 2009, van de Voort et al., 2011, etc.



# 4) COLD GAS INFLOWS

High- $z$  low mass halos: most of the gas reaching the center of a galaxy is able to arrive cold without going through a heating phase.

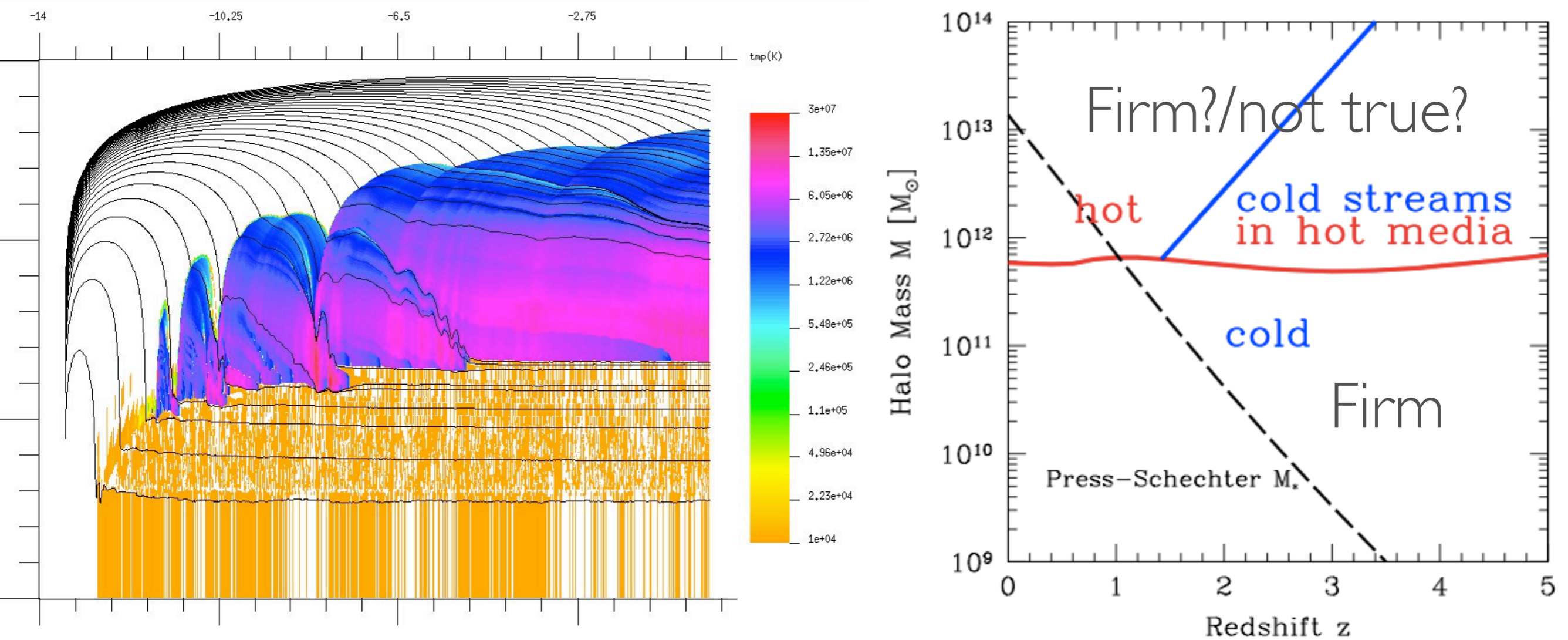


Dekel, Birnboim, et al., 2009

see also Keres et al., 2009, van de Voort et al., 2011, etc.

# 4) COLD GAS INFLOWS

High- $z$  low mass halos: most of the gas reaching the center of a galaxy is able to arrive cold without going through a heating phase.

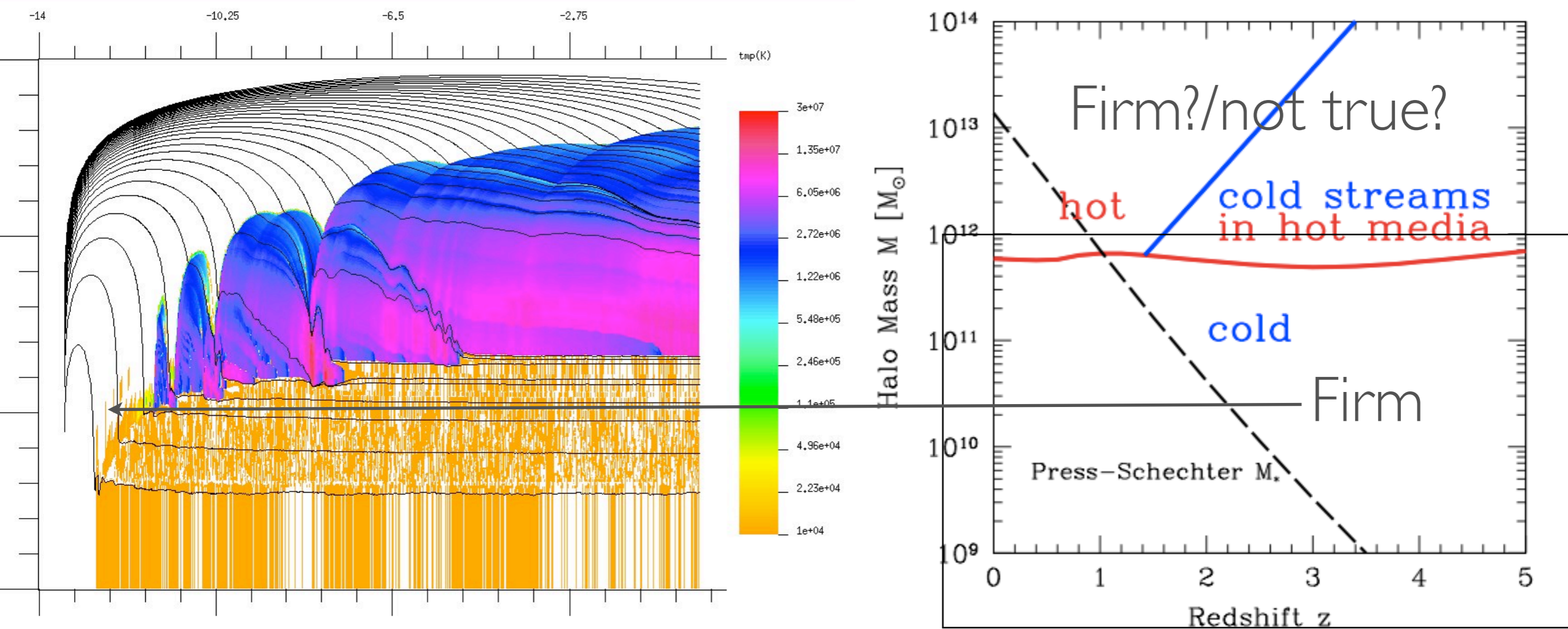


Dekel, Birnboim, et al., 2009

see also Keres et al., 2009, van de Voort et al., 2011, etc.

# 4) COLD GAS INFLOWS

High- $z$  low mass halos: most of the gas reaching the center of a galaxy is able to arrive cold without going through a heating phase.



Dekel, Birnboim, et al., 2009

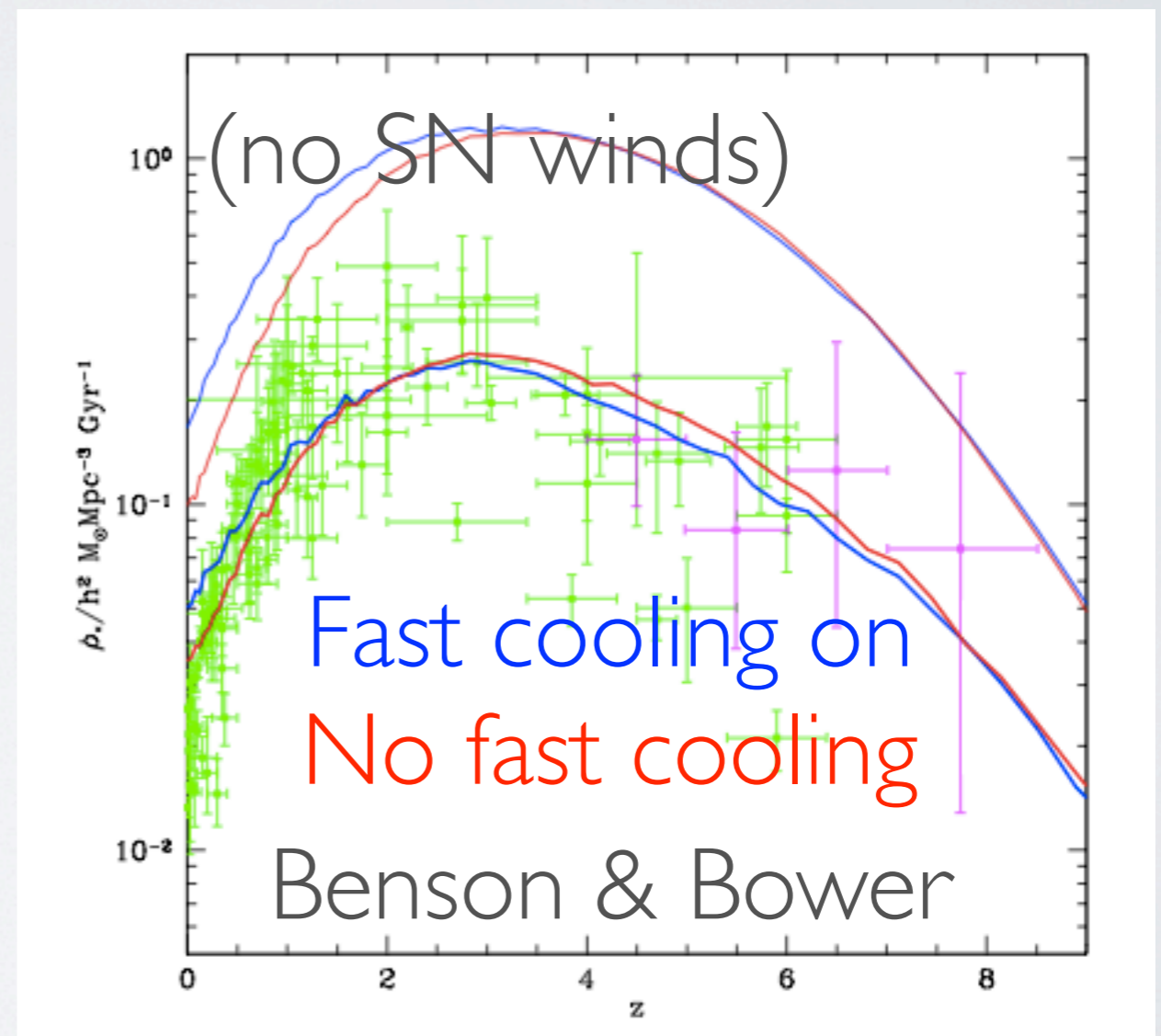
see also Keres et al., 2009, van de Voort et al., 2011, etc.

# 4) COLD GAS INFLOWS

Implemented in the GALFORM semi-analytic model by Benson & Bower (2010):

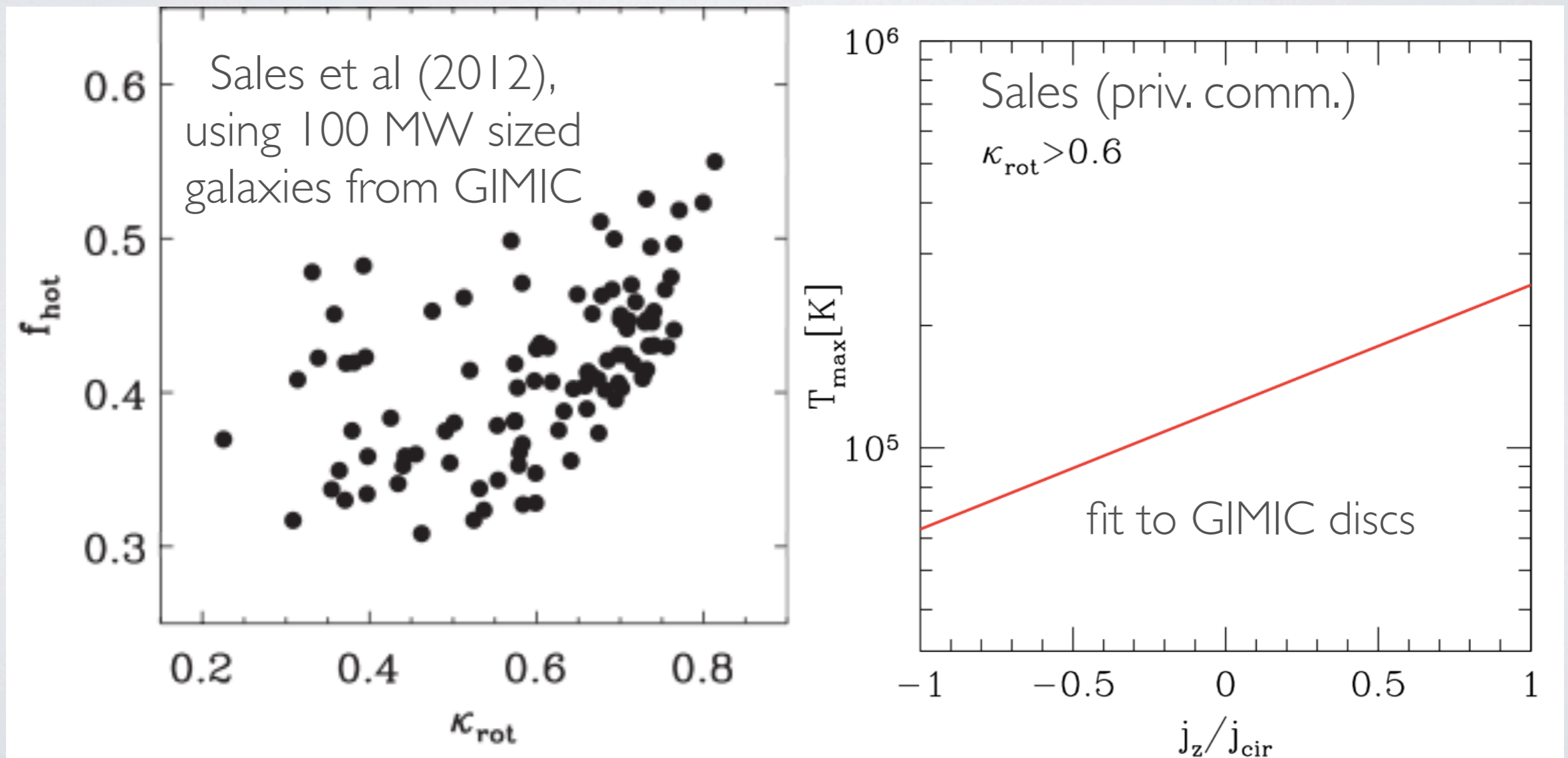
- Analytic approximation.
- Assume infalling cold gas relaxes in halo (also relaxed).

As a result, even though there is more cold gas in galaxies at high- $z$ , the discs are larger: not an important effect on the SFR.



# 4) COLD GAS INFLOWS

However, in gas simulations most of the gas that forms discs has been in a hot phase, indicating that cold flows are somehow responsible for the existence of a spheroid component.



# 4) EFFECT ON SF

We adopt two different treatments:

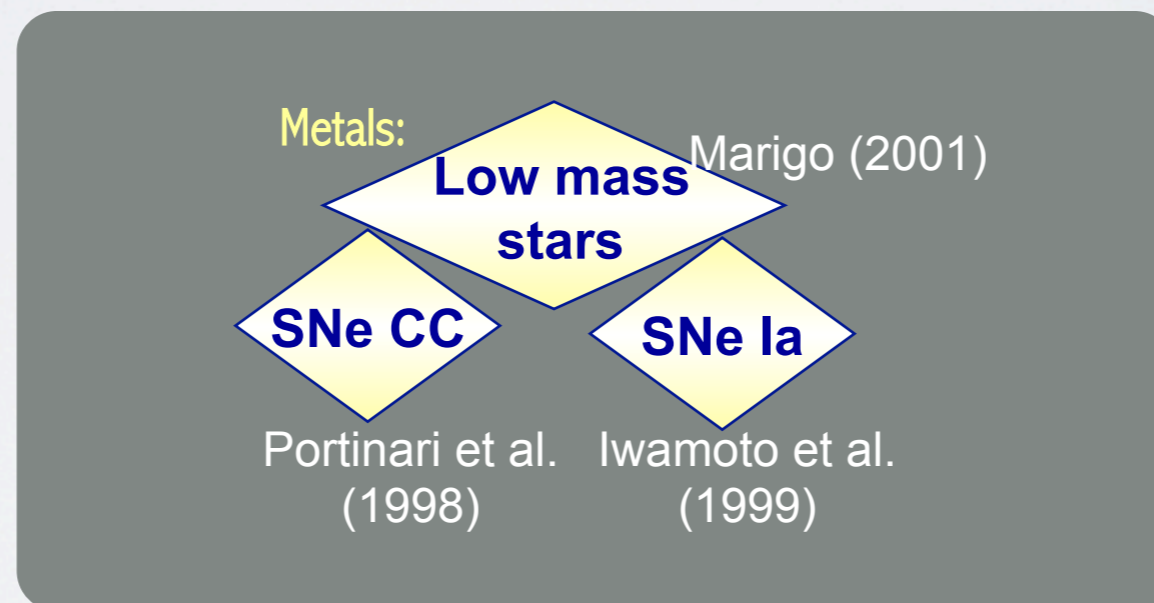
- Angular momentum of filament gas as that of a relaxed DM halo: more angular momentum, more gas, larger disc, may not increase SF.
- Angular momentum assumed to follow **flips** according to the baryonic mass coming with the cold inflows: comparatively smaller gas disc.

# 4) COLD GAS INFLOWS IN SAG

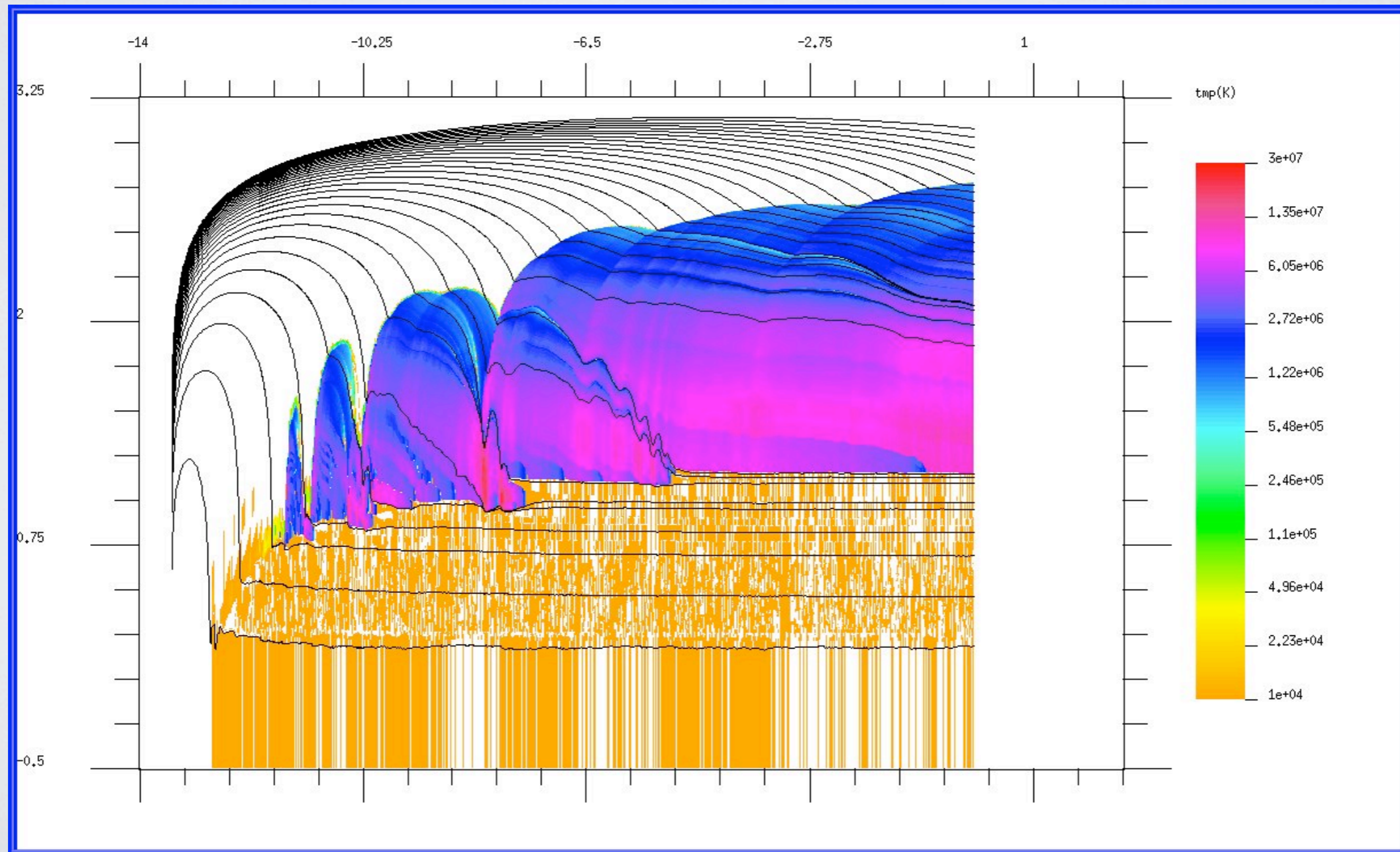
In SAG, we use the Sutherland and Dopita metallicity dependent cooling rates:

$$\frac{dM_{\text{cool}}}{dt} = 4\pi r_{\text{cool}}^2 \frac{dr_{\text{cool}}}{dt}$$

$$t_{\text{cool}}(r) = \frac{3}{2} \frac{kT \rho_g(r)}{\mu m_p n_e^2(r) \Lambda(T, Z)}$$

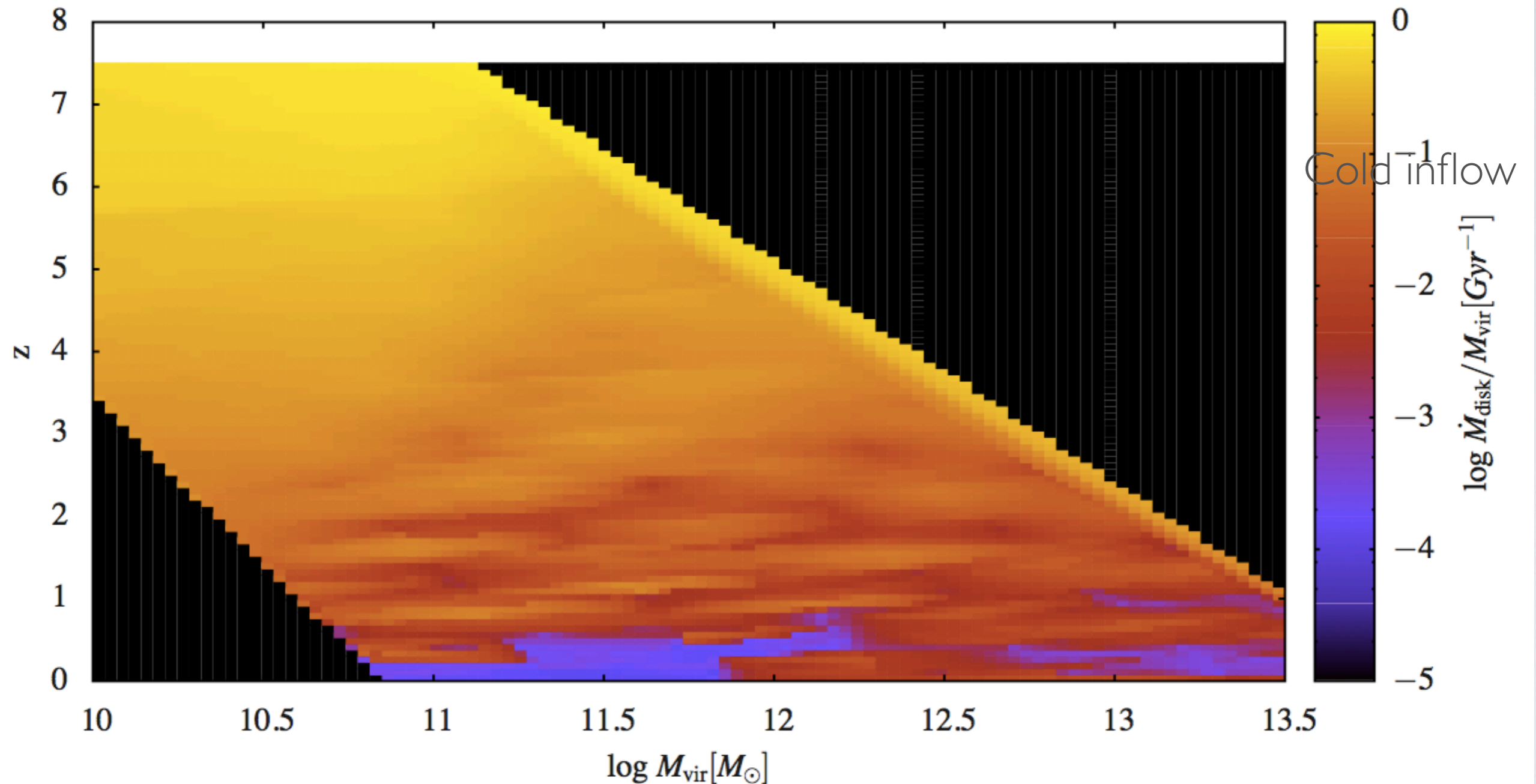


# 4) COLD INFLOWS FROM HYDRODYNAMICAL SIMULATIONS:



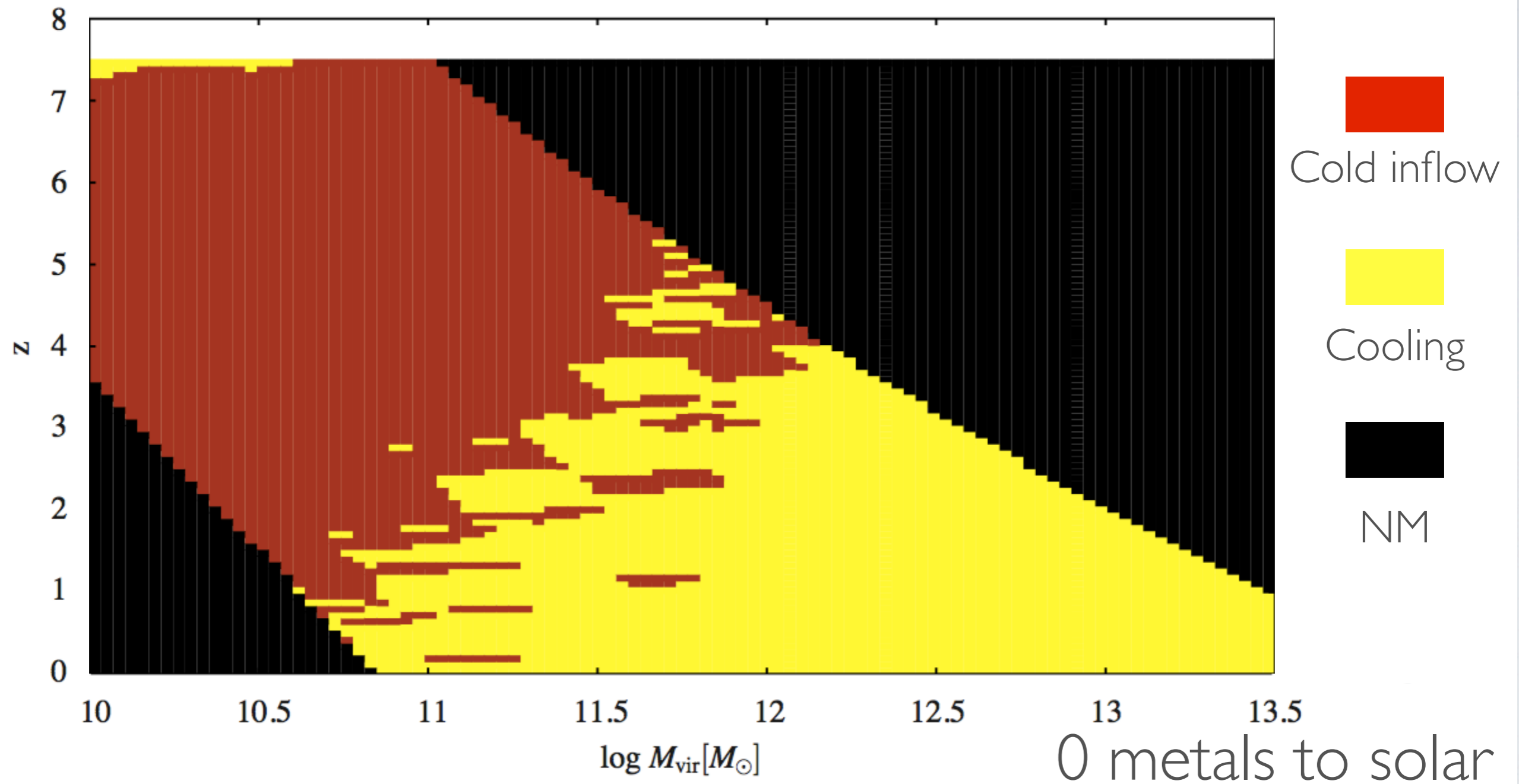


# 4) RATE OF COLD GAS INFLOW:



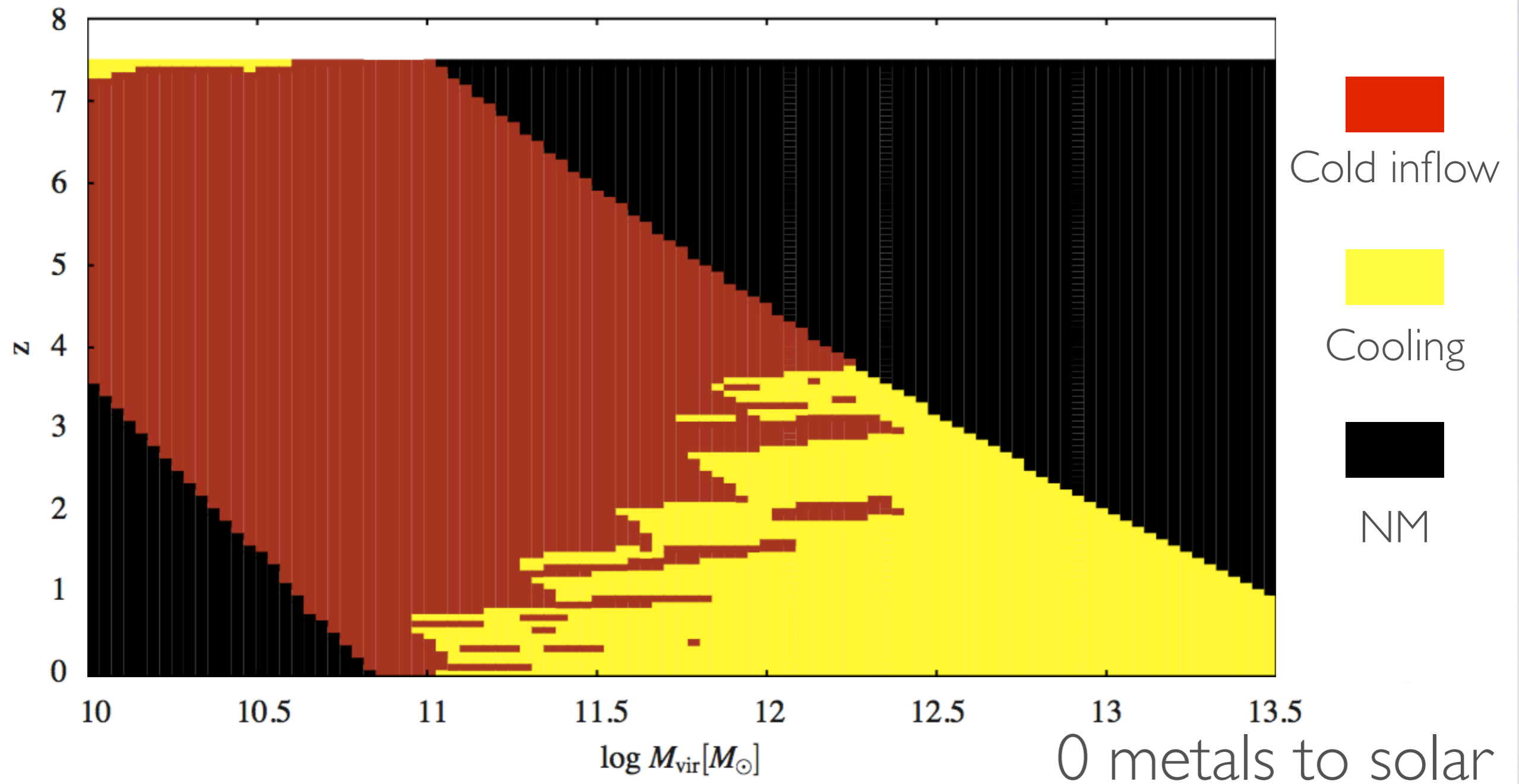
incorporated in SAG via metallicity dependent fit (variables: metallicity, mass, redshift)  
keeping the SD cooling rates for slow cooling

# 4) RATE OF COLD GAS INFLOW:



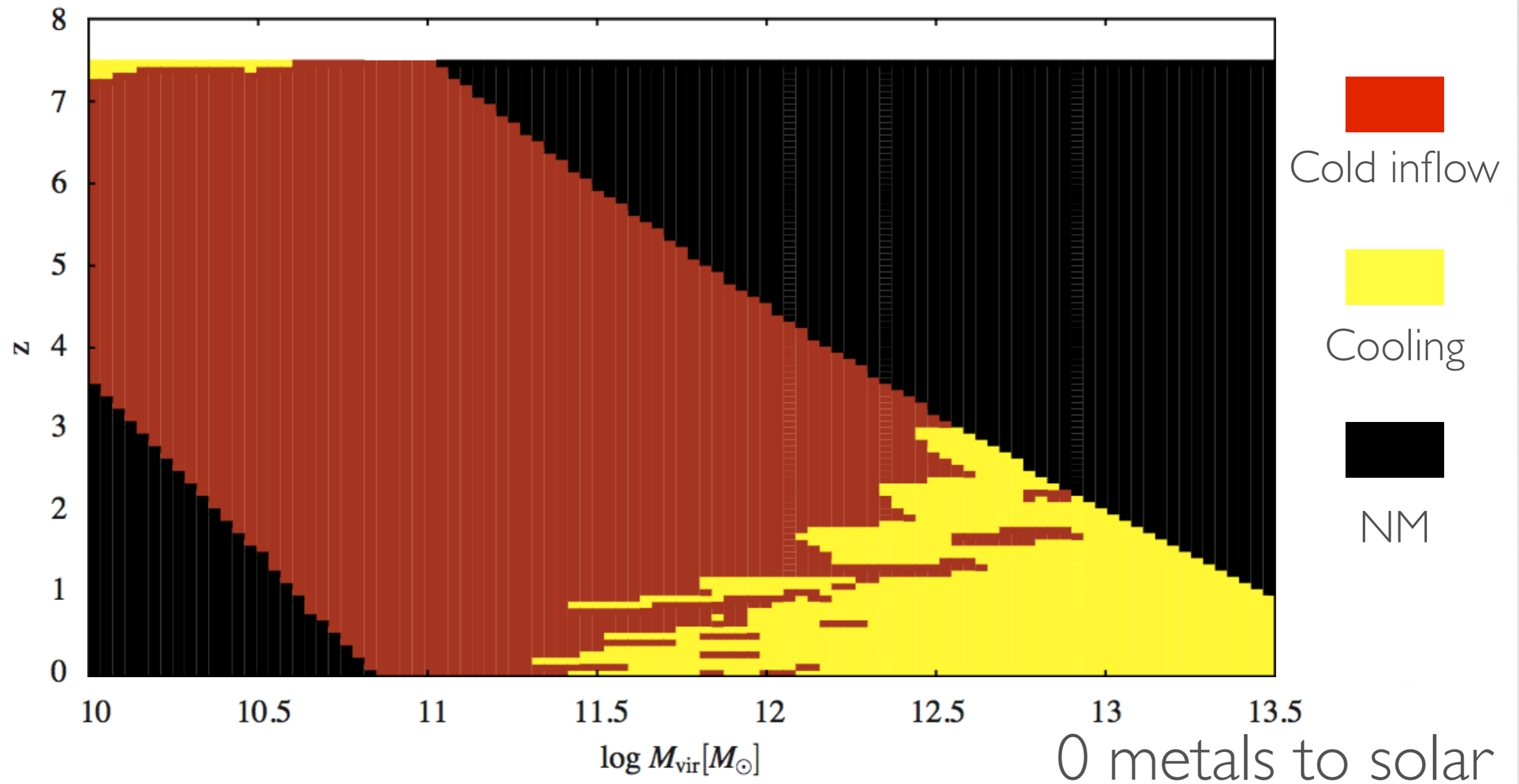
incorporated in SAG via metallicity dependent fit (variables: metallicity, mass, redshift)  
keeping the SD cooling rates for slow cooling

# 4) RATE OF COLD GAS INFLOW:



incorporated in SAG via metallicity dependent fit (variables: metallicity, mass, redshift)  
keeping the SD cooling rates for slow cooling

# 4) RATE OF COLD GAS INFLOW:

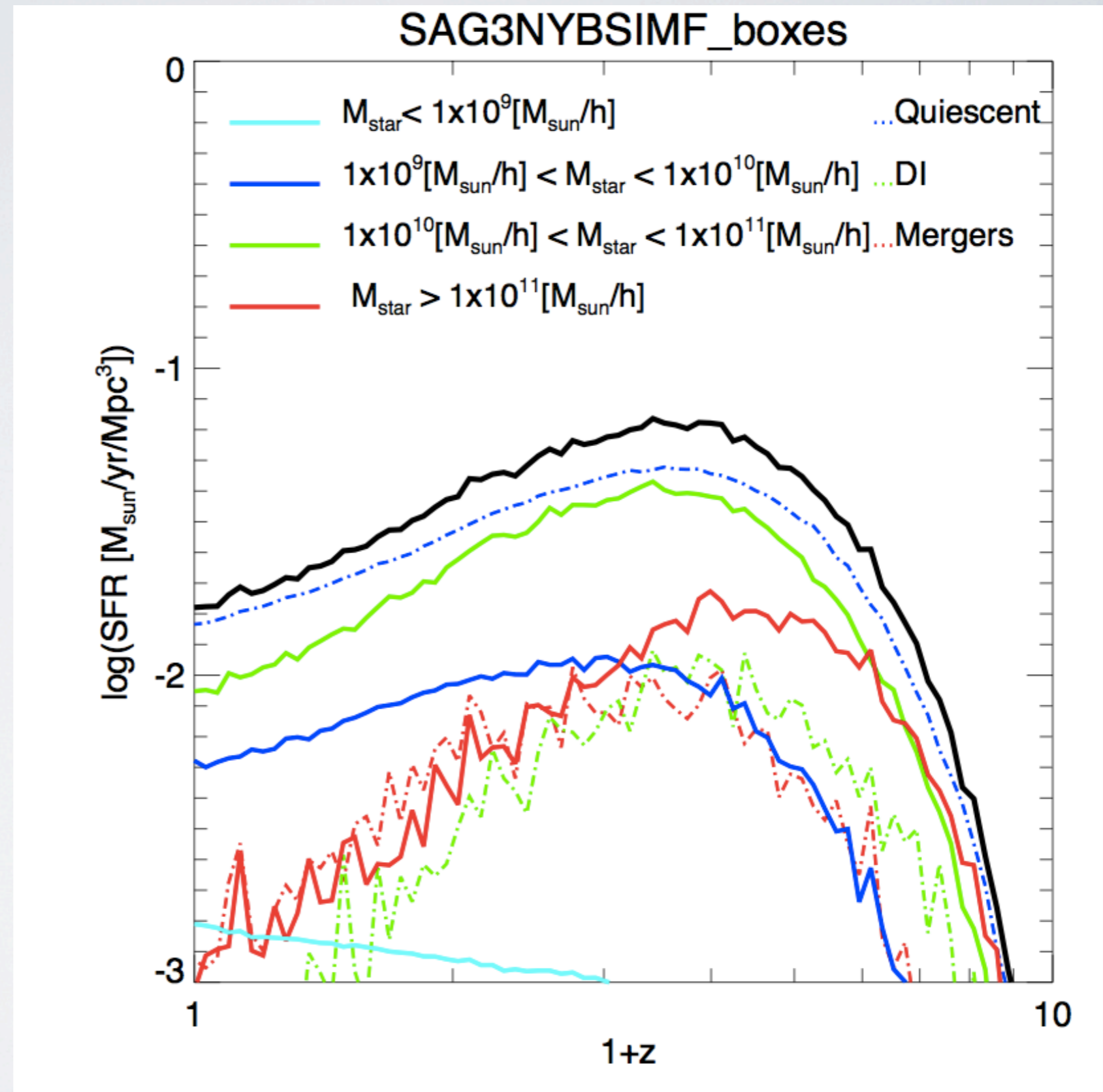


incorporated in SAG via metallicity dependent fit (variables: metallicity, mass, redshift)  
keeping the SD cooling rates for slow cooling

# 4) RESULTS: MADAU PLOT

Almost no effect from cold-inflows when relaxing filaments and no flips.

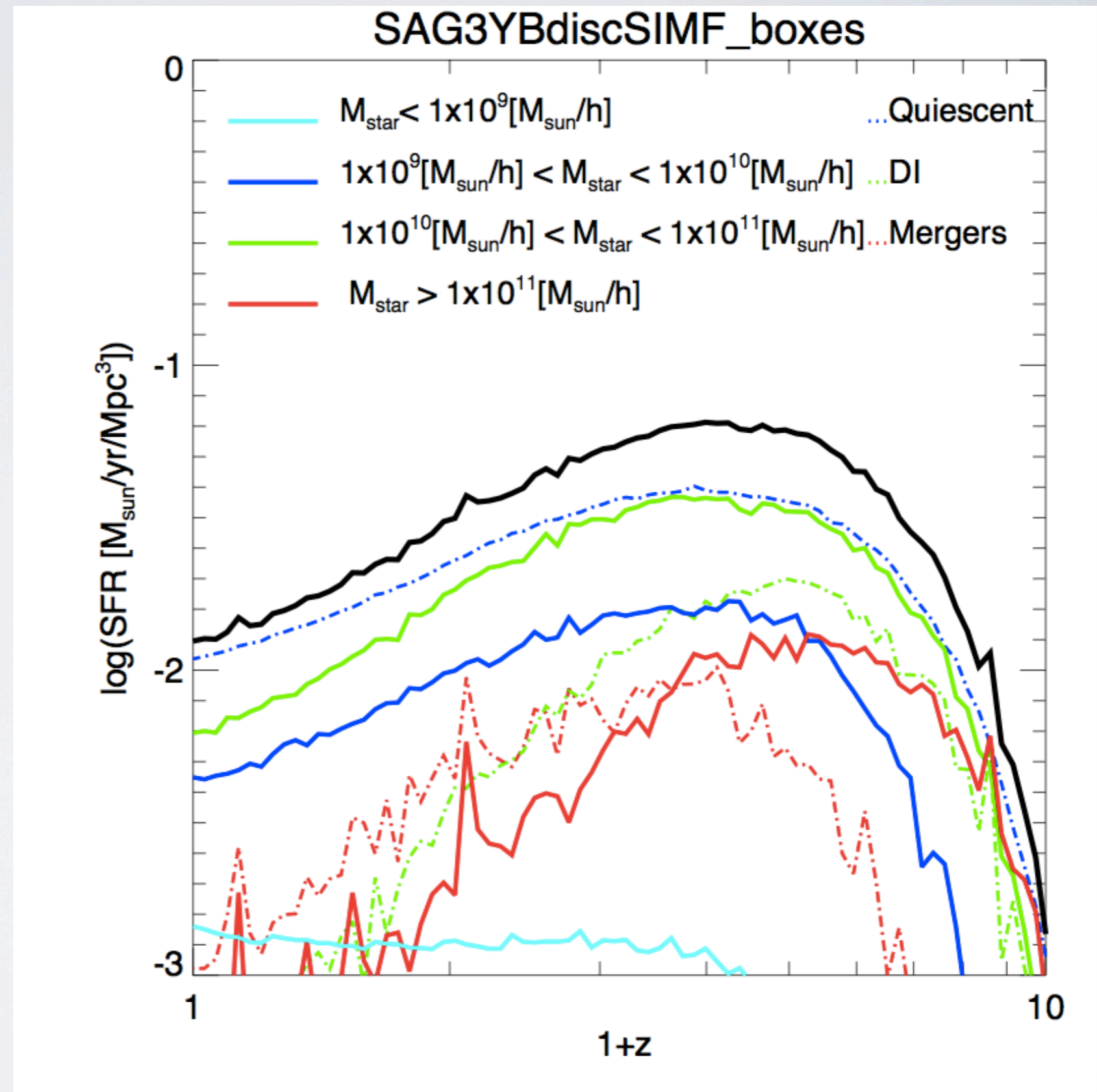
Factor of up to x2 increase in high-z SFR in flips case.



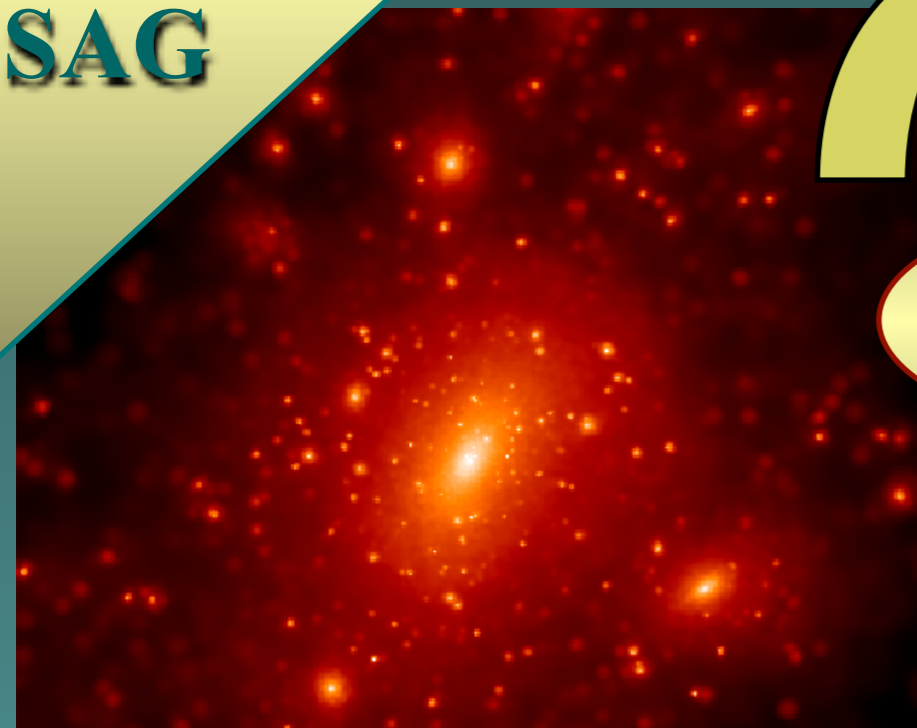
# 4) RESULTS: MADAU PLOT

Almost no effect from cold-inflows when relaxing filaments and no flips.

Factor of up to x2 increase in high-z SFR in flips case.



SAG



**HOT GAS**

$$M_{\text{hot}} = \Omega_b M_{\text{vir}} - \sum_i (M_{\text{star}}^{(i)} + M_{\text{cold}}^{(i)})$$

**COLD GAS**

$$\frac{dM_{\text{cool}}}{dt} = 4\pi r_{\text{cool}}^2 \frac{dr_{\text{cool}}}{dt}$$

$$t_{\text{cool}}(r) = \frac{3}{2} \frac{kT \rho_g(r)}{\mu m_p n_e^2(r) \Lambda(T, Z)}$$

**STARS**

$$\Delta M_{\text{reheat}} = \frac{4}{3} \epsilon \frac{\eta_{\text{SNCC}} E_{\text{SNCC}}}{V_{\text{vir}}^2} \Delta M_*$$

**FEEDBACK**

$$\frac{dM_*}{dt} = \alpha \left( \frac{V_{\text{vir}}}{220 \text{ km s}^{-1}} \right)^n \frac{M_{\text{cold}}}{t_{\text{dyn}}}$$

Option 1

$$\frac{dM_*}{dt} = \alpha \frac{(M_{\text{cold}} - M_{\text{crit}})}{t_{\text{dyn}}}$$

Option 2:  
Croton et al. (2006)

Metals:

**Low mass stars**

Marigo (2001)

Simple degenerate model

(Lia et al. 2002)

**SNe CC**

**SNe Ia**

Portinari et al. (1998)

Iwamoto et al. (1999)

**Stellar life time:**

Padovani & Matteucci (1993)

Cora (2006)

**Improvement**

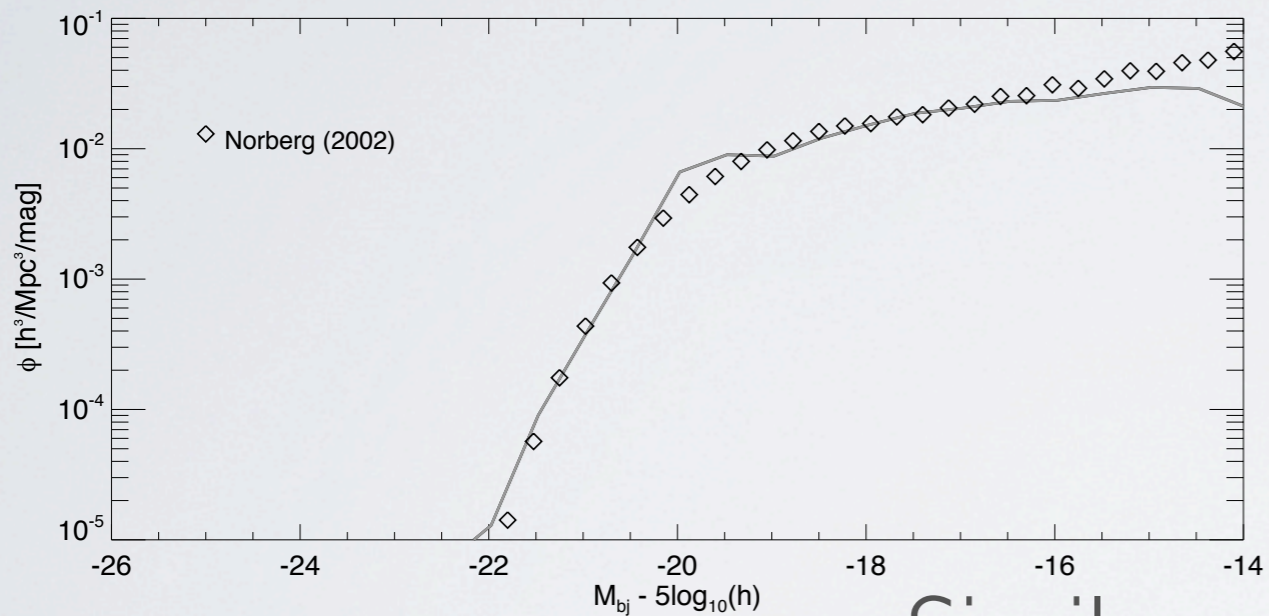
**AGN FEEDBACK**

Lagos, Cora & Padilla (2008)

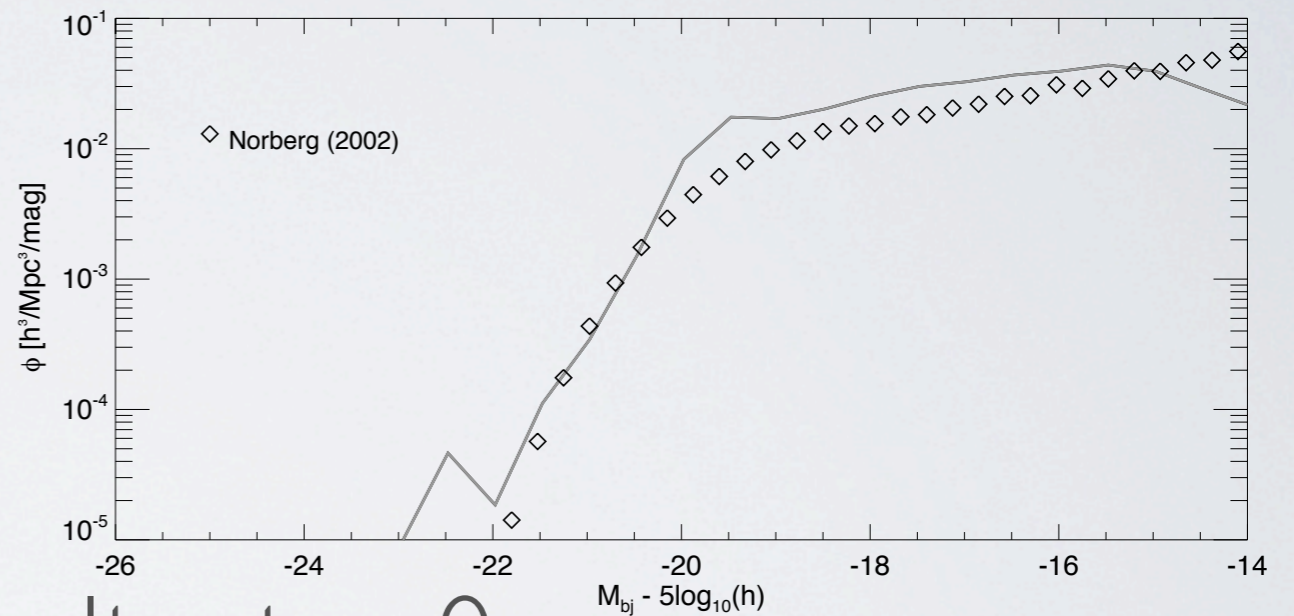
# 4) RESULTS: Z=0 LF

Do we still reproduce z=0 properties?

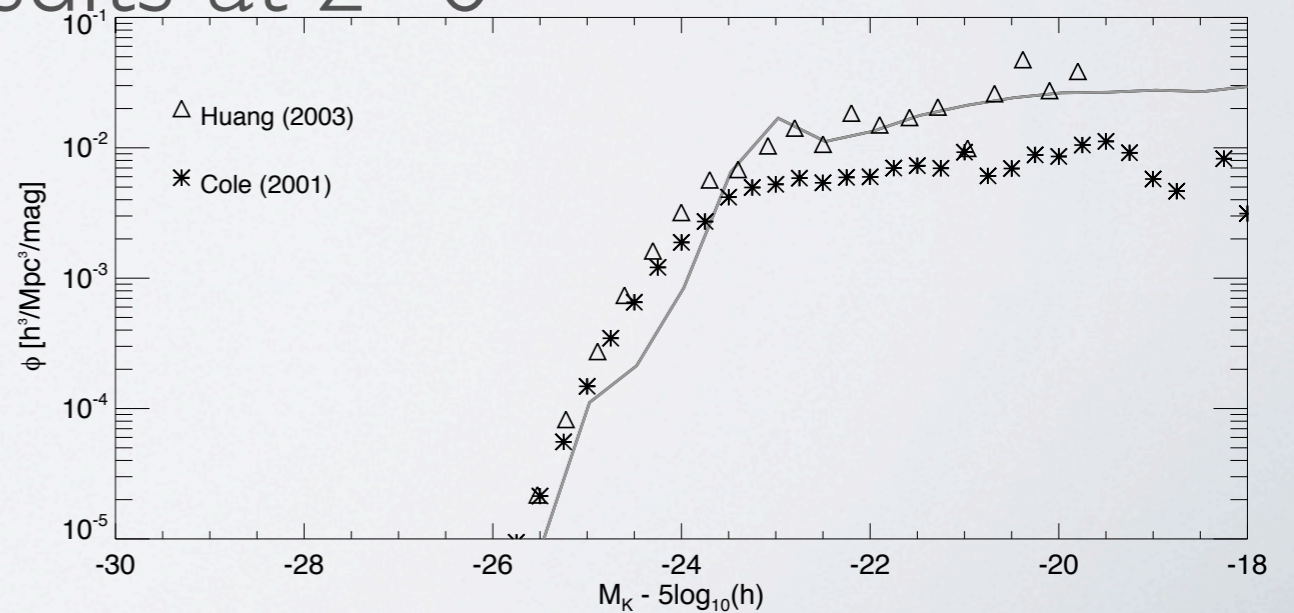
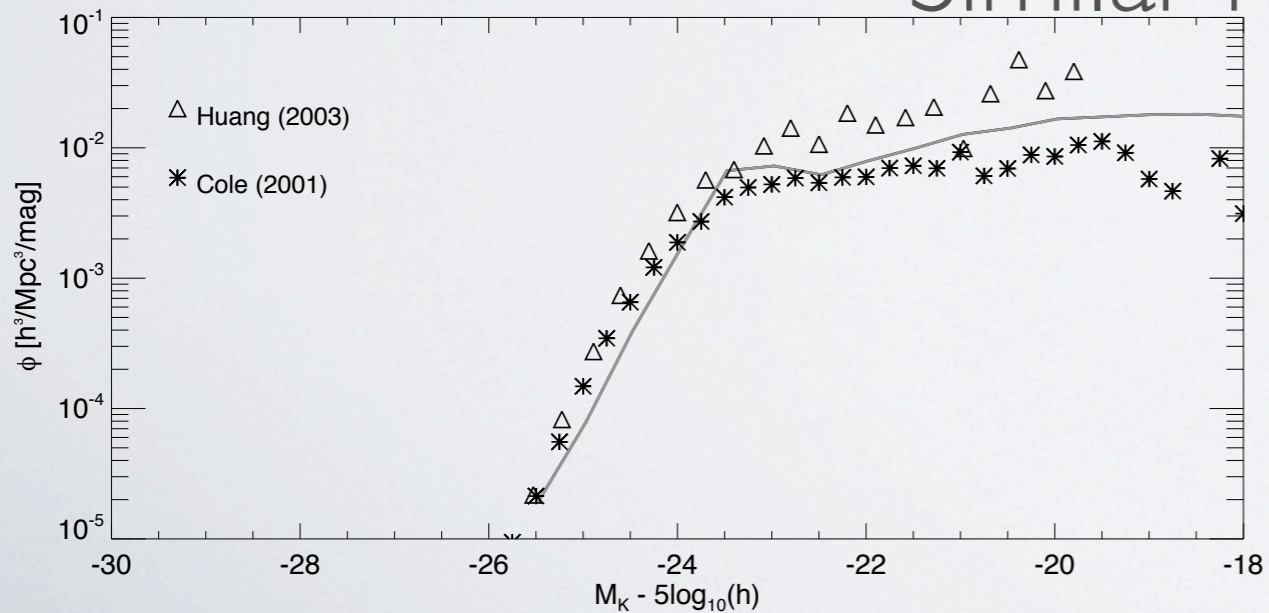
No cold inflows



Cold inflows zero J



Similar results at z=0





4) SPIN OF BHS:

## Base model:

We have 3 different mechanism of BH growth: Bondi-Hoyle

- The QSO mode

$$\dot{M}_{\text{BH}} = \frac{f_{\text{BH}}}{\Delta T} \times \frac{M^{\text{sat}}}{M^{\text{central}}} \times \frac{M_{\text{ColdGas}}}{1 + (200 \text{ km s}^{-1}/V_{\text{vir}})^2},$$

with  $f_{\text{BH}} = 0,76$ .

- The Radio mode

$$\dot{M}_{\text{BH}} = \kappa_{\text{AGN}} \frac{M_{\text{BH}}}{10^8 M_{\odot}} \times \frac{f_{\text{hot}}}{0,1} \times \left( \frac{V_{\text{vir}}}{200 \text{ km s}^{-1}} \right)^3,$$

with  $\kappa_{\text{AGN}} = 6 \times 10^{-2} M_{\odot} \text{ yr}^{-1}$ .

- Mergers of BHs

$$M_{\text{BH}}^{\text{final}} = M_{\text{BH}}^1 + M_{\text{BH}}^2$$

- The BH luminosity

$$L_{\text{BH}} = \eta \dot{M}_{\text{BH}},$$

with  $\eta = 0,1$ .

- The modification of the cooling rate is given by

$$\dot{M}'_{\text{cool}} = \dot{M}_{\text{cool}} - \frac{L_{\text{BH}}}{V_{\text{vir}}^2/2}$$

- We limit the luminosity by the "Eddington limit"

$$L_{\text{edd}} = \frac{4\pi G m_p}{\sigma_T} M_{\text{BH}}$$

## Model with BH spin:

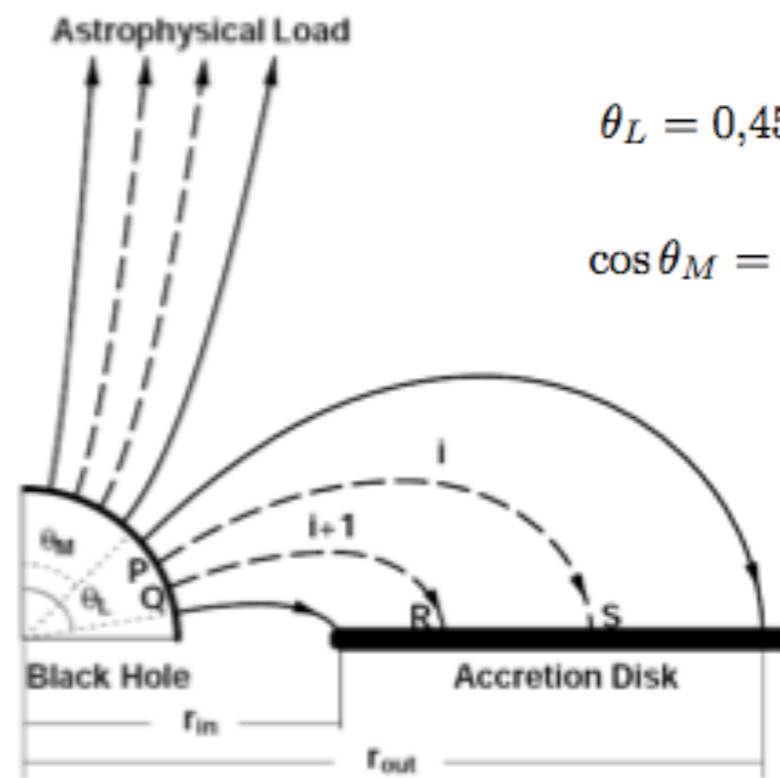
Spin:

last stable orbit  
lies further in.

$$F(r) = \frac{\dot{M}_0}{4\pi r} f + \frac{1}{r} \frac{-\Omega_{,r}}{(E^+ - \Omega L^+)^2} \int_{r_{\text{ms}}}^r (E^+ - \Omega L^+) H r dr,$$

Higher accretion  
disc flux.

We use the model of Wang, Xiao & Lei (2002), with the improvement of Wang et al. (2003)



$$\theta_L = 0,45\pi$$

$$\cos \theta_M = \cos \theta_L + \int_1^{\xi_{out}} G(a_*, \xi, n) d\xi.$$

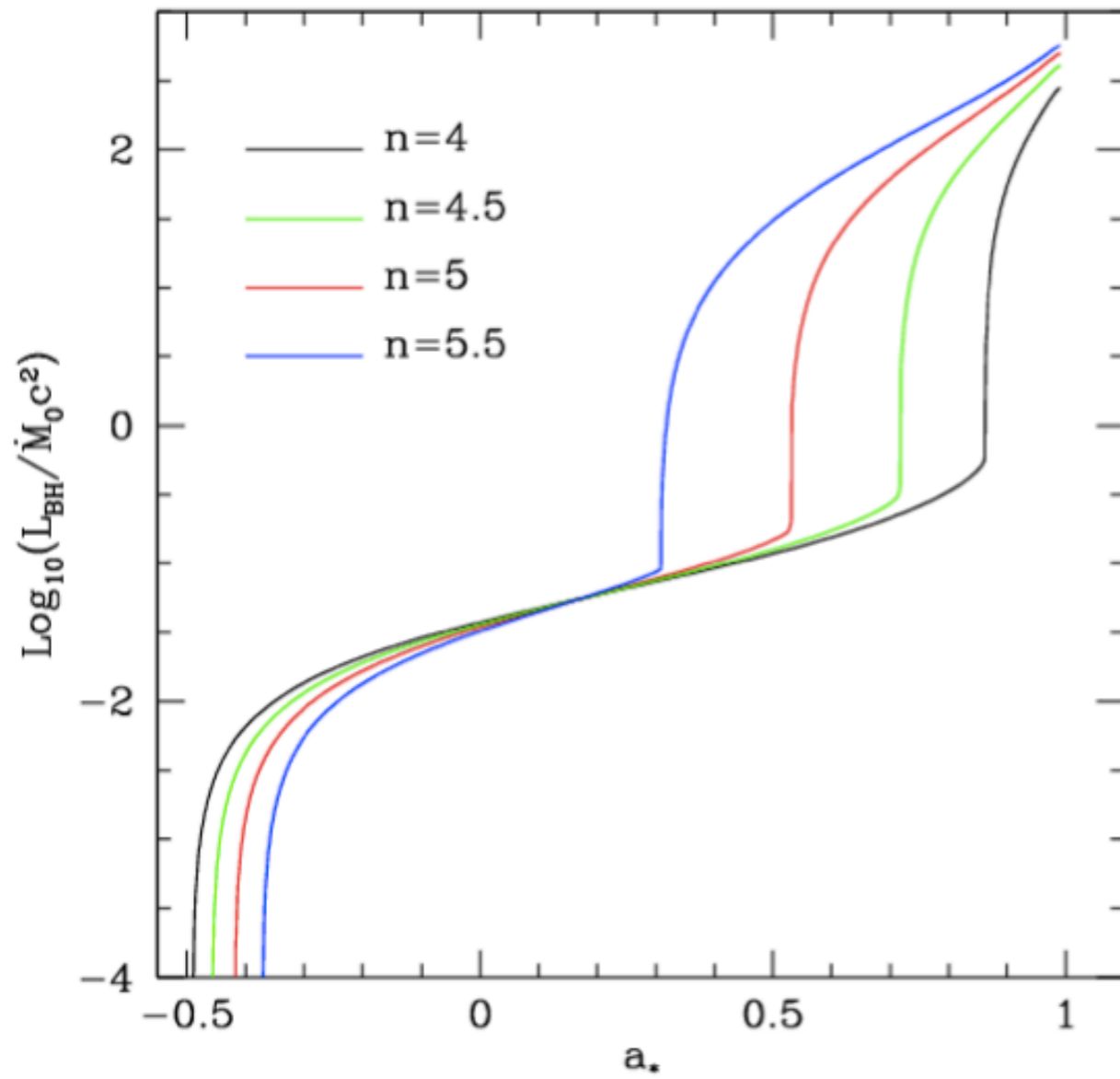
This model allows the coexistence of the BZ and MC processes (CEBZMC).

The magnetic field on the horizon

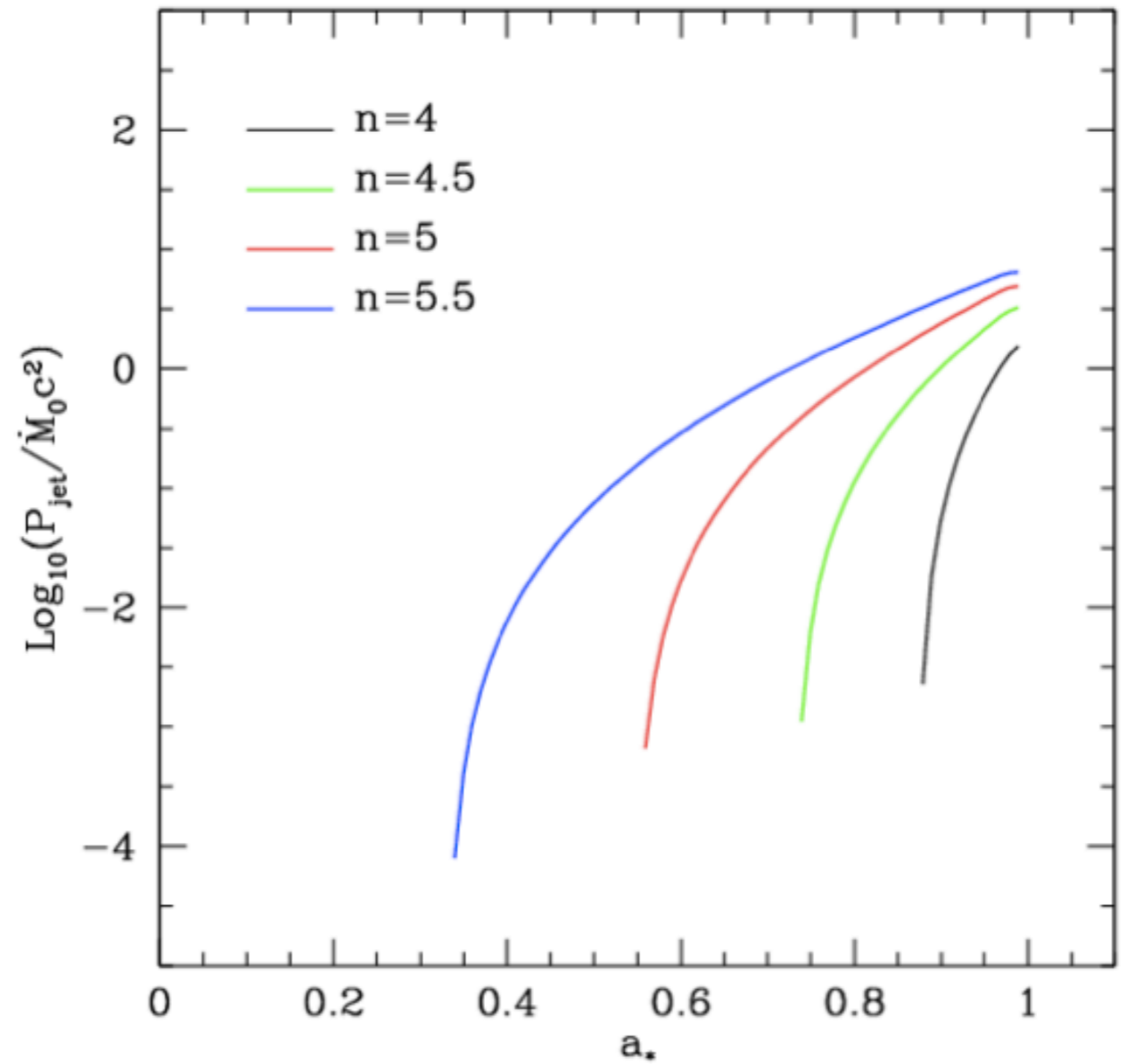
$$B_H^2 = \frac{2\dot{M}_0}{r_H^2}$$

$$\begin{aligned} L_{BH} &\equiv 2 \int_{r_{ms}}^{\infty} FE^+ 2\pi r dr \\ &= \dot{M}_0 (1 - E_{ms}^+) + 4\pi \int_{r_{ms}}^{\infty} H\Omega r dr \\ &= \epsilon_0 \dot{M}_0 + L_{MC} \end{aligned}$$

# 4) SPIN OF BHS:

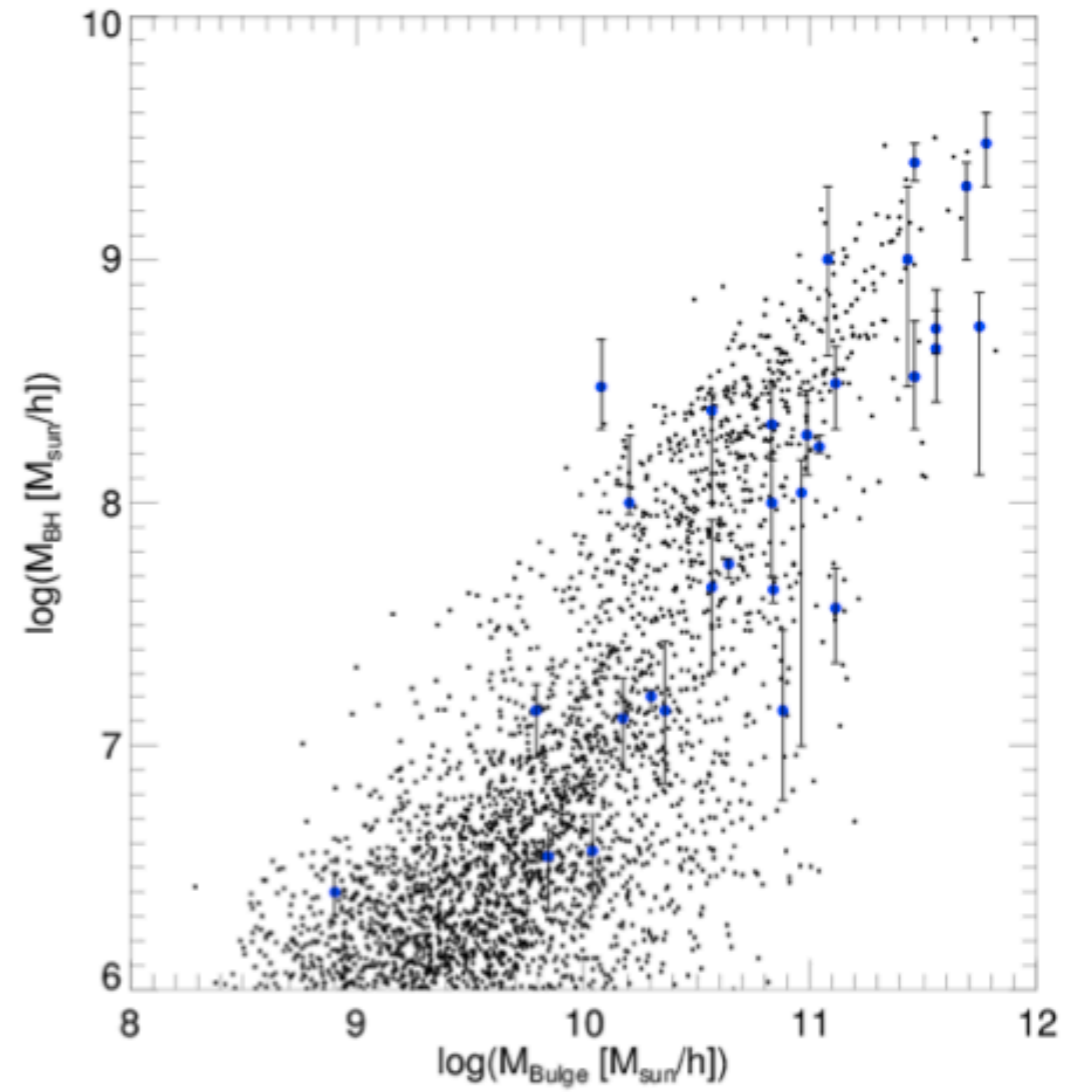
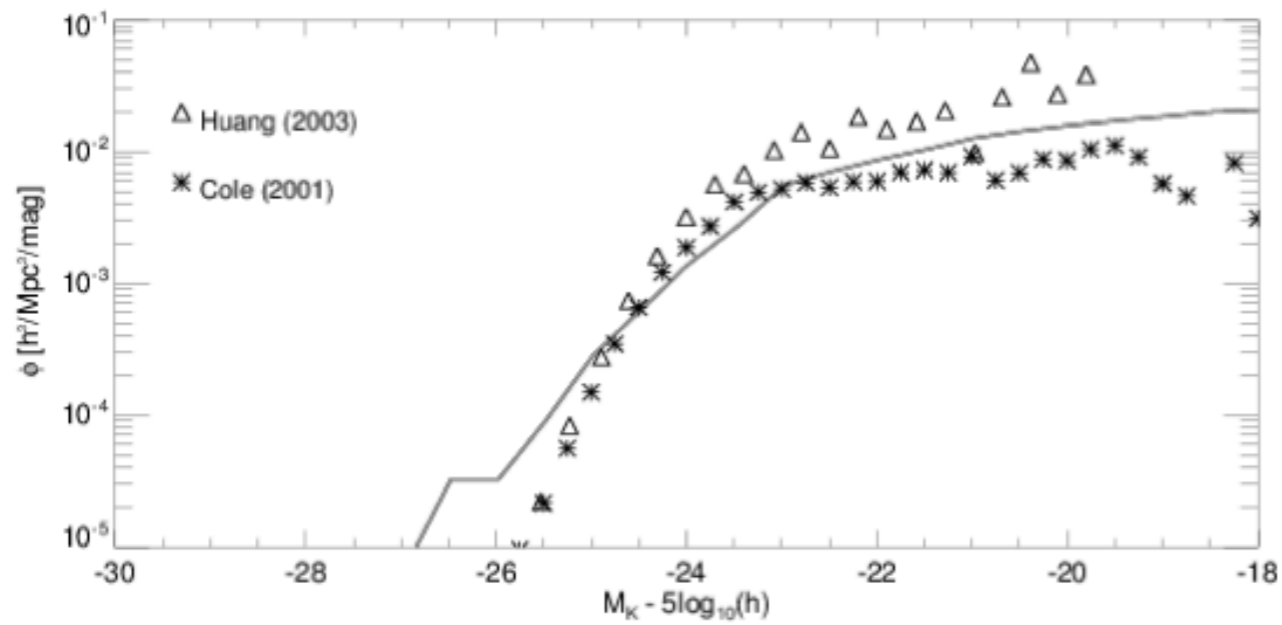
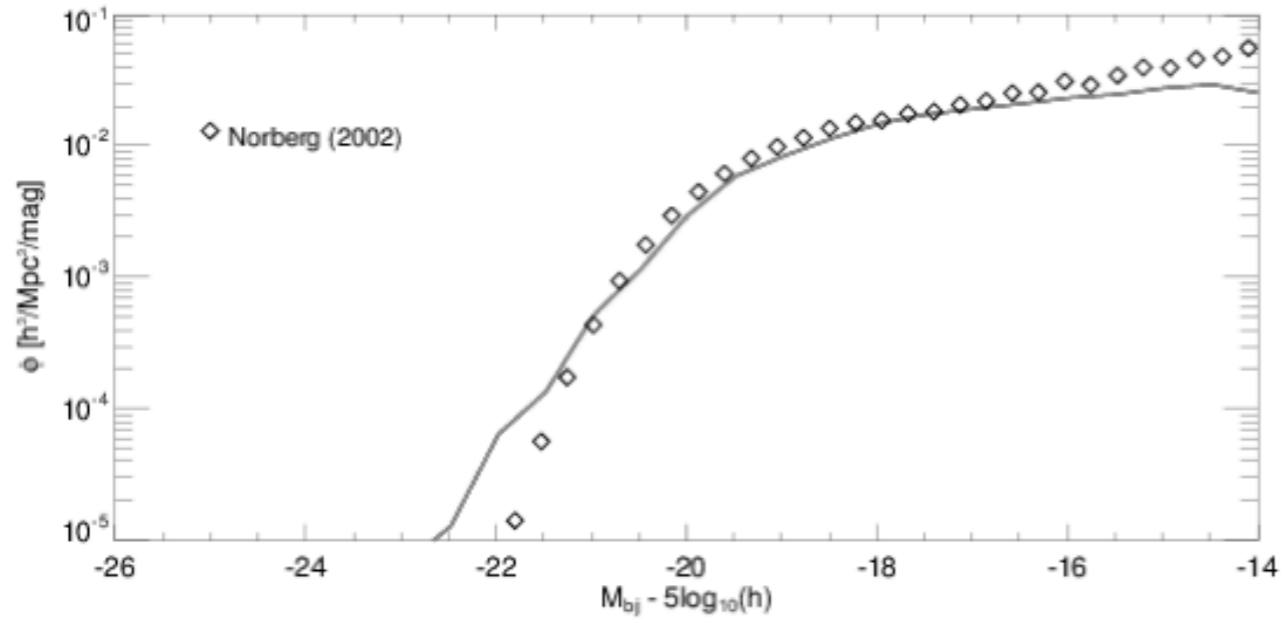


$$(\Delta M_{\text{reheated}})_{\text{AGN}} = \eta_{\text{BH}} \frac{L_{\text{BH}}}{V_{\text{vir}}^2/2}$$



$$\dot{M}'_{\text{cool}} = \dot{M}_{\text{cool}} - \eta_{\text{FB}} \frac{P_{\text{jet}}}{V_{\text{vir}}^2/2}$$

# 4) SPIN OF BHS:

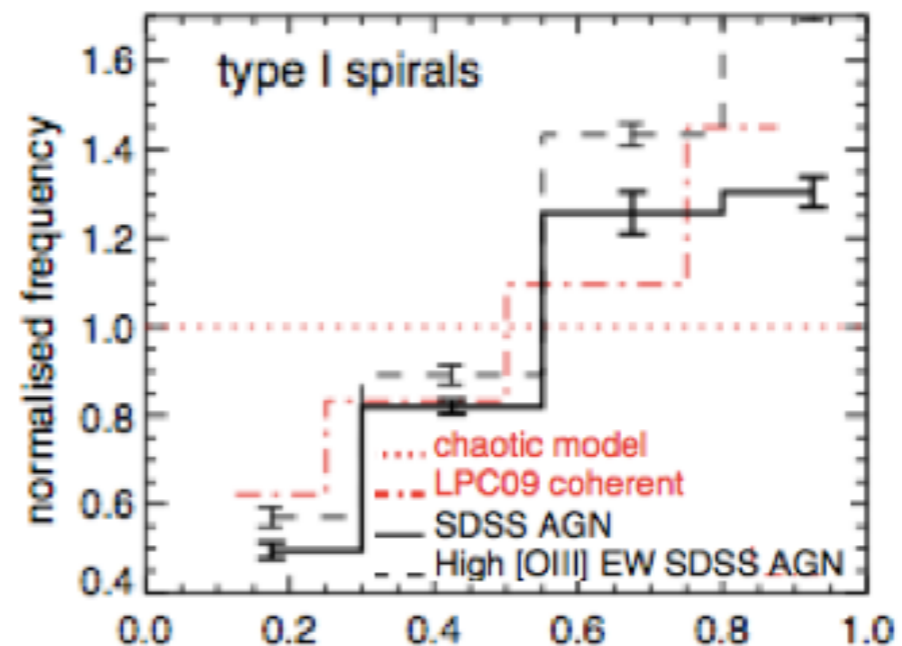
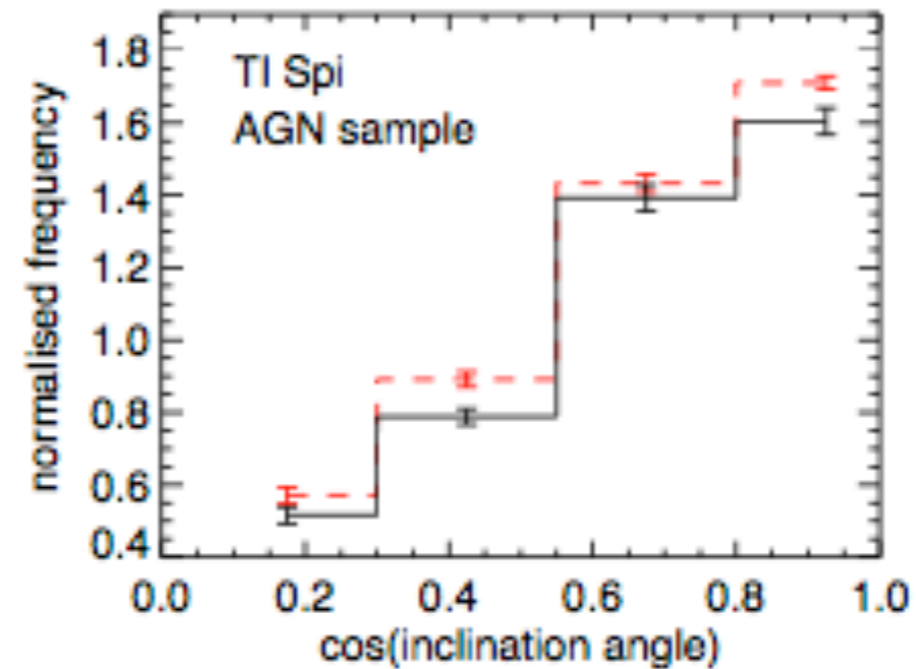


# 4) IS THERE EVIDENCE OF ALIGNMENTS?:

Evidence is conflicting:

Positive in Schmitt et al. (2002) and in Battye & Browne (2008)

Lagos et al. (2011):



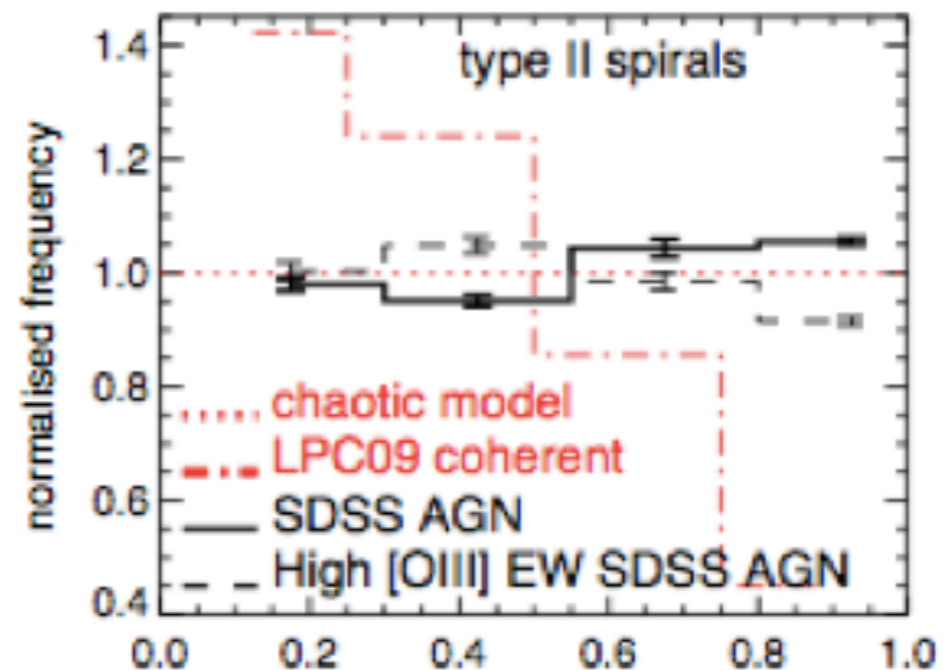
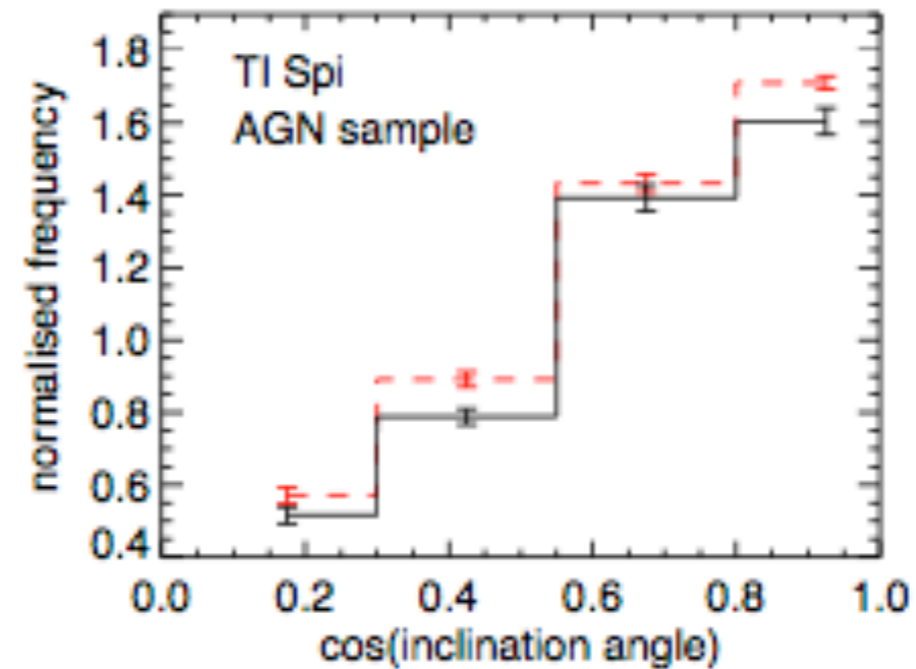
dotted  
horizontal:  
random  
orientations

# 4) IS THERE EVIDENCE OF ALIGNMENTS?:

Evidence is conflicting:

Positive in Schmitt et al. (2002) and in Battye & Browne (2008)

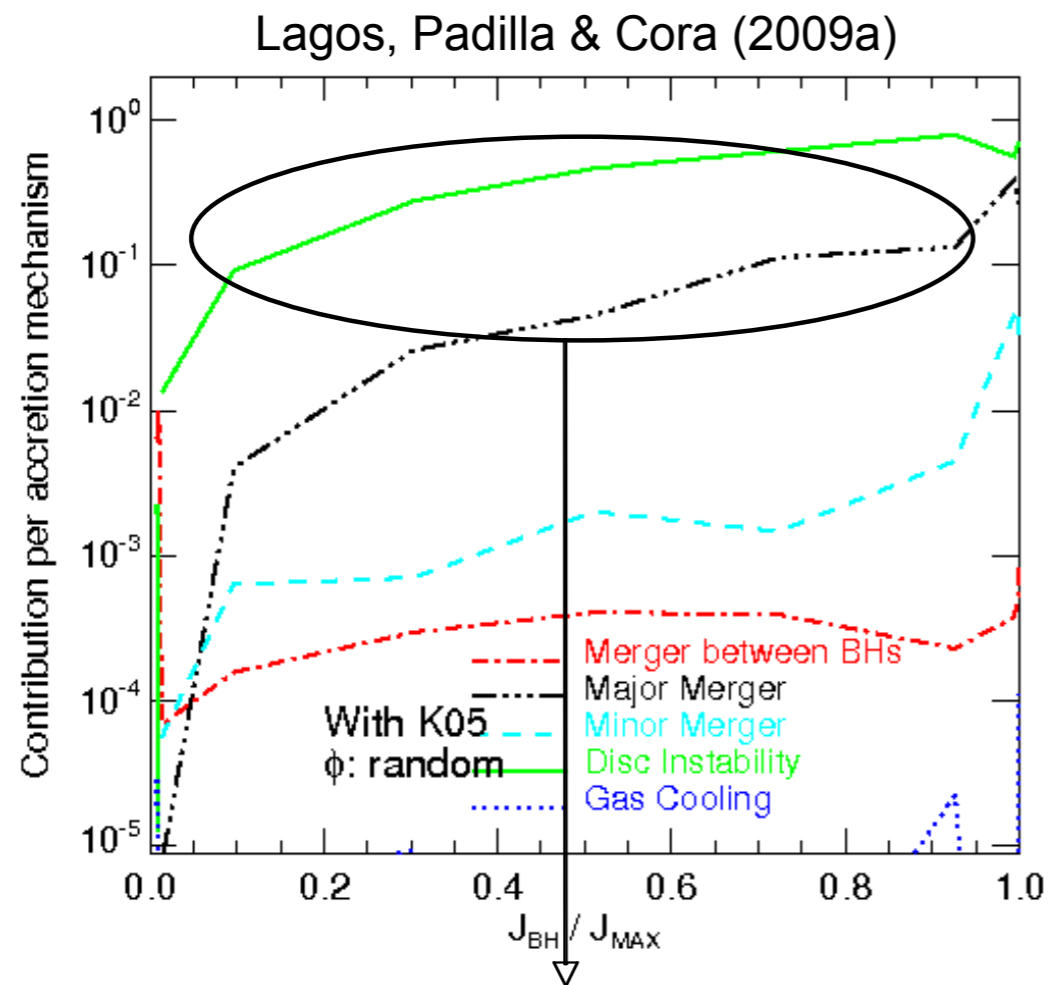
Lagos et al. (2011):



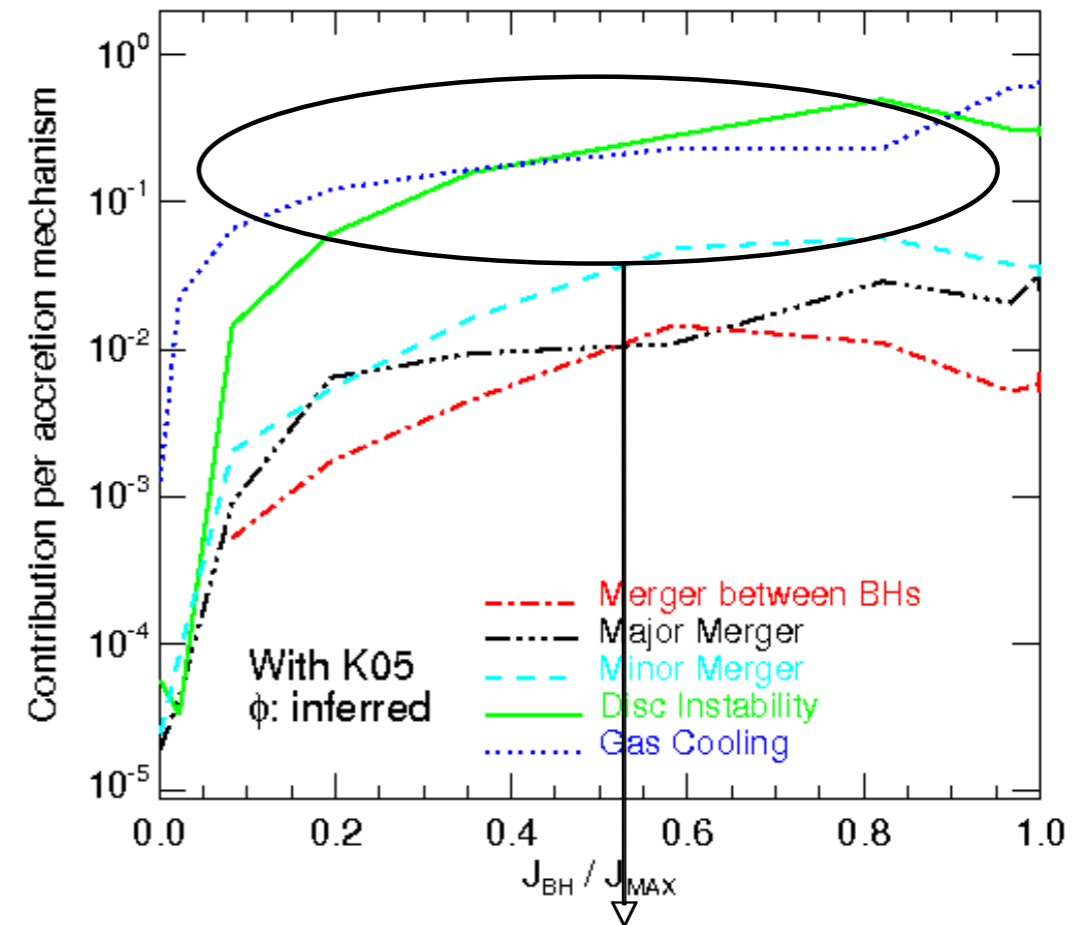
dotted  
horizontal:  
random  
orientations

# 4) IS THERE AN EFFECT OF ALIGNMENTS IN THE MODEL?:

- One of the main advantages in use a SAM is to **follow the baryon physics** and to distinguish between different phenomena in the galaxy SFH



same mechanisms that produce the main BH growth



processes involving same galaxy components